Development of a Photo-Controlled Polymeric Dry Adhesive

by

B. Kailey Wright

B.Sc. (Hons.), University of Victoria, 2014

Thesis Submitted in Partial Fulfillment of the
Requirements for the Degree of
Master of Science

in the
Department of Chemistry
Faculty of Science

SIMON FRASER UNIVERSITY
Fall 2017

Approval

Name:	**B. Kailey Wright**
Degree:	**Master of Science (Chemistry)**
Title:	**Development of a Photo-Controlled Polymeric Adhesive**
Examining Committee:	**Chair:** **Dr. Tim Storr** Associate Professor
	Dr. Neil Branda Senior Supervisor Professor
	Dr. Gary Leach Supervisor Associate Professor
	Dr. Loren Kaake Supervisor Assistant Professor
	Dr. Vance Williams Internal Examiner Associate Professor
Date Defended/Approved:	August 28, 2017

Abstract

The work presented in this thesis describes the design, synthesis, and analysis of a polymeric donor-acceptor Stenhouse adduct (DASA). This photoswitch was chosen as it switches between two isomeric states, open and closed, that are neutral and zwitterionic respectively. The goal of this project was to manipulate this change in polarity to induce a stronger adhesive response in the polymer, due to an increase in the dipole-dipole interaction between the polymer and a contact piece. While the single molecule exhibits reversibility in solution, the polymer does not appear to reverse in solution or in the solid state. There was a change of 18° in the contact angle, indicating a photoinduced change in the intermolecular forces did occur, however this has no significant effect on the bulk adhesive properties.

Keywords: photochromism; photoswitching; dry adhesives; donor-acceptor Stenhouse adducts; polymer; ROMP

Acknowledgements

I would like to thank Gary Leach and Loren Kaake for being on my committee and providing feedback and suggestions throughout the years. I would also like to thank the Internal Examiner, Vance Williams, for his participation on my examining committee.

I would also like to extend my thanks to those who have assisted with practical tasks over the years; Scott Beaupre (Engineering) for adhesion measurements, Jonathan Ward (Holdcroft Group) for GPC measurements, David Ester (Williams Group) and Clayton Schultz (Yu Group) for instrument training and help, Hongwen Chen (SFU) for Mass Spectrometry services, and Nathalie Fournier and Leslie Butler for their assistance with administrative tasks.

To the entire Branda Group—particularly Scott Beaupré, Pamela Tannouri, Danielle Wilson, Brahmjot Kaur, Khaled Arafeh, Amir Asadirad, and Tony Wu—your advice and support has been limitless and for that I will always be grateful.

This work made use of 4D LABS shared facilities supported by the Canada Foundation for Innovation (CFI), British Columbia Knowledge Development Fund (BCKDF) and Simon Fraser University (SFU).

Table of Contents

List of Figures

List of Tables

List of Equations

List of Schemes

List of Acronyms

°C	degrees Celsius
CD_2Cl_2	deuterated dichloromethane
CD_3OD	deuterated methanol
$CDCl_3$	deuterated chloroform
cm^{-1}	wavenumber
d	doublet (NMR)
Da	Dalton
DAE	diarylethene
DASA	donor-acceptor Stenhouse adduct
DCM	dichloromethane
dd	doublet of doublets (NMR)
dec.	decomposed
DSC	differential scanning calorimetry
dt	doublet of triplets (NMR)
DTE	dithienylethene
ESI	electrospray ionization
Et_2O	diethyl ether
GPC	gel permeation chromatography
H	proton
hr	hours
HRMS	high resolution mass spectrometry
Hz	hertz
J	coupling constant (NMR)
JKR	Johnson-Kendall-Roberts
K	Kelvin
LC-MS	liquid chromatography mass spectrometry
M	molarity ($moles \cdot L^{-1}$)
m	multiplet (NMR)
M.P.	melting point
m/z	mass to charge ratio
MeOH	methanol
$MgSO_4$	magnesium sulphate

MHz	megahertz
min	minute
mL	milliliters
mm	millimeters
mN	milliNewtons
$\bar{M}_n$	number average molecular weight
mW	milliwatts
$\bar{M}_w$	weight average molecular weight
nm	nanometers
NMR	nuclear magnetic resonance
PDI	polydispersity index
PDMS	polydimethylsiloxane
PSS	photostationary state
ROMP	ring-opening metathesis polymerisation
RT	room temperature
s	singlet (NMR)
s	seconds
t	triplet (NMR)
t	time
T_g	glass transition temperature
UV	ultraviolet
UV-vis	ultraviolet-visible
W	watts
Δ	heat
δ	chemical shift
ε	molar absorptivity
λ	wavelength
μL	microliter
μm	micrometer

Chapter 1. Introduction

The primary goal of this project was to synthesise a photo-switchable dry adhesive material. Initially, the small molecule and polymer form of the donor-acceptor Stenhouse adducts (DASA) were synthesised and their photochemistry studied. Then, the adhesion characteristics of the material were probed. This chapter details the background for interest in dry-adhesives, as well as the background for photochromism and the particular interest in the DASAs. Chapter two details the previous work done, along with the project design and further findings of this work. Chapter three contains the experimental details. All spectra and other data are contained in the appendices.

1.1. Dry Adhesives

It would be almost impossible for anyone to look around without seeing an adhesive of some kind. From the labels on bottles, to the caulking around windows, their existence is integral in the day to day lives of most people. Wet adhesives are the most common, but they are rarely reusable. Their sticky nature causes them to become easily contaminated, or the mode in which they are set prevents them from being removed once adhered to a surface. Dry adhesives offer an alternative because they can be removed and reapplied without damage to either the adhesive or the surface on which it is placed.[1] The ability to bind two surfaces together and separate them on command, without causing damage is highly desirable in robotic applications,[2–4] for biomedical devices and dressings,[1,5,6] and in many other environments[7,8].

An effective dry adhesive relies on two factors. The first is surface compliance, which is the amount of surface area contact between two layers. This is best described using the Johnson-Kendall-Roberts (JKR) model, which shows that small fibrillar structures are able to enhance adhesion by improving compliance with surfaces, which are naturally rough on the micron scale.[9,10] This is the primary mode through which geckos can adhere to seemingly sheer surfaces, such as glass. Their feet have small divisions, known as setae, which are then further separated into spatulae that are on the order of 0.2 μm (Figure 1.1.1). These small fibrillar structures allow the geckos to make contact with the micro-imperfections of the surface and thus they are able to stick. Several research groups in chemistry, physics, engineering, and other disciplines have been

inspired by the JKR model, and have developed several strategies for the synthesis of artificially structured materials to increase the surface compliance, and therefore the overall adhesion of a material to a surface.[11–17]

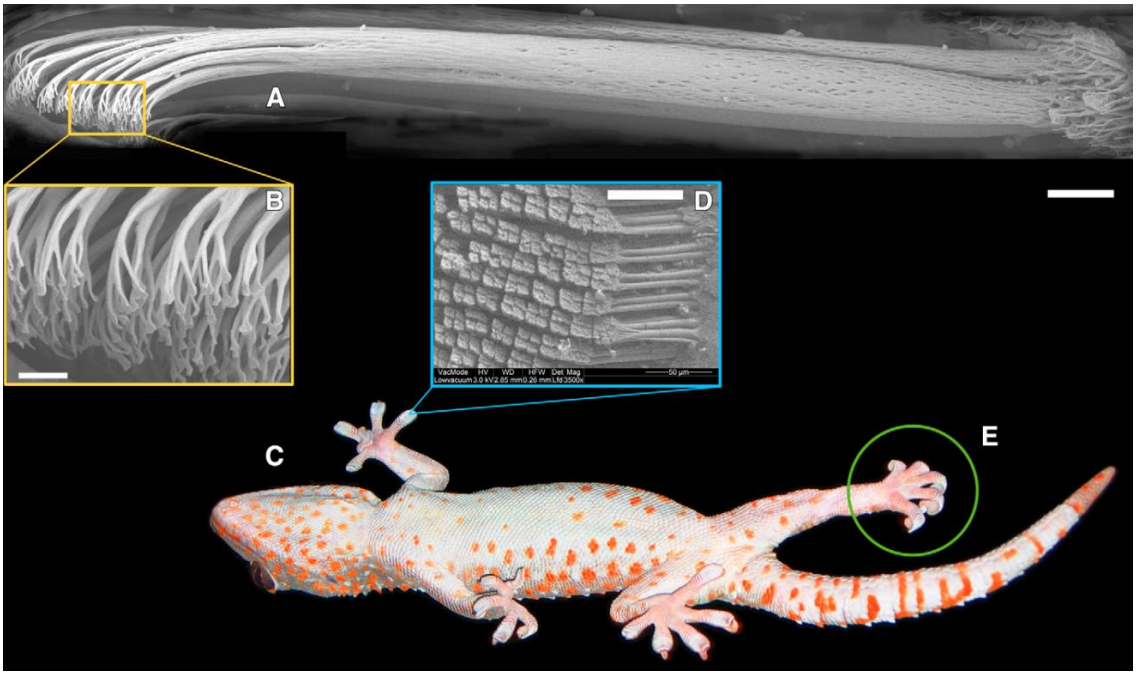

Figure 1.1.1. *Figure of the full adhesive system of the tokay gecko (C) showing the micron-scale features of a gecko's foot. Each toe on the foot (E) has four setae (A) which are further sub-divided into spatulae (B). The grid-like arrangement of the setae is shown in (D). Micrograph scale bars represent 50μm (D), 5μm (A), and 1μm (B).*[18]

The second factor that dry adhesives rely on is the degree of electrostatic interaction between them.[14,19] A molecule with a strong dipole moment will be able to induce a strong inverse dipole moment in the neighbouring molecules, and these opposite dipoles will create adhesion between the layers (Figure 1.1.2). The potential energy of this dipole-induced-dipole interaction (V) depends on the polarizability volume of molecule 1 (α; in this case the surface), the strength of the permanent dipole of molecule 2 (μ; in this case the dipole of the adhesive layer), and the distance between them (r), as shown in Equation 1.1.1. The direction of the induced dipole follows the direction of the permanent dipole, and so the net interaction between them does not average to zero.[20]

$$V = -\frac{\alpha\mu^2}{4\pi\varepsilon_o r^6} \qquad \text{(Equation 1.1.1)}$$

Essentially, when two materials are in contact with each other, the dipole-induced-dipole interactions allows them to stick together.

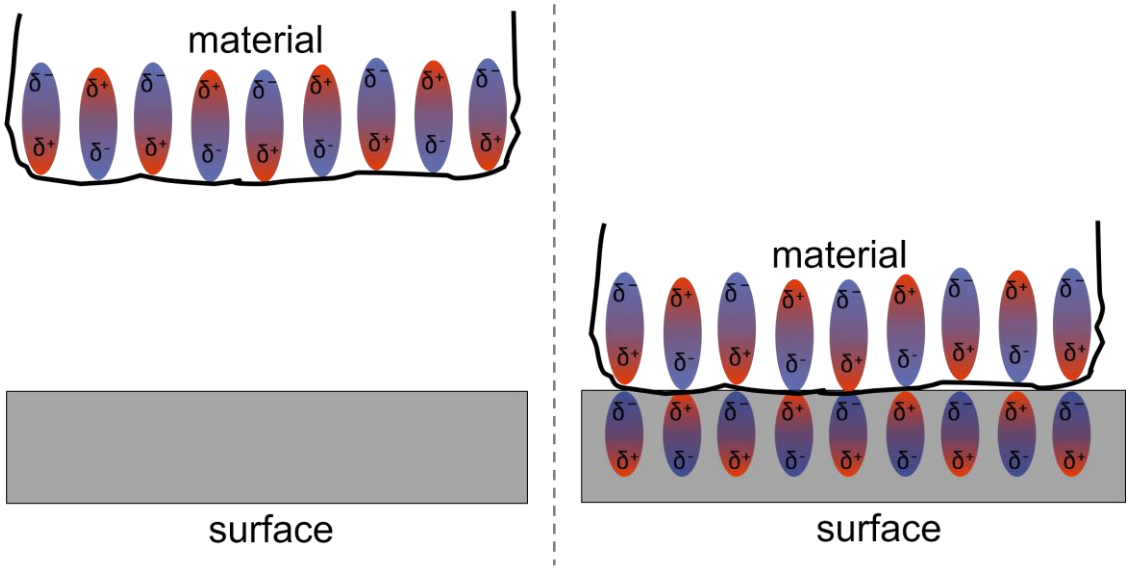

Figure 1.1.2. ***(A)*** *Shows a material with a series of dipoles at the surface, some distance from a surface.* ***(B)*** *When the material comes into contact with the surface, the dipole of the molecules in the material induces a dipole on the surface molecules. The net effect is adhesion of the material to the surface by electrostatic interactions.*

While the surface compliance is often manipulated by engineers and other materials scientists to increase adhesion, the van der Waals forces are manipulated by microbiologists and biochemists to ensure (or prevent) adhesion of bacteria colonies to solid surfaces.[21–24] Some bacterium exhibit a charge either naturally or at a certain pH range, and the level of electrostatic interaction between the bacteria and the surface allow them to grow even on traditionally non-stick environments, such as Teflon.[24] More recently, these observations have informed the development of several materials that make use only of these electrostatic interactions to increase their adhesion.[25,26]

Therefore, the best way to increase the effectiveness of a dry adhesive is to increase the surface compliance (through micro-structuring of the material) and the electrostatic interactions (through a permanent dipole or ionization) of the material. Several studies have addressed the issue of surface compliance,[10,11,15,27] and such work is outside the scope of this thesis. Of particular interest for this project is the alteration of the dipole within the material, specifically one that can be incorporated into a polymer matrix.

1.2. Controlling Materials with Light

While several types of stimuli can affect change upon a chemical system, none are quite as elegant as light. The advantages of using light to influence the state of a material are numerous; it can be focused with very high spatial resolution, there are no chemical contaminants, and the wavelength range can be adjusted to be extremely narrow or extremely broad as needed. Light can also be used as an energy source to enact reversible transformations in specially designed molecules, and these molecules are said to be photochromic.

Photochromic systems are best known for their ability to change colour when irradiated with light. These colour changes occur as a direct result of a configurational change of the specific molecule and often these structural changes result in other significant changes to the behaviour of the molecule. Selective singlet oxygen generation[28] and tunable metal bonding[29,30] using photochromic materials have been explored. Some photoswitches, such as azobenzenes, show a significant change in volume when they isomerise and this feature has been used to manipulate ferroelectricity[31] and enzyme inhibition[32].

Of direct interest in this project is the formation of zwitterionic species upon irradiation, and this occurs in the spirooxazines and spiropyrans, as well as the new class of donor-acceptor Stenhouse adduct (DASA) photochromic molecules. Zwitterions—molecules that contain both a positively and negatively charged group—have been used to affect adhesion,[33,34] and more recently work within the Branda group at Simon Fraser University has made use of a zwitterionic spiropyran to alter the adhesive properties of polydimethylsiloxane (PDMS)[27].

The following sections describe the concept of photochromism and introduce some common synthetically derived organic photochromic molecules, before moving on to discussion of the DASAs, which is the photoswitch of interest for this project. The project is further explored in Chapter 2.

1.2.1. Photochromism

The first recorded occurrence of photochromism was reported in 1867, when Fritzsche observed that tetracene loses its bright orange colouration in sunlight, and the

colour is then regenerated in the dark.[35] The word photochromism is derived from the Greek words phos (light) and chroma (colour), and describes a light-induced reversible transformation of a chemical species between two or more isomers having distinct absorption spectra.[36] In lay terms, a molecule is said to be photochromic if it exhibits a reversible colour change upon exposure to light. This interconversion is demonstrated in Figure 1.2.1. The interconversion of these materials between distinct and stable isomeric states has given rise to the term "photoswitch". The reverse process (B→A) can be either thermally or photochemically driven. This gives rise to the two main classifications of organic photochromic molecules: P-type (photochemically reversible) and T-type (thermally reversible).

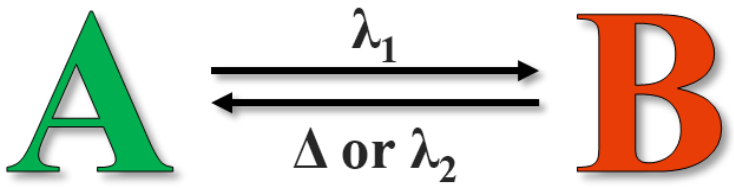

Figure 1.2.1. *Simplified illustration of a photochromic reaction. Isomer 'A' absorbs light at wavelength λ_1, and is converted to isomer 'B'. The reverse process is driven thermally (Δ) or by application of a second wavelength of light λ_2.*

P-type photoswitches are of interest due to their inability to convert between forms without external optical stimulus. These compounds are converted from one form to another with a specific wavelength of light, and remain in this state until irradiated with another wavelength. The two most widely studied P-type photoswitches are the diarylethenes and fulgide types (representative structures are shown in Scheme 1.2.1). Both structures contain a 1,3,5-hexatriene moiety within their structures, which results in ring-closure when exposed to UV light. The high energy barrier (on the order of 10-50 kJ/mol)[37] between the two isomers prevents the spontaneous reversion to the ring-open isomer in the dark, which can only be attained by absorption of lower energy (usually visible) light. An important sub-class of diarylethenes, the 1,2-dithienylethenes (DTEs), are of practical significance as they undergo some of the most efficient photoreactions and are often resistant to photo-degradation.[37,38]

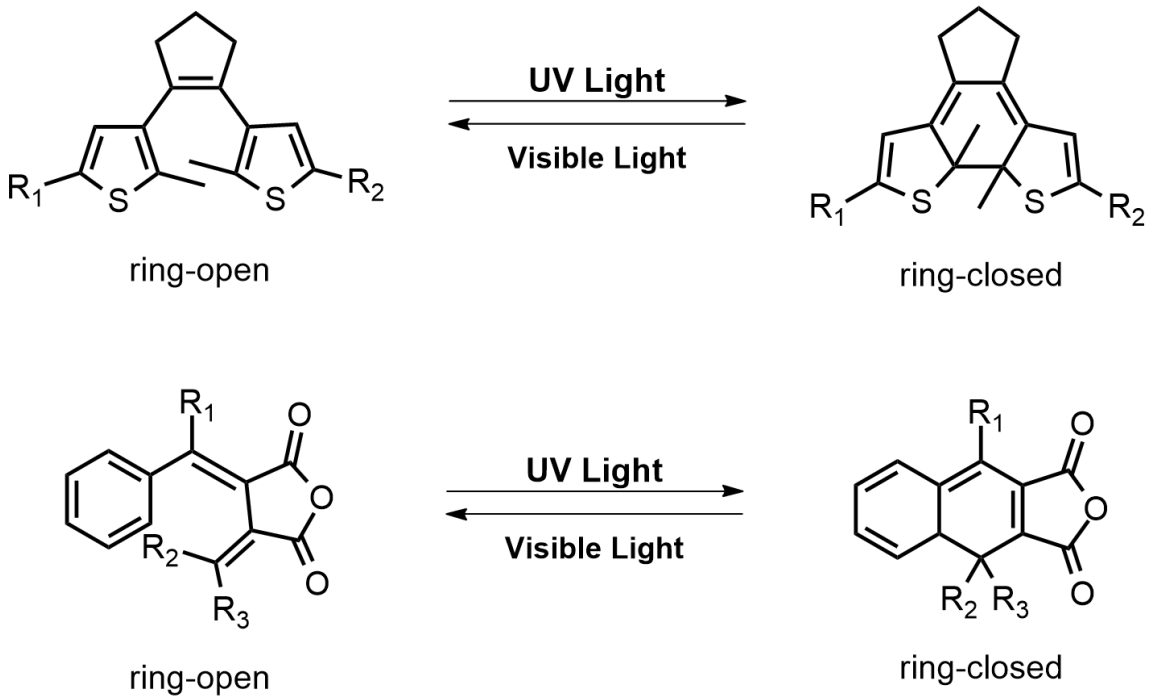

Scheme 1.2.1. *Representative examples of some common P-type photoswitches; (top) diarylethene and (bottom) fulgide.*

In contrast to the P-type photoswitches, T-type photoswitches will convert back to their original state, through a thermal back-reaction, when they are no longer exposed to the initial light source. Some of these T-type photoswitches can also be forced to revert more rapidly through application of a secondary light source. The most well-known use for these photoswitches are in dyes and eyeglass lenses.[39] Upon exposure to sunlight these materials switch to their coloured form, and in the absence of light they revert back to their colourless forms. Spiropyrans and spirooxazines are some of the best studied classes of these T-type photoswitches, and much like with the diarylethenes and fulgides described above, the photochromic nature of these spiro molecules is the result of an electrocyclization reaction.[36,38,39]

Arguably even more popular than the spiro-photoswitches are the azobenzenes, which display isomerism about the double bond. The more thermodynamically stable *(E)* isomer is converted into the *(Z)* isomer upon irradiation. The *(E)* isomer can then be thermally recovered.[38] Representative structures of these two classes of photoswitch are shown in Scheme 1.2.2.

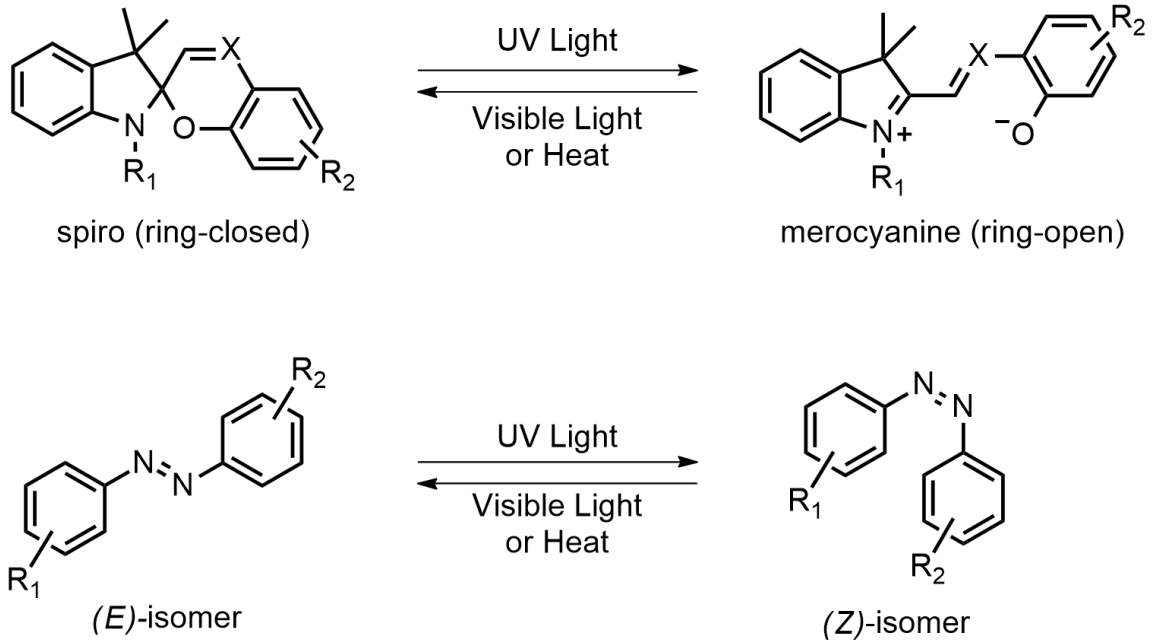

Scheme 1.2.2. *Representative examples of some common T-type photoswitches; (top) spirooxazine (X=N), spiropyran (X=CH), and (bottom) azobenzene.*

1.2.2. Donor-Acceptor Stenhouse Adducts (DASAs)

An exciting class of T-type photoswitch, donor-acceptor Stenhouse adducts (DASAs), have recently been reported by Read de Alaniz and coworkers.[40] What follows is a brief description of their history, structure, photochemical behaviour, and how light can be used to influence their electronic and physical properties.

These DASA photoswitches are the product of over a century of observations, starting with those of Stenhouse in 1870. Stenhouse obtained a series of vibrantly coloured cyanine dyes when ring-opening a 2-furaldehyde in the presence of two equivalents of amine and one equivalent of protic acid.[41] These compounds were not probed any further until the 1980s, when Honda reported the photobleaching of these 'Stenhouse salts', and their dependence on the incorporated alcohol for photobleaching.[42] Later, in 2000, Šafář reported a preliminary study on the rearrangement of a Meldrum's acid derivative.[43] This system made further use of the electron withdrawing nature of the cyclic dicarbonyl in place of the imine/iminium in the Stenhouse salts. Furthermore, reaction of the Meldrum's acid furan derivative with one equivalent of piperidine resulted in two molecules that were unable to be separated: the Stenhouse-type adduct and the corresponding cyclopentenone. However, the photochemistry of these systems was never

examined. Building on these results, Read de Alaniz and coworkers reported the first case of the negative T-type photoswitches, termed as donor-acceptor Stenhouse adducts or DASAs, in 2014[40,44].

Structurally, these photoswitches are very interesting, as they are among a select group of negative photoswitches, which means that the thermally stable form is coloured, and the photoinduced isomerised form is colourless. The core structure of the DASA class of photoresponsive molecules is made up of a donor amine and an acceptor dicarbonyl ring motif (Figure 1.2.2.). Most often a Meldrum's acid or barbituric acid are used here, but other acceptors have been used, such as 1,3-indanedione.[44] The molecule contains a hexatriene with a pendant alcohol that is required for cyclisation of the molecule.[42] Both the donor and acceptor portions of the molecule are highly amenable to synthetic modifications, and alteration to either part of the molecule allows tunability of the optical and chemical behaviour of the photoisomer.[45–47] Being able to alter both portions of the molecule opens a huge potential library for these photochromic compounds in the future.

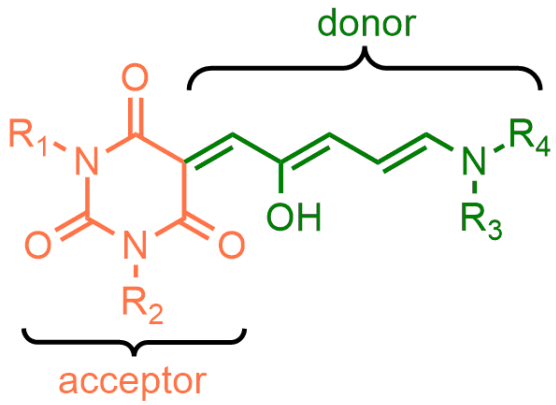

Figure 1.2.2. *Generic DASA molecule showing the acceptor dicarbonyl (in orange) and the donor amine (in green). Positions R_1-R_4 show potential areas for synthetic modification.*

DASAs show T-type photochromism between the coloured, spatially extended π-conjugated form and a colourless, compact zwitterionic form. Thus, these molecules stand in stark contrast to the spiropyrans that start from the compact, colourless, neutral spiro form and open into the conjugated, coloured, charged merocyanine form. The isomerisation not only affects the extension of the molecule, but also the hydrophobicity. The open form of the DASA molecule is hydrophobic, while the closed form is hydrophilic.[48,47]

The triene (open) isomer of the DASA can absorb light of a specific wavelength, typically visible light, and undergo an intramolecular cyclization to produce the cyclopentenone (closed) structure. The isomerization reaction is accompanied by a change in the molecule's absorption spectrum and a visible colour-change can often be detected as the open isomer has an extended π-conjugated system which is completely removed in the closed system. Reversion of the cyclized form to the open conjugated form occurs in the dark, though this is known to be solvent-dependent. It is now known that first generation DASAs (such as those outlined in this research) do not switch in the solid state or in solid matrices.[46] This research was conducted concurrent to the research outlined in this thesis, and the results are consistent with what was found here. Further implications of these findings are discussed in Section 2.9.

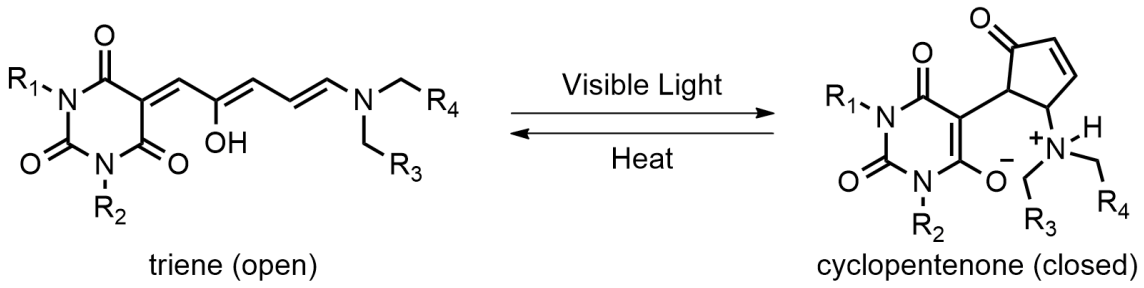

Scheme 1.2.3. *Generic DASA molecule showing the triene (open) coloured form and the cyclopentenone (closed) colourless form.*

DASAs are relatively new photoswitches, and as such mechanistic and energetic studies are ongoing. It has been calculated theoretically that the DASA isomers are nearly isoenergetic, with a difference of 8-20 kJ/mol.[48] In 2016, Feringa et al[49] proposed the mechanism as a photoinduced alkene *E/Z* isomerism followed by a thermal conrotatory 4π-electrocyclisation and proton transfer to the colourless form, shown in Scheme 1.2.4.

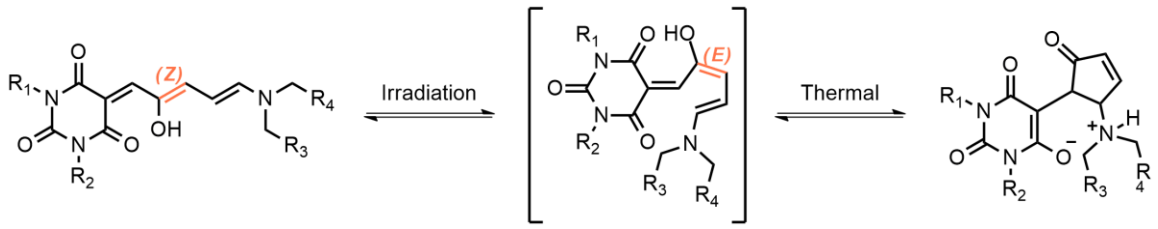

Scheme 1.2.4. *Proposed photoswitching mechanism of the DASA photoswitch. Irradiation induces the E/Z isomerism about the highlighted double bond, and a thermal cyclisation yields the cyclopentenone.*[49]

Chapter 2. Controlling Adhesion with Light

2.1. Previous Work and Project Design

Preliminary research by P. Tannouri in the Branda group involved doping a microstructured PDMS substrate with spiropyran molecules. In a proof of concept study, the spiropyran was found to selectively alter the adhesive properties of the material dependant on whether it was in the open (merocyanine) or closed (spiro) form.[27] However, this system had some potential issues, and several improvements were identified for further development.

2.1.1. Photoswitch

There is a potential drawback when using spiropyrans; they can form the quinoid open form in addition to the merocyanine upon exposure to light (Scheme 2.1.1), limiting the availability of the zwitterionic form. Stabilisation of either the merocyanine or quinoid form is known to be solvent dependant,[39,50] and it is therefore likely that within the hydrophobic PDMS matrix the quinoid form will dominate.

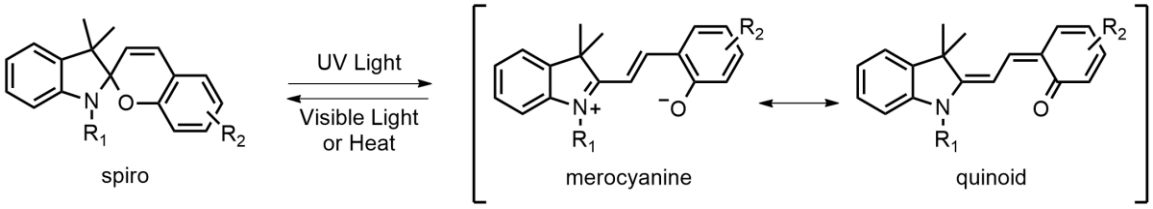

Scheme 2.1.1. *Spiropyran showing spiro (closed) form as well as the open merocyanine (zwitterionic) and quinoid (neutral) forms.*

Though previous work in the Branda group focused on the use of spiropyrans as the photoresponsive molecule of choice, the decision to move forward with the DASA molecule is based on their status as completely zwitterionic in their closed form. As seen in Chapter 1.2.2, the donor-acceptor Stenhouse adducts (DASAs) switch completely to the zwitterionic form, and so the overall change in surface charge from open to closed forms should be much greater than that of the spiropyrans. The DASA molecules have also been incorporated into several materials since their initial development such as polymers[40,51,52] and in multi-photoswitch systems.[53] They are currently the only known photoswitch that exists in a completely zwitterionic form when switched, which has

important implications for modulating their electrostatic interactions. Despite some performance limitations, such as thermal back reactions[46] and limited solid state switching[47,51], these DASAs are promising photoswitches to alter the adhesive properties of the polymer.

Though the DASA class of molecules are highly amenable to synthetic modification the DASA molecule for this project is kept relatively simple. In three locations, we make use of ethyl groups (Figure 2.1.1). In the final position we have attached the oxanorbornene adduct to facilitate polymerisation, which is further discussed in Section 2.1.2.

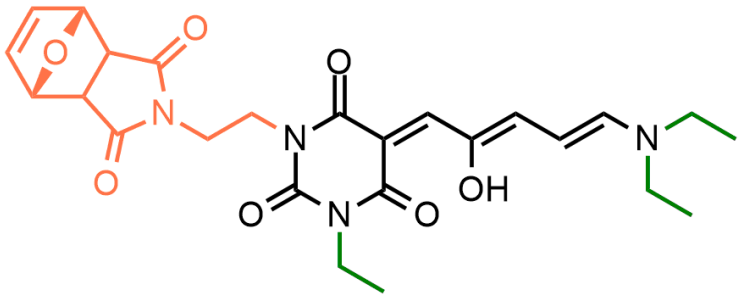

Figure 2.1.1. *The DASA target for this project. Ethyl groups (highlighted in green) are chosen for simplicity, and can be seen attached to all but one of the modifiable nitrogen sites. The oxanorbornene adduct (highlighted in orange) is the exception, and this is the synthetic handle through which the polymerisation will occur.*

2.1.2. Doping

Doping is not a long-term solution for adhesion in PDMS films. This is because the PDMS matrix inherently contains several small channels, thus creating an environment in which these small molecules can "flow" around the polymer chains.[54–56] This can cause either ejection of the dopant from the substrate over time or pooling of the small molecules, reducing the overall effectiveness in altering the bulk properties of the polymer. PDMS is a hydrophobic polymer that is easily able to take on other hydrophobic molecules.[56–59] This can be problematic when doping with zwitterionic switches as these molecules exist as the hydrophobic and hydrophilic isomers, causing rejection of the dopant over time. Polymer doping is also limited, as most polymers will only accept small amounts of dopant.[55,58]

To avoid the issues with doping, the photoswitches need to be covalently bound to the polymer backbone. This can be done by bonding the photoswitch directly to the PDMS substrate, or by creating a photoswitchable polymer that will not be ejected from the substrate of interest. For this project, and owing to the institutional procedures available within the Branda Group, it was decided to move forward with the synthesis of a photoswitchable polymer material. We can address the issue of small molecules in a polymer matrix by creating a photoswitchable polymer made up almost entirely of photoswitches, thus circumventing the issue of doping percent as well as separation and ejection of the photoswitch from a PDMS matrix.

Connecting an oxanorbornene to the DASA allows for direct polymerisation of the monomer with itself through a ring-opening metathesis polymerisation (ROMP),[60,61] and the dicarboximide allows a convenient synthetic handle with which to attach this pendant to the DASA photoswitch.

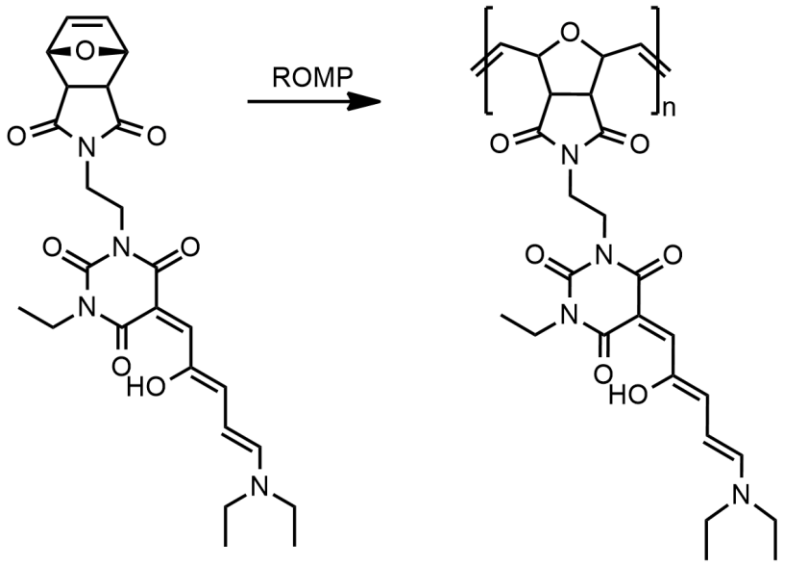

Scheme 2.1.2. *Polymerization of the target DASA molecule. 7-oxabicyclo[2.2.1]hept-5-ene-2,3-dicarboximide is the synthetic handle attached to the DASA to facilitate the ring opening metathesis polymerisation (ROMP).*

ROMP was chosen because it offers stoichiometric yields (using appropriate initiator-to-monomer ratios) with low polydispersity, the polymerisation is performed under mild conditions, and it is highly tolerant of multiple functional groups. The Grubbs catalyst is selective towards the constrained ring system, which makes it relatively straightforward to exploit specific functional groups.

This design allows us to create a polymer that potentially has more varied usage than simply being doped into PDMS, as it could potentially be used alone or further modified for copolymerisation or block polymerisation with another monomer.

In order to ensure potential differences in the measured adhesion and electrostatic differences come from the photoswitch and not from the polymer backbone a control compound was synthesised and polymerised. N-(2-dimethylamino)ethyl)-7-oxabicyclo-[2.2.1]hept-5-ene-2,3-dicarboximide (Scheme 2.1.3) was synthesised and polymerised to act as a control for experimental measurements. This compound was also used to determine the activity of the Grubbs Catalyst and to test the general polymerisation procedure.

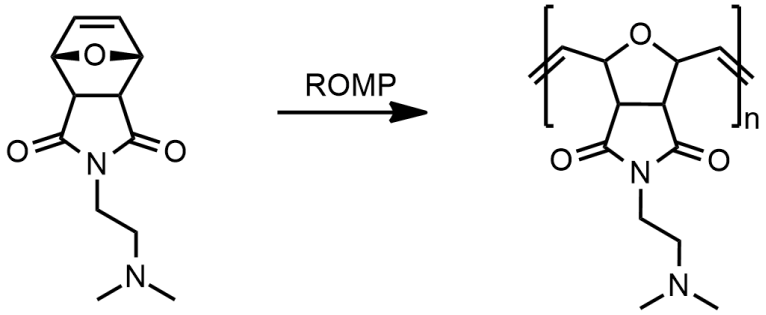

Scheme 2.1.3. *ROMP polymerization of the control molecule. This control polymer is used as a control for the experimental results from the target DASA because the structure of this molecule is representative of the target polymer backbone.*

2.2. Project Overview

First, the reversible light-induced changes of the original (unpolymerised) material in the solution state were examined. This material was then polymerised. However, this "pure photoswitch" polymer was insoluble in all common laboratory solvents, which led to considerable problems in characterising it. The control polymer, however, was incredibly soluble in almost all common laboratory solvents and at long chain lengths (in excess of 80 000 Da). Therefore, it was decided to copolymerize the control compound with the DASA photoswitch. This control was an ideal compound to form a random copolymer with the DASA as both units should be equally reactive toward the Grubbs catalyst, because they contain the same constrained ring target. Three different ratios of switch to control were synthesised (1:1, 1:2, and 1:4), and in all cases this copolymerisation had the desired

effect of increasing the solubility of the polymers. The representative structures for these polymers is shown in Figure 2.2.1.

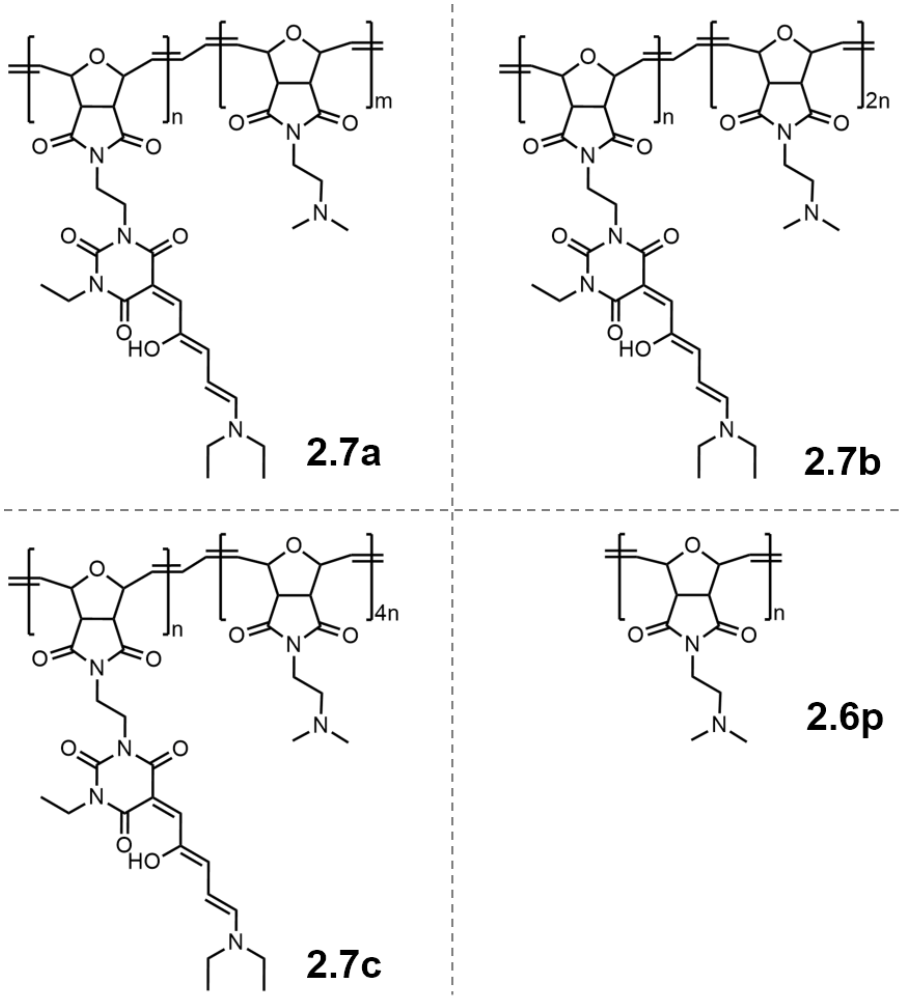

Figure 2.2.1. *Representative structure of the target polymers and their relative DASA photoswitch to control ratios.Polymer **2.7a** is 1:1 (switch:control), **2.7b** is 1:2 (switch:control), **2.7c** is 1:4 (switch:control), and **2.6p** is pure control monomer.*

Further synthetic detail is given in Sections 2.3-2.5 and Chapter 3.2, and all new compounds were characterised by ^{1}H and ^{13}C NMR, UV-Vis spectroscopy, and mass spectrometry as appropriate. The results were consistent with the structures shown in Schemes 2.3.1. – 2.3.3. The photo-controlled contact angle change of the polymers was measured by contact angle goniometry. Adhesion was also tested through a custom force-loaded stage.

2.3. Synthesis of DASA Precursor

All compounds described below were prepared in gram quantities and moderate yield. Further detail is in Chapter 3, and ^{1}H and ^{13}C NMR spectra are presented in Appendix A.

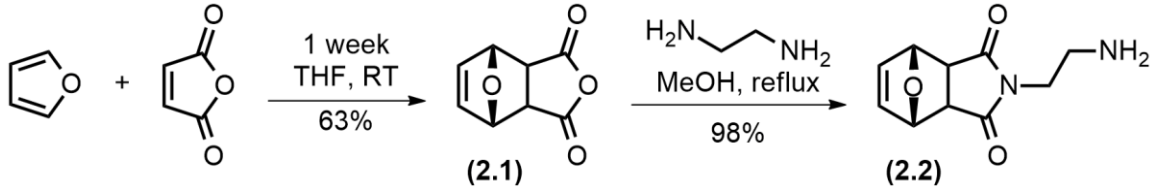

Scheme 2.3.1. *Synthesis of oxanorbornene **2.1** and the subsequent aminoethyl-oxanorbornene **2.2.***

The oxanorbornene pendant molecule, 7-oxabicyclo[2.2.1]hept-5-ene-2,3-dicarboxylic anhydride **2.1**, was prepared by Diels-Alder reaction of maleic anhydride with furan, as per literature procedure.[62] Though Diels-Alder reactions usually yield endo products, the endo isomer for this particular reaction forms reversibly and therefore the product is thermodynamically controlled resulting in the exo isomer.[60] The difference can be seen by 1H NMR, using the coupling constants of the bridgehead protons. The structure of **2.1** is rigid, resulting in distinct dihedral angles of either 34° (endo) or 88° (exo). Using the Karplus equation the coupling constants are calculated to be 5.4 Hz (endo) and 0.04 Hz (exo). This results in all signals for the exo isomer appearing as singlets, and this is what is observed. The structure was sufficiently pure (>95% by ^{1}H NMR) for the next synthetic step. This oxanorbornene was then condensed with ethylenediamine in a modified literature procedure[63] to yield N-(2-aminoethyl)-7-oxabicyclo[2.2.1]hept-5-ene-2,3-dicarboximide **2.2**. Purification was carried out by trituration with diethyl ether. In the ^{1}H NMR the presence of two triplet signals from the aminoethyl group confirms the success of this reaction. This primary amine is the synthetic handle that is used to synthesise the barbituric acid precursor to the final DASA.

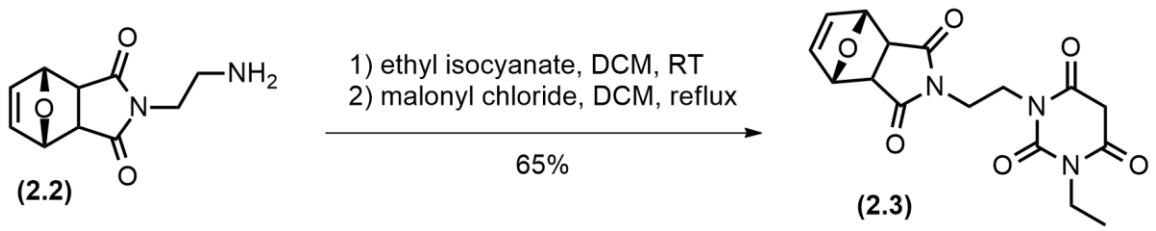

Scheme 2.3.2. *Synthesis of barbituric acid **2.3.***

The synthesis of DASA precursor **2.3**, 1-(7-oxabicyclo [2.2.1]hept-5-ene-2,3-dicarboximidoethyl)-3-ethylbarbituric acid, was accomplished in two steps, first with nucleophilic attack of **2.2** with ethyl isocyanate to form a urea adduct, and then a subsequent condensation with malonyl chloride.[44] The compound was purified by flash chromatography and ^{1}H NMR proton signals corresponding to ethyl amine as well as the barbituric acid segment confirm the formation of product **2.3**.

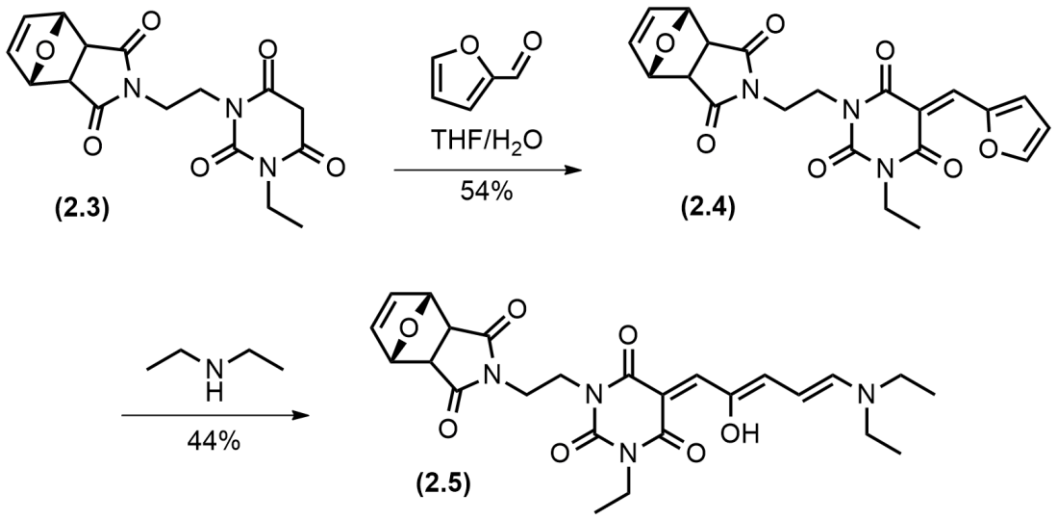

Scheme 2.3.3. *Synthesis of DASA precursor **2.5** from barbituric acid **2.3***

(*E*)-5-((2*Z*,4*E*)-5-(N,N-diethylamino)-2-hydroxypenta-2,4-dien-1-ylidene)3-ethyl-5-(furan-2-ylmethylene)-1-(7-oxabicyclo[2.2.1]hept-5-ene-2,3-dicarboximidoethyl)barbituric acid **2.5** was synthesised in a two-step, one-pot synthesis wherein condensation of furfural with **2.3** yields the isolable intermediate 3-ethyl-5-(furan-2-ylmethylene)-1-(7-oxabicyclo[2.2.1]hept-5-ene-2,3-dicarboximido-ethyl)barbituric acid, **2.4**. Diethylamine is then used to induce ring opening of the furan group to give **2.5**. The DASA precursor was purified by column chromatography, its structure was confirmed by ^{1}H NMR, ^{13}C NMR, and COSY.

2.4. Control Precursor Synthesis

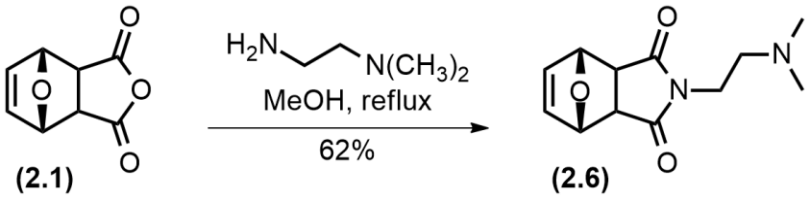

Scheme 2.4.1. *Synthesis of oxanorbornene **2.6***

N-(2-(Dimethylamino)ethyl)-7-oxabicyclo[2.2.1]hept-5-ene-2,3-dicarboximide **2.6** was synthesised analogously to **2.2**, but with N,N-dimethyl ethylenediamine as the nucleophile (Scheme 2.3.1). Compound **2.6** is used as the precursor to the control polymer.

2.5. General Synthesis of Polymers

In preliminary testing with **2.6**, the Grubbs Catalyst was found to be ~15% active using the following procedure, and the monomer to initiator ratios were chosen to yield polymers of approximately 100 units long.

Polymers **2.5p**, **2.6p** and **2.7a**-**c** were prepared under typical ROMP conditions by treating the appropriate precursor(s) with first generation Grubbs catalyst (bis(tricyclohexylphosphine)benzylineruthenium(IV) dichloride) to initiate the living polymerisation, and an excess of ethyl vinyl ether to terminate the polymerisation after stirring at room temperature in dichloromethane for two hours. The resulting polymers were then either evaporated to dryness (**2.7b**, **2.7c**), or precipitated directly from the crude mixture with cold diethyl ether (**2.5p**, **2.6p**, **2.7a**). All polymers were then washed with diethyl ether to remove impurities.

The polymer **2.5p** was insoluble in all common laboratory solvents and was tested in concentrations as low as 0.1 mg/mL. Solvents tested include (but are not limited to) xylene, chloroform, ethyl acetate, dichloromethane, diethyl ether, acetone, methanol, ethanol, n-butanol, n-hexanes, toluene, tetrahydrofuran, water, dimethylformamide, dimethyl sulfoxide, and dioxane. By comparison, polymer **2.6p** was found to be soluble in a large majority of these solvents at concentrations of 1 mg/mL. Polymers **2.7a**-**c** were

also tested for solubility at concentrations of 1 mg/mL. The solubility of these compounds as well as their respective precursors is summarised in Table 2.5.1.

Table 2.5.1. *Polymer Solubilty. All compounds tested at 1 mg/mL and 295 K.*

	2.5	**2.6**	**2.5p**	**2.6p[a]**	**2.7a**	**2.7b**	**2.7c**
xylene	s	s	i	s	sl	sl	sl
chloroform	vs	vs	i	vs	s	s	s
dichloromethane	vs	vs	i	vs	s	s	s
methanol	vs	vs	i	vs	s	s	s
diethyl ether	s	vs	i	sl	i	i	sl
water	s	s	i	s	i	i	sl
dimethylformamide	vs	s	i	s	s	s	s

i = insoluble; sl = slightly soluble, s = soluble; vs = very soluble

2.5.1. Polymer Characterisation

The polymers were characterised by ^{1}H NMR. Gel permeation chromatography (GPC) was used to determine the molecular weights of the polymers, and differential scanning calorimetry (DSC) was used to show their thermal properties. The details of characterisation follow and the results are summarised in Table 2.5.2.

Table 2.5.2. *Summary of polymer characterisation showing yield, composition, weight average molecular weight, number average molecular weight, polydispersity index, and glass transition temperature.*

Compound	**Yield**	**Switch/Control (Number of Units)[a]**	$\bar{M}_w$ **(×10^3 Da)**	$\bar{M}_n$ **(×10^3 Da)**	**PDI** ($\bar{M}_w/\bar{M}_n$)	T_g **(°C)**
2.6p	24 %	0 / 91 (91 Total)	21.5	20.1	1.07	135
2.7a	78 %	56 / 56 (112 Total)	41.0	35.0	1.17	125
2.7b	92 %	39 / 78 (117 total)	38.0	31.9	1.19	ND[b]
2.7c	82 %	21 / 86 (107 total)	31.0	27.2	1.14	110

a. Representative average for the polymers in question; calculations are in Appendix C
b. the glass transition for this polymer was not detected

2.5.1.1. Gel Permeation Chromatography

Gel Permeation Chromatography data was collected, analysed, and provided by Jonathan Ward (Holdcroft Group – SFU).

The relative molecular weights of the polymers were determined by GPC, which is a type of size exclusion chromatography used for separating polymers by size. The separation takes place through a column packed with beads of a porous gel. A dilute solution of the polymer is introduced into the column and as the molecules flow past the beads, they can diffuse into the pores to an extent depending on their size. Large molecules can only partially enter these pores (or are completely excluded) while smaller molecules make their way deeper within the beads. Thus, the larger molecules spend less time within the gel and are eluted first. GPC columns are typically calibrated using polystyrene standards of a known molecular weight, and this provides a direct relationship between the molecular weight and the elution time.[64,65]

Polymers are long chains of molecules, and these chains have a range of lengths. Typically, the measured molecular weights are given as an average, rather than a definitive number. There are two ways of considering the molecular weight average of polymers; either as a weighted average (the average weight of all polymer chains) or as a number average (the average number of polymers at a specific chain length). Mathematically, the number average molecular weight (Equation 2.4.1) and the weight average molecular weight (Equation 2.4.2), where M_i is the size and N_i is the number of molecules of that size) are shown below.

$$\bar{M}_n = \frac{\sum N_i M_i}{\sum N_i} \qquad \text{(Equation 2.5.1)}$$

$$\bar{M}_w = \frac{\sum N_i M_i^2}{\sum N_i M_i} \qquad \text{(Equation 2.5.2)}$$

From the GPC analysis both the number average molecular weight ($\bar{M}_n$) and the weight average molecular weight ($\bar{M}_w$) of a polymer sample were provided. The ratio of ($\bar{M}_w$)/($\bar{M}_n$) is the polydispersity index, and is a useful measure of the spread of the molecular distribution curve.

The result of the GPC analysis of polymers **2.7a**-**c** and **2.6p** are shown in Table 2.5.2 with the number average molecular weights corresponding to polymers with a length of roughly 100 units (Appendix C), which is consistent with the amount of catalyst used and its previously determined activity. The PDIs for these polymers are close to 1.0, indicating that these polymers have low polydispersity. This is expected as the Grubbs catalyst was used specifically to generate polymers of low PDI.

^{1}H NMR spectroscopy was not used to determine the composition of these mixtures as the signal intensities were disproportionate and therefore the ratio of these signals yielded inconclusive results. Therefore, the amount of switch and control units that make up the composition of the polymer was determined algebraically. To determine the composition either one of two assumptions can be made: either the chain length is restricted to the same as the full control polymer (determined to be 91 units) or by assuming the reactivity of the control and the switch precursors is the same and that they are included in the polymer in the same ratio as they are added to the reaction mixture. This second assumption was found to yield calculated results that are consistent with the results from the UV-vis spectroscopy (further discussed in Section 2.7), which found that the amount of switch component in each polymer was consistent with the synthetic switch to control ratios. The GPC chromatograms and composition calculations are contained in Appendices B and C respectively.

2.5.1.2. Differential Scanning Calorimetry

Differential scanning calorimetry (DSC) gives information about the exothermic and endothermic processes that occur as a polymer sample is heated or cooled over a specific temperature range. A computer controls and measures the temperature of the sample (in a small metal pan) and a reference (an empty pan). The temperature of each pan is increased at a set rate (usually 10°C/min), and the amount of power (heat flux) required to heat each pan at the same rate is recorded. Because one pan contains the polymer sample while the other does not, the pans will require a different amount of power to heat them at the same rate, and a signal proportional to the power difference is plotted. The area under the curve is a direct measure of the heat of transition.[65]

Of interest is the glass transition temperature (T_g), which represents the boundary between the amorphous (glass) phase of a polymer and the more viscous rubber-like region. In the glass phase the polymer chains have minimal free volume, but as the sample

is heated through the glass transition temperature, the sample is transformed into a more disordered rubber phase. The rubber phase has a larger free volume and allows the polymer chains to rotate more freely. This transition is visible as a step in the DSC thermogram. Melting and crystallisation can also be determined using DSC; melting appears as an endothermic peak while crystallisation appears as an exothermic well.[65]

Polymers **2.7a**-**c** are random copolymers, and therefore the glass transitions are more difficult to observe as they occur over an extended temperature range due to the long-range disorder.[65] In order to get a more accurate value, the first derivative was taken to confirm the points of inflection corresponding to the T_g. Polymer **2.7a** has a small step at 115°C, corresponding to the glass transition temperature. The T_g for **2.7b** is undiscernible from the thermogram. Polymer **2.7c**, at a ratio of 1:4 (switch:control) behaves the most like **2.6p** (T_g of 135°C) as the amount of switch is low enough to act as an impurity in the control polymer, disrupting the overall order of the polymer and slightly reducing the glass transition temperature to 125°C.

The glass transition temperature is important for these polymers because the DASA units change shape when they photo-isomerise, and a polymer above the glass transition would be more fluid and thus more adaptable to this structural change. The glass transition measurements for these polymers indicates that there is a minimal amount of free volume in these compounds at room temperature, and consequently the motion required to accommodate the isomerisation reactions are partially restricted by the matrix.[65]

A representative thermogram for polymer 2.6p is shown in Figure 2.5.1. The DSC heating rate was 10°C/min and the T_g values are reported for the second heating cycle and summarised in Table 2.5.2. None of these polymer samples showed melting or crystallisation in the range of 0-300°C. All thermograms are contained in Appendix D.

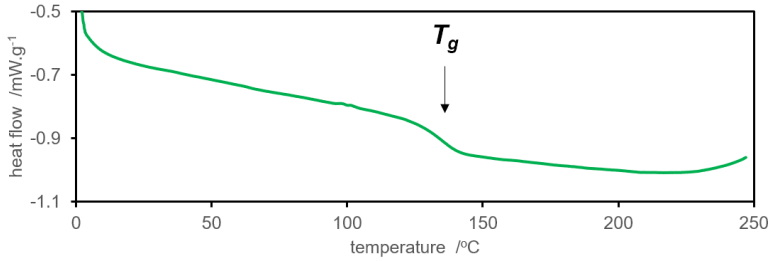

Figure 2.5.1. *DSC Theromgram for polymer* ***2.6p****, showing the* T_g *at 135°C.*

2.6. Photochromism

The practical efficiency of photochromic molecules is often evaluated based on the photostationary state (PSS). This is a steady state where the photoconversion of the ring-open isomer and ring-closed isomer is in equilibrium, and subsequent irradiation no longer causes a change in the UV-vis absorption spectrum of the compound.[66] The PSS of a molecule is specific to a set of parameters including, but not limited to, the type of irradiation (wavelength, power, intensity), temperature, concentration, and solvent. The PSS is usually expressed as a percentage to facilitate comparison to other compounds. The calculation of this value is given by Equation 2.5.1.

$$\mathrm{PSS} = \frac{\mathrm{n_{isomerised\ molecules}}}{\mathrm{n_{total\ molecules}}} \times 100\% \qquad \text{(Equation 2.6.1)}$$

The solution state UV-vis spectroscopy data was collected with an OceanOptics USB2000 spectrometer, and the light source was a 300 W halogen lamp with a <520 nm cut-off filter, operating 20 cm from the sample. The sample was irradiated concurrently to the measurements being taken, and was stirred to ensure that the solution was homogenous between the irradiation point (top of the cuvette) and the area where the measurements were being taken (bottom of the cuvette).

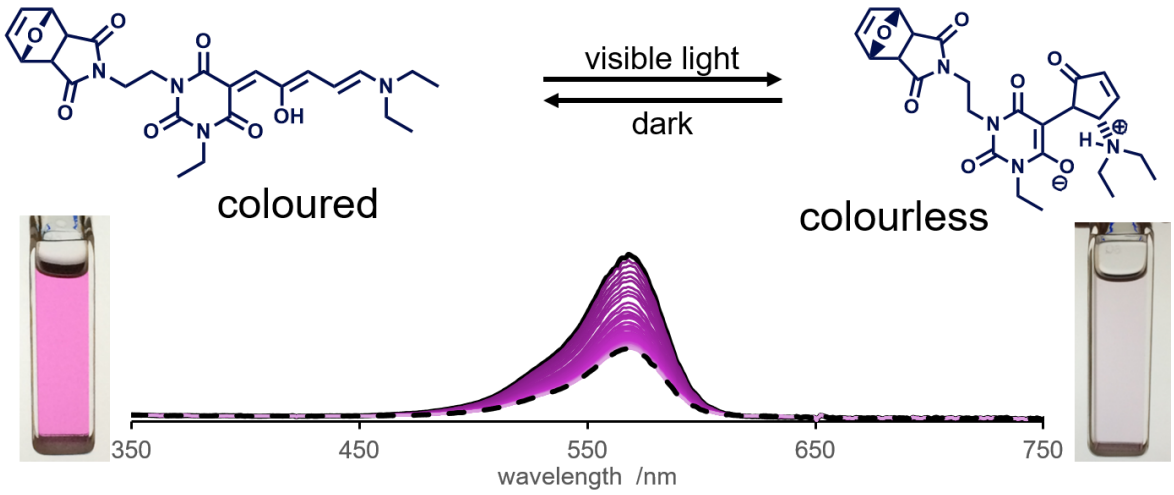

Figure 2.6.1. *Showing the structure, colour in solution (methanol), and UV-vis absorption spectra of the extended triene coloured form (left) and the closed cyclopentenone colourless form (right) of DASA* ***2.5****. The UV-vis spectrum obtained from a solution prepared as 2x10^{-5}M in o-xylene.*

The photostationary state (PSS) was determined by irradiating the sample continuously until no further change was observed in the spectrum. This was found by observing the kinetics at a single wavelength and determining the steady state of irradiation. A representative plot of the kinetics of irradiation (ring open to ring closed) for DASA **2.5** is shown in Figure 2.6.1. After 60 seconds the absorbance levels off, confirming that the photostationary state has been reached. Subsequent calculations on the thermal relaxation (ring closed to ring open) yield a rate constant of 0.042 s^{-1}, which corresponds to a half-life of approximately 15 s. Calculations and graphs are included in Appendix G.

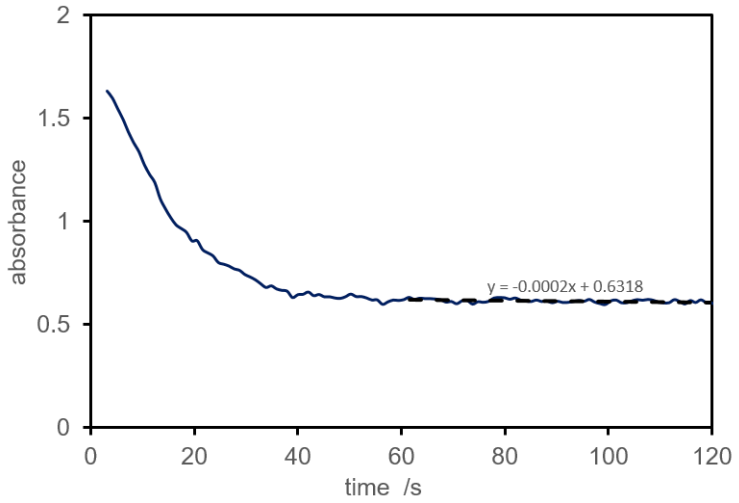

Figure 2.6.2. *Determination of the photostationary state of DASA **2.5**. The sample (2×10^{-5} M in o-xylene) was irradiated until no further change was observed. This trace follows the absorbance of the maximum absorption peak (at 567 nm) over time. At 60s the graph is seen to flatten out, and this is confirmed by the gradient for the trendline tending towards zero.*

The molar absorptivity (ε) values were calculated using the Beer-Lambert law on samples of the ring-open form and the ring-closed form at the PSS. For the PSS of DASA molecule **2.5**, the total number of molecules was calculated from the concentration of the solution before irradiation, and the corresponding ε value was approximated as being a result of all molecules in the open form. It is possible for this assumption to result in slightly lower percent conversion as it is likely that equilibrium in the dark is established at less than 100% open form. However, when the ^{1}H NMR spectrum of **2.5** is analysed there are no peaks corresponding to the closed isomer when the sample has not been irradiated. This indicates that there is at least >95% open form in xylene solutions that have not been irradiated. The number of converted molecules is then assessed from ε at the steady state and the Beer-Lambert Law gives the concentration of molecules that have not been

isomerised. From this, the number of isomerised molecules is then determined, and the PSS calculated.

This process was repeated for the polymers in solution, again assuming that dark measurements were the 100% open form for the baseline. Given that ε describes only the photoswitchable units, we expect these values to be the same for each of the polymers **2.7a-c** in solution, as these as they are prepared to have the same concentration of switch, when assuming the ratios determined algebraically (Section 2.5.1.1 and Appendix C) are correct. In solution, all systems are seen to have ε values that are very close to each other (12096-11625 $L \cdot mol^{-1} \cdot cm^{-1}$), which supports the algebraically determined values. These ε values were then used (as described above) to determine the PSS of the polymer solutions. This process is the same for the polymer thin films, however the concentration and absorbance fluctuate in direct relation to the amount of photoswitchable units in the polymer. This gives ε values for the polymer in the range of 5531-5542 $L \cdot mol^{-1} \cdot cm^{-1}$, again supporting the algebraically determined ratio of DASA to control units.

The results of the photoinduced isomerisation experiments for the polymer (**2.7a-c**) in thin film and solution (methanol, $2x10^{-5}$ M in the DASA component), and their PSS are summarised in Table 2.6.1.

Table.2.6.1. *Photoisomerisation summary of DASA 2.5 and copolymers* ***2.7a-c***

Compound	PSS (%)	λ_{max} (nm)	ε ($L \cdot mol^{-1} \cdot cm^{-1}$) triene open form
2.5 - xylene solution[a]	65	567	85867
2.7a - methanol solution[b]	70	545	12096
2.7a - thin film	55	554	5534
2.7b - methanol solution[b]	65	545	11936
2.7b - thin film	20	554	5531
2.7c - methanol solution[c]	65	545	11625
2.7c - thin film	5	554	5542

a. Concentration of solution is $1.9x10^{-5}$ M
b. Concentration of solution is $2.1x10^{-5}$ M in the DASA component
c. Concentration of solution is $1.8x10^{-5}$ M in the DASA component

2.6.1. Solution State Photoisomerisation Studies

The DASA switch **2.5** and the derived polymers **2.7** are solvatochromic, which means that the maximum wavelength of absorption shifts depending on the solvent. While these effects are often dependent on the polarity of the solvent, other solute-solvent interactions (such as induction, dipole-induced dipole, and dispersion forces) can also affect this.[39] Given the difference between the open (neutral) and closed (zwitterionic) forms the solvatochromic effects for these compounds are not strictly dependent on a the dielectric of the solvent, and it can be inferred from these structural changes that all of these interactions need to be considered when determining whether a particular solvent will result in a red or blue shift. Relative to DASA **2.5**, the polymer **2.7a** shows a slight hypsochromic shift of the absorption band. These values are detailed in Table 2.6.2.

Table 2.6.2. *Wavelength of maximum absorption of DASA **2.5** and polymer **2.7a**. Polymers **2.7b** and **2.7c** show the same behaviour as polymer **2.7a**.*

Compound	λ_{max} (nm) in xylene	λ_{max} (nm) in methanol	λ_{max} (nm) in chloroform
2.5	567	552	570
2.7a	560	545	565

The photoisomerisation of DASA photoswitch **2.5** was monitored by UV-vis absorption spectroscopy (Figure 2.6.3) in a xylene solution, as DASAs are able to ring-open and ring-close in xylene, while methanol stabilises the closed form and chloroform stabilises the open form.[40] Irradiation of a xylene solution containing **2.5** with a >520 nm light results in an immediate decrease in the intensity of the absorption band at 567 nm corresponding to the disappearance of the ring-open isomer. While literature indicates a concomitant increase of an absorption in the 250 nm region,[45] this is not observed because of the spectral cut-off window for o-xylene at 300 nm. The photostationary state was calculated to be 65% under these conditions, though this is likely to be very solvent dependant, and an even higher PSS could be expected in a solvent such as methanol.

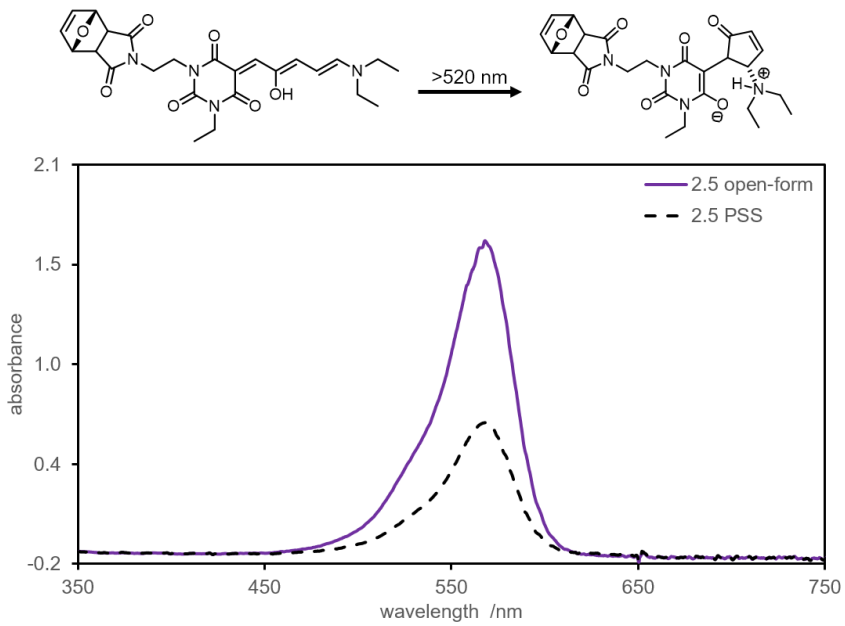

Figure 2.6.3. *UV-visible absorption spectrum of compound **2.5**, 2×10^{-5} M in o-xylene. Irradiation with >520 nm light yields the PSS at 60 s.*

Solutions of polymer **2.7b** in o-xylene that are irradiated form lightly coloured aggregates (Figure 2.6.4.) that do not re-dissolve upon standing. The formation of aggregates in xylene (a non-polar solvent) is indicative of a polarity shift in the polymer from the open (neutral) to the closed (zwitterionic) form.

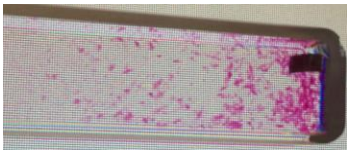

Figure 2.6.4. *Polymer **2.7b,** prepared in o-xylene, showing the pink aggregate after 1 hour of irradiation.*

The formation of these aggregates necessitated the use of a different solvent for the PSS measurements of the polymer in solution. Methanol was chosen as it is quite polar, and thus would ideally prevent the formation of aggregates with irradiation and it tends to permit higher photostationary states (which are known to be solvent-dependent)[38,39]. A series of solutions of polymers **2.7a**-**c** were prepared with a concentration of 2×10^{-5} M in the DASA component, and the absorption changes with irradiation are shown in Figure 2.6.5. The ring open DASA unit has an absorption band at 545 nm, which is blue shifted in comparison to the absorption band of **2.5**. With irradiation (>520 nm) this peak decreases quite significantly in intensity. This behaviour is nearly identical for all three polymers, which suggests that the ratio of control units in the

copolymer does not affect the photoswitching nature of these polymers in solution. This is supported by the observation that these polymers take approximately one hour to reach the PSS.

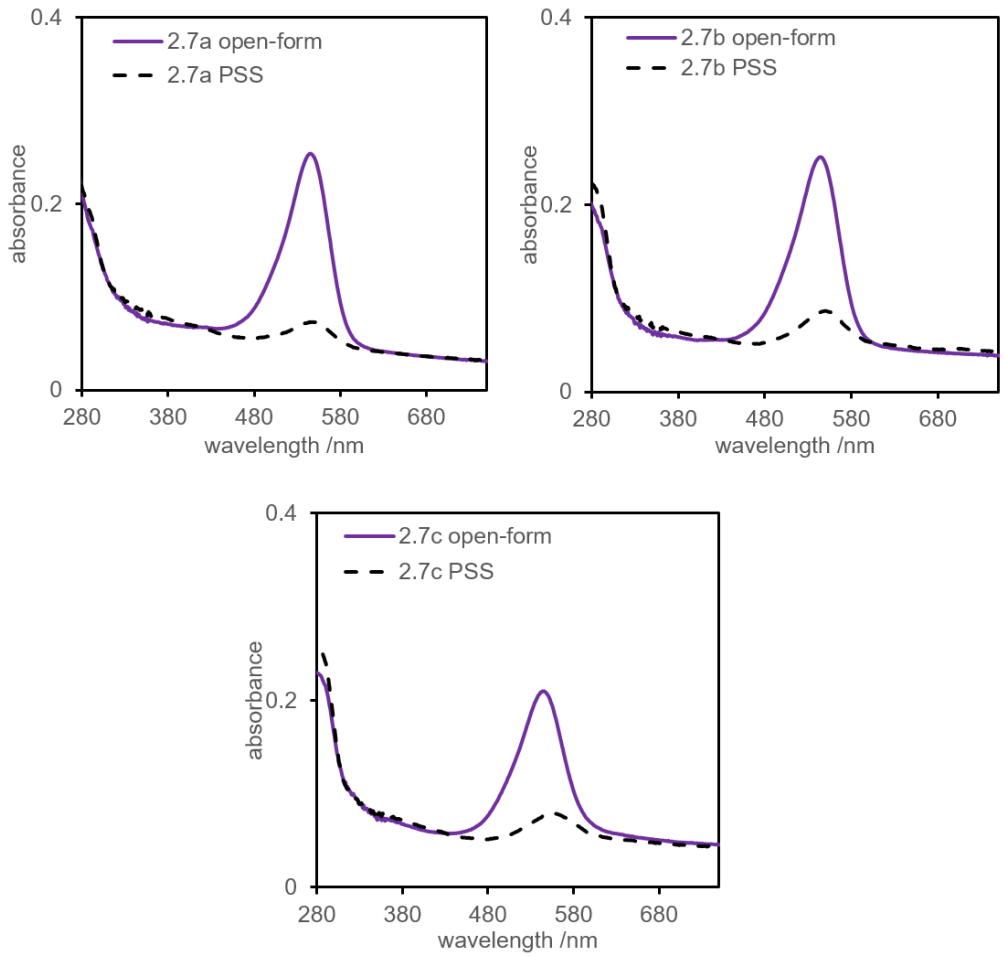

Figure 2.6.5. *UV-visible absorption spectra of polymer* ***2.7a-c****, 2×10^{-5} M in methanol. Irradiation with >520 nm light yields the PSS after one hour.*

2.6.1.1. Photochemical Cycling

Fatigue resistance is the ability of a photoswitch to be converted between the open and closed forms without forming side products or degrading. There are some molecules (such as DTEs) that can be cycled thousands of times without showing any significant degradation (less than 10%).[38] The DASA precursor **2.5** shows rapid thermal reversion, and so the fatigue resistance could be determined. As we do not have access to an automated cycling system, nine cycles were conducted manually by subsequent light on (75 s of broad-band light with a <520 nm cut-off filter) and light off (120 s) cycles. The monomer showed relatively high fatigue resistance as the absorbance of the ring open

form was reduced to only 95% of the original value after nine cycles. The polymer molecules showed no reversion to the open form either thermally or with multiple wavelengths of irradiation in either the thin film or solution state studies.

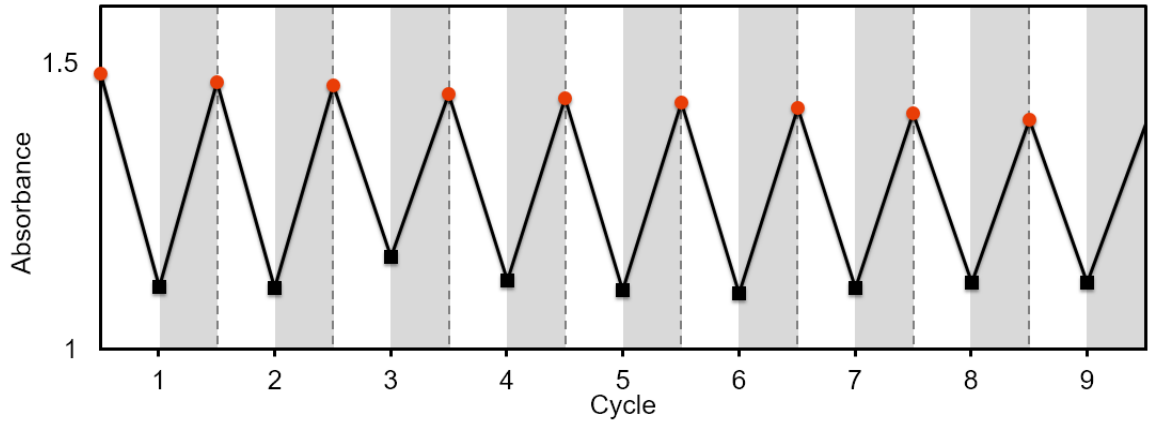

Figure 2.6.6. *Photochemical cycling of a 2x10^{-5}M solution of monomer **2.5** in xylene. The orange circle represents the start of the light on phase (>520 nm light, 75 s duration). The black square represents the light off (120 s duration).*

2.6.2. Determination of Open and Closed Structure of DASA 2.5

The thermal back-reaction of the DASA switch **2.5** occurs rapidly in solution, even when cooled to -70°C, and we do not have the equipment to simultaneously irradiate the sample and obtain the NMR spectra. However, using a polar solvent mixture does allow for detection of the closed cyclopentenone after irradiation. The light set-up was taken to the NMR room, and the sample irradiated and the spectrum taken. The auto-sampler was bypassed in an effort to minimise the time between irradiation and analysis. The presence of the zwitterionic form was confirmed by ^{1}H NMR in a polar solvent mixture (1:1 d_4-methanol and d_2-water). This mixture was used as water is best able to stabilise the closed zwitterionic form.[44] Methanol was mixed with water to reduce the photochemical degradation that was observed to occur when samples in water are irradiated. In the ^{1}H NMR spectra the signals of interest for the open triene form of the molecule were found at δ7.95, 7.12, 6.71, 6.32 ppm and are consistent with literature peaks for similar compounds.[46] After irradiation, the open form peaks were seen to decrease relative to the solvent peak, and the closed cyclopentenone form peaks at δ7.70, 6.61, 5.51, 3.75 ppm showed a relative increase in height (Figure 2.6.7). The peaks corresponding to the closed form, while slightly visible in this polar mixture, are not visible in spectra obtained in chlorinated solvents (which are known to stabilise the open form of this compound).[44]

These changes are consistent with the formation of the closed cyclopentenone ring. This transformation from open to closed zwitterion is further supported by the photoswitching nature of the monomer.

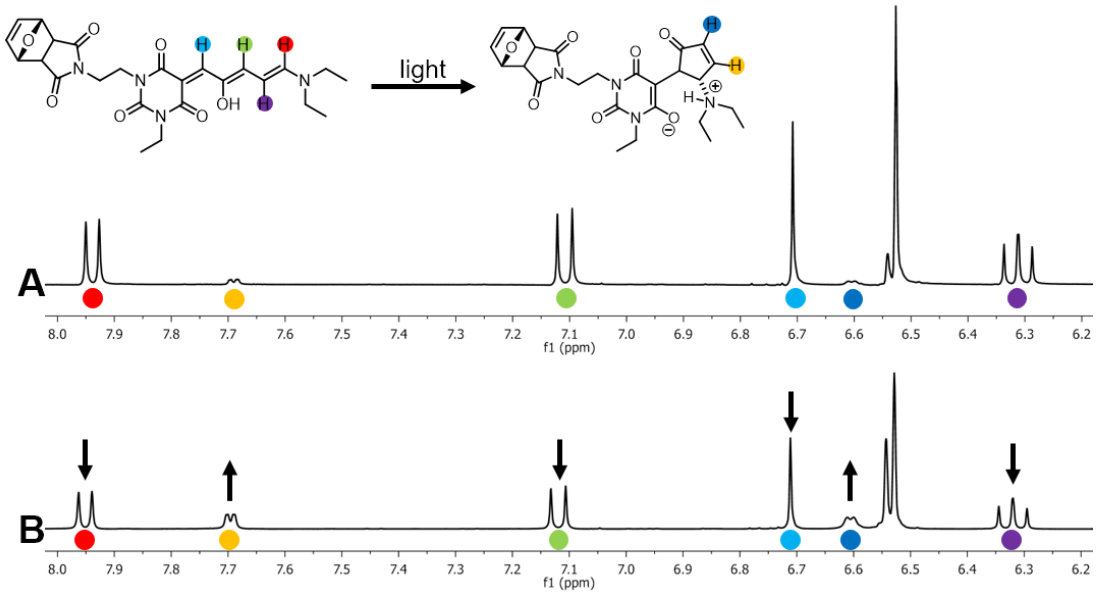

Figure 2.6.7. *Partial ^{1}H NMR of compound **2.5**. The signals are colour coded to represent the same coloured protons in the inset scheme of **2.5**. Trace A shows the initial spectrum with no irradiation, while Trace B shows the spectrum after 15 min of irradiation. The increase and decrease of peaks of interest is highlighted by the up and down arrows.*

Photoswitching of the monomer was observed by solution UV-vis spectroscopy studies upon irradiation with a broadband light source with a <520 nm cut-off filter (Figure 2.6.7.).

2.6.3. Thin Film Photoisomerisation Studies

The thin films were created by drop-casting, which involved dissolving 3 mg of polymer in 2 mL of dichloromethane, and then dropping onto a quartz slide. The solvent was allowed to evaporate, leaving a thin film of the polymer on the quartz slide. While these films exhibit several irregularities, there are some regions that are continuous and uniform, and testing was localised to these areas. Using the density estimation calculations outlined by Girolami,[67] the thicknesses of the thin films were estimated to be approximately 3 μm. These calculations are included as Appendix F.

A series of thin films of polymers **2.7a**-**c** were prepared with 3 mg of material, and as such the variation in absorbance is a comparative measure for the ratio of DASA units in each polymer. The absorption changes with irradiation are shown in Figure 2.6.8. The ring open DASA unit has an absorption band at 554 nm, which is in the range expected, but is difficult to compare to solution measurements as these compounds are solvatochromic (and therefore have fluctuating λ_{max} values). While some concomitant increase in the UV range is expected,[45] it is masked by the absorbance of the polymer backbone, and no clear isosbestic point is observed. However, if this band were of particular interest, thinner films would allow this region to be observed with greater clarity and perhaps the change could be better quantified.

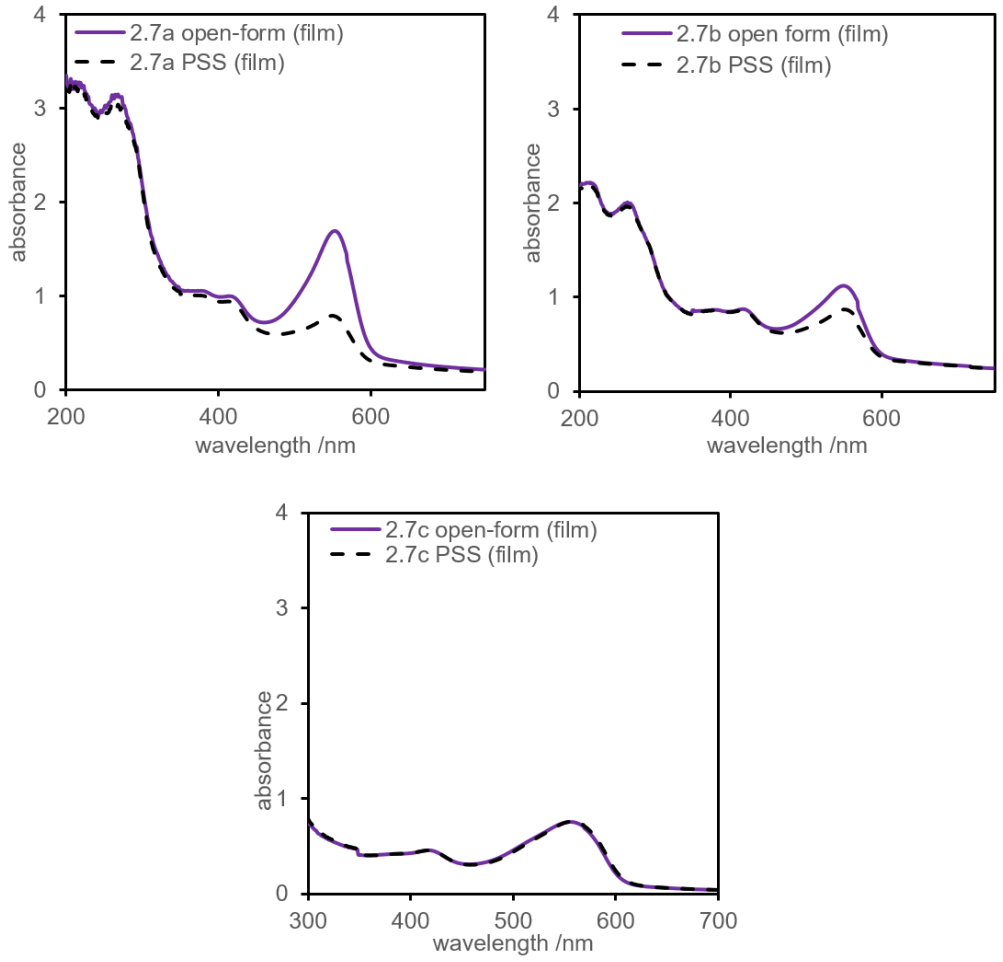

Figure 2.6.8. *UV-visible absorption spectra of polymer **2.7a-c** thin films. Irradiation with >520 nm light yields the PSS after 7 hours (**2.7a**), 3 hours (**2.7b**), and 1.5 hours (**2.7c**).*

In contrast to the solution studies, the amount of photoswitch in the polymers seems to have a significant impact on their ability to switch in the solid state. This may be

due to the inflexibility of the control units—having more of them impedes the ability of the DASA units to isomerise, leading to lower PSSs for the polymers that contain more control units than switchable units. This is consistent with glass transition temperatures above room temperature (discussed in Section 2.5.1.2) that demonstrate a lack of free rotation due to the polymers being in the glass-like phase rather than the rubber phase, which would be a direct hindrance to switching.[68]

The value for the PSS of the polymers and monomer are estimated using UV-vis, assuming the original coloured spectrum is 100% open form. Calculation of the molar absorptivity (ε) of the polymers gives consistent results across all three films. This agreement in molar absorptivity is consistent with the stoichiometric ratio of switch to control for all three polymers (calculated in Appendix C). This also shows that all three films have the same initial percentage of open form (assumed to be 100%).

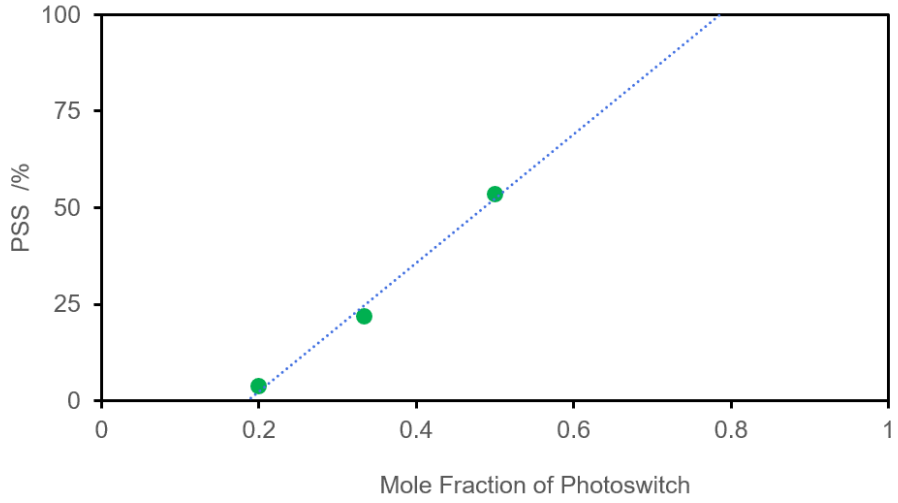

Figure 2.6.9. *Graph of photostationary state vs mole fraction of DASA photoswitch in the polymer. Linear trend-line extrapolation implies a photostationary state of 100% is possible near 0.8 mole fraction of photoswitch.*

A simple plot of PSS vs DASA mole fraction (Figure 2.6.9) implies that there is a linear relationship between the photostationary state and the number of photoswitch units contained in the polymer. Extrapolation of the data implies that a polymer composed of 4:1 photoswitch to control would yield a photostationary state close to 100%. However, due to the limited data set, this relationship would need to be explored in more detail to yield truly conclusive results.

2.7. Contact Angle Goniometry

The contact angle is the angle at which a liquid meets a solid surface, and is specific for a particular system. Contact angle goniometry is used to determine the wettability of a surface, and it can also be used to calculate the surface energy (using Young's equation). The wetting behaviour of a surface is an important property, and is governed by both the chemical composition and the geometric structure of the surface. 'Wetting' describes the contact between a liquid (usually water) and a solid surface and is a result of the intermolecular interactions between them. The amount of wetting is described by the contact angle. ; smaller than 90° is indicative of a hydrophilic surface and greater than 90° indicates that the surface is hydrophobic.[69,70]

Contact angle measurements are easily affected by the nature of the surface, including the electrostatic interactions, surface landscape, and possible contaminants. Even small deviations in the quality of the surface can affect the accuracy of the measurements, and it is a practical limitation that the difference between the left and right side contact angles of the same droplet can vary by a few degrees.

Many polymers are hydrophobic in nature, and the contact angles observed for polyethylene is 105°,[71] while that of PDMS is 115°.[72] This is consistent with the observations of Tannouri *et al*[27] who saw a contact angle of 102° for the non-structured spiropyran doped films. The micro-structured doped polymers showed a contact angle of 130°, which is likely due to the lotus leaf effect (small air pockets beneath the liquid droplet result in an increase in the contact angle). In contrast, the contact angle of clean glass is 0°, as a water droplet on this surface will spread out on the surface as a result of the strong hydrophilic interaction.

For this particular set of measurements, a 2 µL drop of highly purified water is dispensed directly onto the surface of a thin film of polymer via Eppendorf pipette. A digital video camera is used to obtain a side-on view of the surface and the drop, and specialised software is used to obtain the angle between the droplet and the surface.

The polymer systems described in this thesis are chosen based on the concept that photoisomerism of the DASA compounds between the neutral triene and the zwitterionic cyclopentenone will affect the electrostatic forces on the surface of the polymer. Therefore, the contact angle measurements of the open and closed forms should

give information about the electrostatic interactions on the surface of the polymer films. In thin film, all three polymers (**2.7a**-**c**) show at least some photoinduced isomerisation when monitored by UV-vis absorption spectroscopy, although this is greatly affected by the number of photoswitchable units in the polymer.

For the contact angle measurements, each polymer was used to make a single glass slide (as per experimental procedure outlined in Section 2.6.3.), and on each slide, there were five separate sites isolated for consistency and uniformity. These sites were marked (on the reverse side of the glass) and the first set of 'dark' contact angle measurements was then taken. At the time of measurement, the water droplet had partially dissolved the film of control polymer **2.6p** and therefore only one set of readings was taken for this slide. Because the films require irradiation over long time periods, and because of the demonstrated solubility of **2.6p** in water, the droplets were removed from all films before irradiation, rather than observing the change of the droplets over time. The slides were irradiated for one hour with broad-band light with a <520 nm cut-off filter (using the same set-up as previously described). The same sites were then used to obtain a set of 'light' contact angle measurements. This data is presented in Table 2.7.1 and a representative diagram of the contact angle is shown in Figure 2.7.1. Raw data is presented in Appendix H.

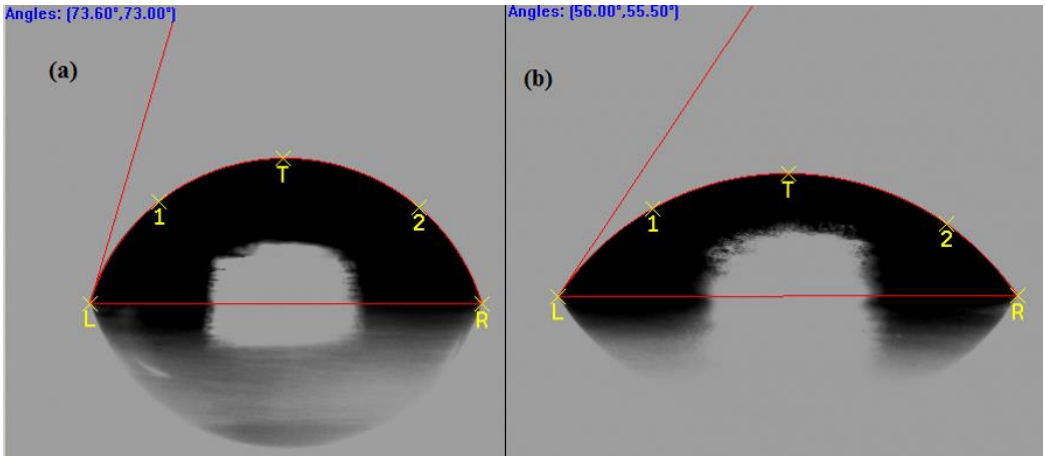

Figure 2.7.1. *Representative example of a contact angle measurement of a water droplet on top of (a) polymer **2.7a** in the dark and (b) polymer **2.7a** after one hour of irradiation.*

Table 2.7.1. *Contact angle measurements for water droplets on top of thin films before and after irradiation with >520 nm light source for one hour.*

	Polymer 2.6p	Polymer 2.7a		Polymer 2.7b		Polymer 2.7c	
	Dark	Dark	Light	Dark	Light	Dark	Light
Angle (degrees)	14.1	76.7	57.1	67.0	62.4	49.0	57.0
	21.3	73.0	56.1	63.2	66.5	49.5	52.6
	18.9	73.6	54.6	67.9	68.5	55.1	58.0
	27.4	72.4	54.0	62.6	69.5	52.5	54.2
	26.2	76.4	55.7	68.3	62.9	51.3	54.4
	12.7	72.7	53.7	65.1	70.8	51.8	52.8
	22.7	73.0	55.5	65.8	68.8	55.1	59.1
	20.6	72.1	56.0	63.1	68.3	52.4	50.8
		73.7		68.2	65.2	50.7	59.9
		72.4		68.4	70.5	46.9	58.5
Mean:	20.4	73.6	55.3	66.0	67.3	51.4	55.7
SD:	5.2	1.6	1.2	2.3	3.0	2.6	3.2

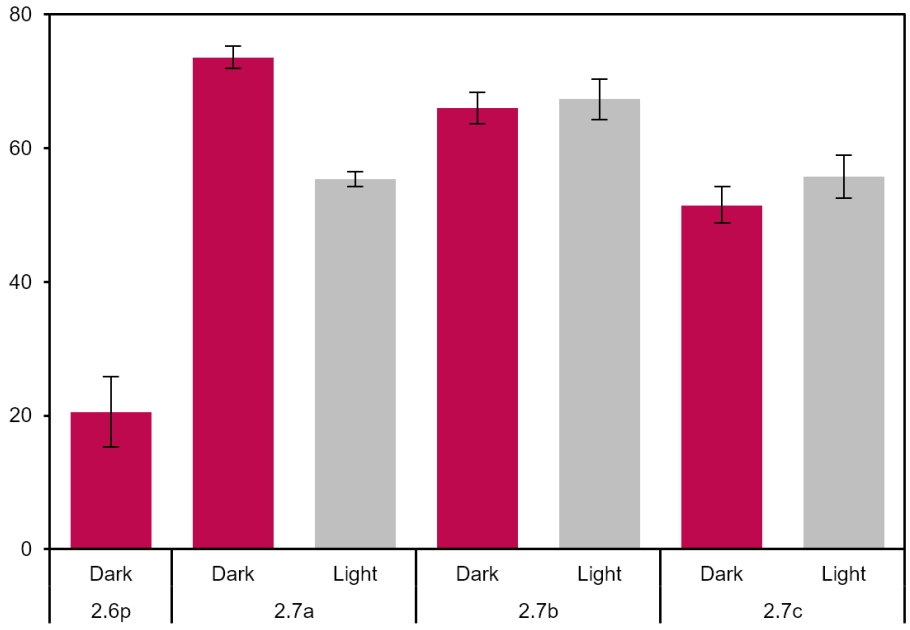

Figure 2.7.2. *This plot shows the average values for all measurements taken (raw data in Appendix H). Light measurements are taken at the same spot on the film as the dark measurements, subsequent to 1 hour of >520 nm irradiation.*

While polymers **2.7b** and **2.7c** showed no significant changes in the contact angle upon irradiation, the dark measurements show a general trend towards hydrophilicity with increasing amounts of control units. This is consistent with the finding that the polymer **2.6p** is soluble in water. Due to the long switching times, it is possible that a longer irradiation period would have yielded some statistically significant results for thin films **2.7b** and **2.7c**, but they would have been minimal, and solvation with water would have become a greater concern.

The contact angle of the water droplets resting upon the thin film of **2.7a** increases when it is irradiated with >520nm light, which is a result of a change in the wetting behaviour of this thin film. This is most likely as a result of isomerisation of the DASA units, as this polymer is largely insoluble in water (Table 2.5.1). However, it is possible that there are some surface interactions occurring because of insufficient drying of the surface between measurements. Still, there was one hour between measurements, which should have been sufficient time for the surface to dry completely, and this seems to be the case upon inspection. In future, it would be of benefit to perform contact angle measurements on a slide that had been irradiated and then a single set of light measurements taken from it, to determine if (and how much) of these contact angle changes are due to the irradiation alone, and if there are any residual solvent-interactions that are altering the measurement.

Polymer **2.7a** showed a decrease of 18.3°, which is probably due to correspond to an increase in wettability between the open and closed forms of the photoswitch. This is a significant improvement over the 8° difference that was observed in previous work[27] for the unstructured spiropyran-doped PDMS films. This result illustrates the change in the electrostatic interactions at the surface of the polymer because of the photoswitching mechanism of the incorporated DASA units.

2.8. Adhesion Strength Measurements

Adhesion strength measurements were collected and data provided by Scott Beaupré (SFU Engineering), from which the analysis was conducted.

With the change in surface wettability (determined by contact angle goniometry in Section 2.7), there can, in principle, be a change to the adhesion of the surface as well. As described in Chapter 1.1, the adhesion of a surface is determined by the geometry of the surface as well as the molecular interactions. With the confirmed change in the molecular interaction (from the goniometry experiments) due to photoswitching, the surface adhesion may also be affected.

Adhesion tests were performed with a custom apparatus consisting of a probe attached to a load cell and positioned with a linear motorized stage. Software lowers the probe via the load cell until contact is made with the sample, and then the probe is retracted. The force required to remove the probe tip from the surface measures the adhesion between the probe and the surfaces.

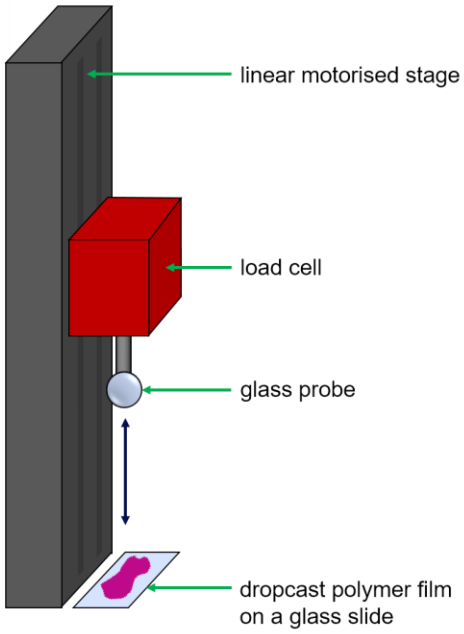

Figure 2.8.1. *Cartoon of the apparatus used to determine the adhesion strength. Software controls the lowering of the load cell via the linear stage with a set force until contact with the sample is detected. The force required to remove the probe from the surface is a measure of the adhesion betweeen the two surfaces. In this case, a glass probe is used, and the sample is prepared as a dropcast film on a glass slide.*

The polymer thin-film samples (**2.6p, 2.7a-c**) were prepared as drop-cast films on glass slides, as described previously. Polymer **2.6p** was used as a reference film and prepared in the same manner. Areas of uniformity were isolated for testing. The load cell was set to apply 100 mN of preload force. This value was chosen as the highest value the set-up was reliably able to maintain over several iterations. At significantly higher preload forces, the probe tip caused visible cracking of the thin films, and the software had difficulty in maintaining consistency of the higher preload forces. In previous work,[27] there was negligible difference observed for varying preload forces.

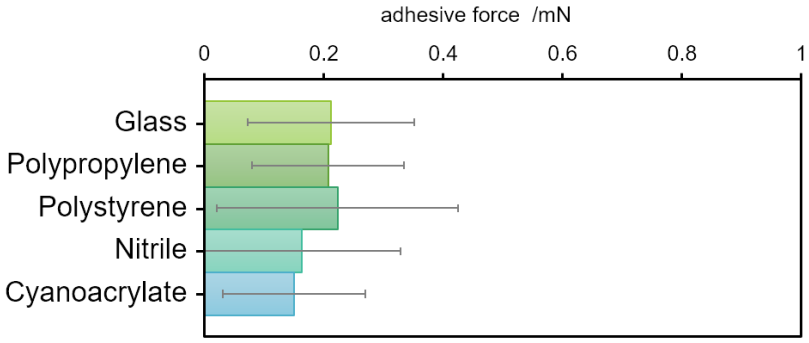

Figure 2.8.2. *Adhesion of various materials (100 mN preload force) to a thin film of polymer* ***2.6p.***

Several probe tips were prepared and tested, and the glass probe tip was chosen as the best candidate for further testing because it showed the greatest amount of preliminary adhesion to the control surface, as well as the lowest amount of error in readings (Figure 2.8.2). All probes were roughly spherical in shape, with the approximate contact surface amounting to 3 mm^2. While the readings for the glass probe were similar of those to the polypropylene probe, the near-perfect spherical nature of the glass bead made it a more consistent probe for repeated measurements.

With the chosen probe in place, measurements were taken on all samples every 15 minutes for one hour and the force required to retract the glass tip from the film directly measures the adhesion strength between the two surfaces. The error appears to be so significant because the linear stage, while moderately sensitive, is designed to detect loads of 1 N to 100 N. The equipment sensors had been previously modified to detect force loads as low as 10 mN, but because the average readings for these polymers are below 1 mN, these small measurements are very likely outside the detection limit of this equipment.

Unsurprisingly, as Figure 2.8.3 illustrates, there is no significant adhesion observed under these conditions. However, it appears that the control polymer does exhibit a small amount of adhesion (0.2 mN), as seen in the control **2.6** as well as the sample that is 4 parts control, **2.7c**.

There is no significant change during the irradiation time. There are a few potential reasons for this. First, it may be that the choice of probe was inappropriate for these measurements. Though glass is generally considered to be a hydrophilic surface (the polymer was shown to be hydrophilic in Section 2.7), it may be that another choice of probe would have been better able to elucidate a significant change for this experiment.

Another possible reason why these tests were not successful is that the probe was not pushed far enough into the surface to allow for sticking, which would limit the full contact area and therefore any alteration to the adhesion would undetectable with this equipment. This is the most likely reason for the inconclusive adhesion results, especially when considering the dipole-induced-dipole interactions (Equation 1.1.1) which show that the potential energy of these interactions is strongly governed by the $\frac{1}{r^6}$ term. In practice, this requires the probe to be within a few angstroms of the polymer surface,[20] and this was not possible owing to the brittle nature of these films.

For future experiments of this type, it may be the most beneficial to use a larger probe, as a larger contact area would increase the attractive force between the probe and the surface, and this would ideally bring these signals past the detection limit of the apparatus. Unfortunately, we were not able to perform these experiments due to complications with the equipment.

While it is possible to determine surface energy differences using other techniques, such as atomic force microscopy, we are interested in larger differences in the adhesion that this polymer was not able to provide.

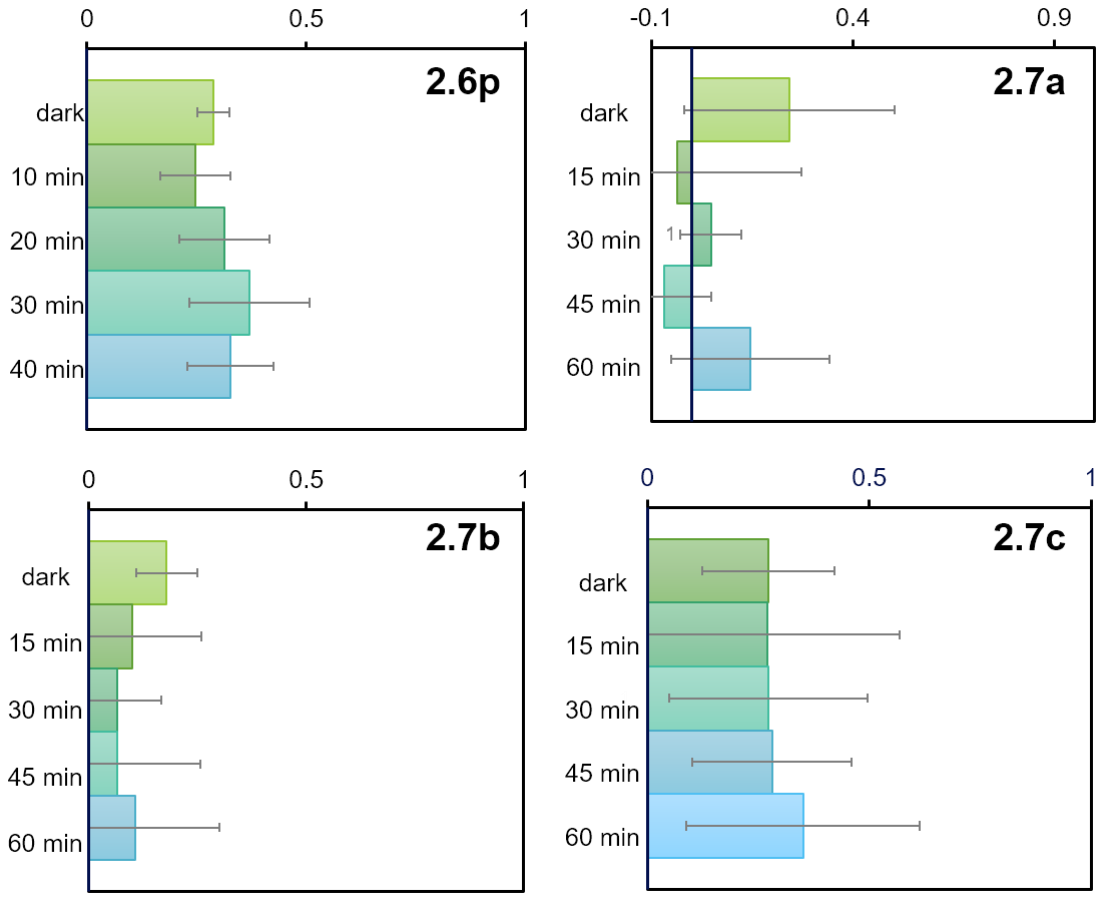

Figure 2.8.3. *Adhesion force of polymer thin films over the course of an hour with irradiation at >520 nm light (y-axis). The x-axis shows adhesive force in mN.*

2.9. Conclusion

The first phase of this project was the synthesis of the pre-polymer molecule, **2.5**, with the pendant oxanorbornene and testing of the photochemistry of this molecule in isolation. This was followed by synthesis of the polymer or pure photoswitchable material compound **2.5p**, which was then compared to a synthesised 'control' polymer of a modified oxanorborene, **2.6p**.

The original photoswitchable polymer **2.5p** was largely insoluble, even at relatively low molecular weights (as low as 15 individual units, Mw: ~11380 Da). Not only did this create significant barriers to its study and characterisation, but it also causes an impediment to its usefulness in mixing with other polymers. To address this issue, compound **2.4** was copolymerised with **2.6** in varying ratios to form copolymers **2.7a**-**c** that were readily soluble in chloroform, and dichloromethane. The synthesis and characterisation of these polymers was described. While these polymerised materials show some photoswitching in solution, there is slightly less conversion in the solid state, and the polymers are completely incapable of reverting in the solid or solution.

Contact angle measurements performed on the polymers showed significant change (18°) for the polymer containing the most switch (**2.7a**), while nothing significant was observed for the other two (**2.7.b and 2.7.c**). Further adhesion tests showed no change in the adhesive properties of these polymers within the detection limit of the equipment.

2.10. Future Work

Since conclusion of this work, other research groups have made significant contributions to the synthesis of new DASA switches that show increased switching in a wide range of solvents.[46] The modifications have been to cyclise the tertiary pendant amine acceptor group. Previously, the majority of work done in polymerising and functionalising these molecules has been done through this amine group. If the photoswitching capabilities of this molecule are tied into the donor portion of the molecule then our polymerisation approach (the pendant oxanorbornene pendant off of the acceptor portion of the DASA) could potentially be the future for the polymerisation of these molecules.

Any future work would greatly benefit from the increased switchability and solubility that the cyclic amine acceptor section has on these molecules. These second generation DASAs may also be more prone to exhibiting multi-directional switching in the solid state, which would open up these materials to several other applications where the reusability of the substrate is desired.

Additionally, while we were unable to successfully show the direct adhesion of these polymers through use of the linear stage, it is possible (and indeed likely based on previous results) that the incorporation of this particular photoswitch (or of the subsequent generation types) into a PDMS (or similar) polymer matrix will impart the known favourable behaviours that have been previously assessed.[1,12,27] This would also likely reduce the inherent brittleness of these materials that caused some problems when measuring the adhesion using the stage, and allow for closer contact between the probe and the photoswitch molecules.

The large change in the contact angle measurements does suggest that there is a significant change to the hydrophilicity of the molecule when switching between the open and closed forms of this molecule, and thus future work should focus on incorporation of these polymers into a PDMS matrix. In particular, focus should be given to tethering second generation DASA molecules directly to the PDMS backbone to prevent their ejection from the polymer over time.

Chapter 3. Experimental

3.1. General Materials

Unless otherwise noted, all solvents used were purchased from Fisher or Sigma Aldrich and used without further purification. NMR solvents were purchased from Cambridge Isotope Laboratories and used as received. All reagents and starting materials were purchased from Sigma-Aldrich and used as received. Nitrogen was purchased from Praxair, and silica for column chromatography was purchased from SiliCycle.

3.2. Instrumentation

All synthetic compounds were characterised by ^{1}H NMR and ^{13}C NMR spectroscopy using a Bruker Avance-400 instrument operating at 400 MHz for ^{1}H NMR and 100 MHz for ^{13}C NMR. Chemical shifts (δ) are reported in parts per million relative to TMS using the solvent residual peak as the reference standard. Coupling constants are reported in Hertz.

High resolution mass spectroscopy (HRMS) measurements were made by Hongwen Chen with an Agilent 6210 TOF LC-MS in ESI-(+) mode.

Melting points (MP) were taken with a Gallenkamp melting point apparatus using a mercury thermometer (-20 to 400°C).

The gel permeation chromatography was performed by Jonathan Ward using a converted Waters HPLC pump, with three in-line Waters Styragel columns: HR 3 (500 to 30K Da separation), HR 4 (5K to 600K Da separation), and HR 5 (50K to 4M Da separation). Columns are kept at 60C via a column oven. The samples were run in N,N-dimethyl formamide with 0.01 mol/L LiBr solution. The chromatography was run at a flow rate of 1.00 mL/min with an injection volume of 20.0µL of an approximately 2mg/mL solution of the polymer dissolved in the eluent solution. A Waters 2487 Dual Wavelength Ultraviolet Detector set at 264nm was utilized to detect polymer being eluted. Samples were compared against a standard calibration curve of polystyrene.

Phase transition temperatures and enthalpies were determined using differential scanning calorimetry (DSC) on a TA Instruments DSC Q2000 equipped with a TA Instruments Cooling System 90 and the values for the temperatures and heat flow were recorded on the second heating cycle at a rate of 10°C/min.

The polymer thin films were created by drop-casting, which involved dissolving the polymer in a small amount of dichloromethane, and then dropping onto a quartz slide. This drop was then spread along the slide using a capillary tube held horizontally with equal amounts of pressure on both sides to thin the solution and spread the polymer along a greater area. The solvent was allowed to evaporate, leaving a thin film of the polymer on the quartz slide. While these films exhibit several irregularities, there are some regions that are continuous and uniform, and testing was localised to these areas. This uniformity was confirmed by UV-vis, showing uniform absorbance over these regions, as well as microscopically, at 10x zoom using an Olympus BX50 optical microscope.

Ring-closing reactions were carried out using light from an Osram halogen lamp (MRW, 300W/120V, part number 93518) source and passed through a <520 nm cut-off filter to block higher energy wavelengths. The light source was kept at a distance of 20 cm from the sample for all irradiation measurements. Photoreactions monitored by UV-visible absorption spectroscopy were performed in 1 cm quartz cuvettes for solution state samples, and on quartz slides for thin film samples. Irradiation times are noted as a cumulative irradiation time, and not interval times. Photocycling experiments and repeat measurements were made with an OceanOptics USB2000 Spectrometer used with a USB-ISS-UV/VIS lamp, and cuvette holder attached, and controlled using OOIBase32 software. Thin film measurements were recorded on a Varian Cary 300 Bio-spectrophotometer. Ring closing with light at any wavelength was unsuccessful and is not reported here.

Wetting measurements on the prepared polymer films were performed using a digital AST Optima contact angle apparatus with a horizontal light beam to illuminate the water droplet. Water droplet volumes of approximately 1.5−2.0 μL were delivered to the film surface with micropipettes.

Adhesion tests were performed with a custom apparatus consisting of a glass probe approximately 5 mm in diameter attached to a tension and compression load cell

(FUTEK LRF400, 2.2lb). The load sensor was connected to a 24-bit amplifier (FUTEK USB210) and positioned with a linear motorized stage (Zaber Technologies T-LS27-SMV) and the reading and positioning was controlled using a custom LabVIEW (National Instruments) script. The load cell was set to apply 100 mN of preload force. The polymer thin-film samples were prepared as drop-cast films on glass slides, as previously outlined.

3.3. Synthesis

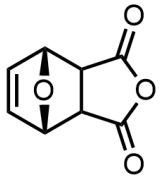

7-oxabicyclo[2.2.1]hept-5-ene-2,3-dicarboxylic anhydride (2.1). A solution of maleic anhydride (16.0701 g, 163.88 mmol) in THF (60 mL) was prepared in an Erlenmeyer flask and swirled to dissolve. Furan (11.7 mL, 160.88 mmol) was added via syringe while stirring. The walls of the Erlenmeyer flask were washed with a further 10 mL of THF, and subsequently placed in a cool dark place. Upon standing for 2 weeks, the product was collected by Buchner filtration, rinsing with ice cold THF. Purification by recrystallisation from warm THF yielded 16.8504 g of oxanorbornene **2.1** (63%) as small white needles. MP: 110-111 °C. ^{1}H NMR ($CDCl_3$, 400 MHz): δ = 6.57 (s, 2H), 5.45 (s, 2H), 3.18 (s, 2H). ^{13}C NMR (CD_2Cl_2, 100 MHz): δ = 170.72, 136.90, 82.34, 48.79.

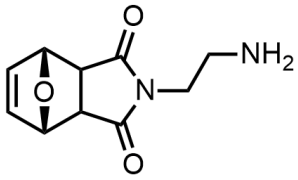

N-(2-aminoethyl)-7-oxabicyclo[2.2.1]hept-5-ene-2,3-dicarboximide (2.2). Compound **2.1** (5.00968 g, 30.15 mmol) in MeOH (250 mL) was stirred vigorously under N_2 at 0 °C for 30 minutes. Ethylene diamine (2.1 mL, 30.65 mmol) in 60 mL MeOH was added via addition funnel over 20 minutes. The mixture was brought to room temperature over 45 minutes and left stirring at room temperature for 1 hour. This solution was then refluxed for 3 hours, and then returned to room temperature. The mixture was reduced to 100 mL by rotary evaporation and left to stand for 1 hour. The solids were filtered off and the liquid

was evaporated to dryness under vacuum. The crude mixture was then brought up in 60 mL MeOH, sonicated, filtered, and evaporated to dryness under vacuum. Purification by trituration from diethyl ether yielded 5.9489 g of oxanorbornene **2.2** (98%) as a yellow oil. ^{1}H NMR (CD_3OD, 400 MHz): δ = 6.58 (s, 2H), 5.18 (s, 2H), 3.57 (t, 2H, *J* = 6.2 Hz), 2.82 (t, 2H, *J* = 6.2 Hz), 2.97 (s, 2H). ^{13}C NMR (CD_3OD, 100 MHz): δ = 177.40, 136.17, 80.91, 48.46, 40.55, 38.83. LC-MS (ESI+, acetonitrile): *m/z* calculated for $C_{10}H_{13}N_2O_3^+$: 209.0946, found 209.0932.

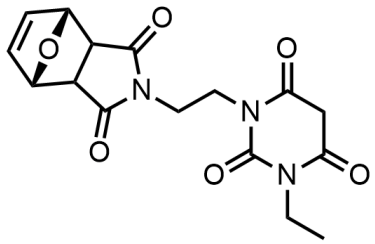

1-(7-oxabicyclo[2.2.1]hept-5-ene-2,3-dicarboximidoethyl)-3-ethylbarbituric acid (2.3). Ethyl isocyanate (1.2 mL, 15.2 mmol) in DCM (30 mL) was added dropwise to a vigorously stirring solution of compound **2.2** (3.1750 g, 15.2 mmol) in DCM (100 mL) under N_2 over 10 minutes. This solution was stirred for 1 hour at room temperature, and followed by TLC (5% MeOH in DCM, visualised in an I_2 chamber). During this time the solution changed to a milky yellow in appearance. Malonyl chloride (1.48 mL, 15.2 mmol) was then added dropwise to the solution and refluxed for 1 hour, followed by TLC (as above, product visualised with 254 nm light, impurities by I_2 chamber), becoming transparent and light brown. The mixture was then cooled to room temperature and quenched with HCl (60 mL, 1M). The aqueous layer was extracted with DCM (3×70mL), and the combined organic phases were washed with a saturated brine (1×50 mL). The organic layer was dried over $MgSO_4$, filtered, and evaporated to dryness under vacuum. Purification by flash chromatography (silica, 9:1 hexanes/EtOAc) yielded 3.4317 g of 1,3-disubstituted barbituric acid **2.3** (65%) as a fluffy light brown powder. MP: 108-114°C. ^{1}H NMR ($CDCl_3$, 400 MHz): δ = 6.52 (s, 2H), 5.23 (s, 2H), 4.17 (2×dd, 2H, *J* = 3.1, 5.1 Hz), 3.92 (q, 2H, *J* = 7.1 Hz), 3.84 (2×dd, 2H, *J* = 3.1, 5.1 Hz), 3.63 (s, 2H), 2.83 (s, 2H), 1.24 (t, 2H, *J* = 7.1 Hz). ^{13}C NMR ($CDCl_3$, 100 MHz): δ = 176.48, 165.32, 164.47, 151.48, 136.62, 80.92, 53.56, 47.65, 39.73, 37.46, 36.94, 13.28. LC-MS (ESI+, acetonitrile): *m/z* calculated for $C_{16}H_{18}N_3O_6^+$: 348.1195, found 348.1227.

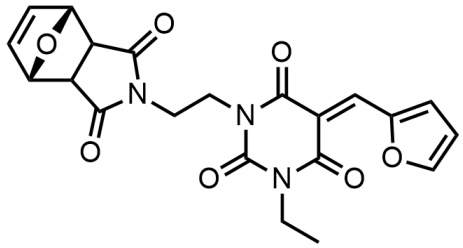

3-ethyl-5-(furan-2-ylmethylene)-1-(7-oxabicyclo[2.2.1]hept-5-ene-2,3-dicarboximido ethyl)barbituric acid (2.4). Furfural (470 µL, 5.66 mmol) was added to vigorously stirring solution of compound **2.3** (1.9737 g, 5.66 mmol) in THF/water (25 mL/20 mL) under N_2. The reaction was stirred at room temperature for 3 hours during which colour changed from amber to dark green and was followed by TLC (3:1 Hex/EtOAc, visualised with 254 nm light). The THF was removed under vacuum and the remaining solids were removed by filtration. The solids were then dissolved in DCM (75 mL) and washed sequentially with 30 mL each of: saturated aqueous $NaHSO_3$, water, saturated aqueous $NaHCO_3$, and saturated brine. The organic layer was dried over $MgSO_4$, filtered, and evaporated to dryness under vacuum. Purification by flash chromatography (silica, 3:1 hexanes/EtOAc) yielded 1.3005 g of 1,3,5-trisubstituted barbituric acid **2.4** (54%) as a chalky light yellow powder. MP: 96-98°C (decomposed). ^{1}H NMR ($CDCl_3$, 400 MHz): δ = 8.61 (dd, 1H, *J* = 3.8, 18.8 Hz), 8.39 (d, 1H, *J* = 14.5 Hz), 7.85 (s, 1H), 6.73 (m, 1H), 6.46 (d, 2H, *J* = 6.6 Hz), 5.19 (d, 2H, *J* = 7.7 Hz), 4.23 (m, 2H), 4.01 (q, 2H, *J* = 7.08 Hz), 3.85 (m, 2H), 2.80 (s, 1H), 2.75 (s, 1H), 1.25 (m, 3H). ^{13}C NMR ($CDCl_3$, 100 MHz): δ = 176.27, 162.59, 161.82, 160.86, 160.26, 151.18, 150.91, 141.04, 136.48, 127.88, 115.09, 111.47, 80.69, 47.50, 40.28, 37.61, 13.25. HRMS (ESI+ of M+H): *m/z* calculated for $C_{21}H_{20}N_3O_7^+$: 426.1301, found 426.1296.

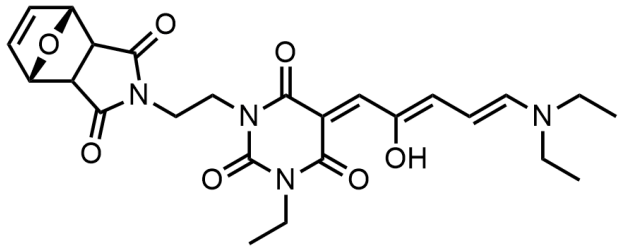

(E)-5-((2Z,4E)-5-(N,N-diethylamino)-2-hydroxypenta-2,4-dien-1-ylidene)3-ethyl-5-(furan-2-ylmethylene)-1-(7-oxabicyclo[2.2.1]hept-5-ene-2,3-dicarboximidoethyl)

barbituric acid (2.5). In dark conditions, compound 2.4 (0.99994 g, 2.35 mmol) was stirred vigorously for 15 minutes in dry degassed THF (5 mL) for 20 minutes under N2. Diethylamine (243 µL, 2.35 mmol) was added slowly to the rapidly stirring solution, which was stirred at room temperature and followed by TLC (19:1 DCM/MeoH, visualised by 254 nm light). After 3 hours the crude mixture was evaporated to dryness under vacuum. Purification by column chromatography (silica, 9:1 DCM/MeOH) yielded 0.5187 g of DASA 2.5 (44%) as a dichroic green/purple powder. MP: 114-118°C. ^{1}H NMR (CD_2Cl_2, 400 MHz): δ = 7.31 (d, *J* = 12.2 Hz, 1H), 7.01 (d, *J* = 7.3 Hz, 1H), 6.47 (s, 2H), 6.11 (td, *J* = 12.4, 5.3 Hz, 2H), 5.16 (d, *J* = 2.5 Hz, 2H), 4.13 – 4.05 (m, 3H), 3.90 (p, *J* = 7.3 Hz, 2H), 3.73 (dt, *J* = 11.3, 5.4 Hz, 2H), 3.50 (dq, *J* = 14.7, 7.2 Hz, 4H), 2.81 (d, *J* = 5.9 Hz, 2H), 1.30 (q, *J* = 7.8 Hz, 2H), 1.15 (dt, *J* = 10.4, 7.0 Hz, 3H). ^{13}C NMR ($CDCl_3$, 100 MHz): δ = 176.48, 165.32, 164.47, 151.48, 136.62, 80.92, 53.56, 47.65, 39.73, 37.46, 36.94, 13.28. HRMS (ESI+ of M+H): *m/z* calculated for $C_{25}H_{31}N_4O_7^+$: 499.2193, found 499.2188.

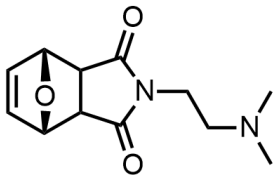

N-(2-(dimethylamino)ethyl)-7-oxabicyclo[2.2.1]hept-5-ene-2,3-dicarboximide (2.6). Compound **2.1** (3.03812 g, 18.29 mmol) in MeOH (100 mL) was stirred vigorously under N_2 at 0 °C for 30 minutes. N,N-dimethyl ethylene diamine (2 mL, 18.20 mmol) in 20 mL MeOH was added via addition funnel over 20 minutes. The mixture was brought to room temperature over 45 minutes and left stirring at room temperature for 1 hour. This solution was then refluxed for 3 hours, and then returned to room temperature. The solvent was removed by rotary evaporation, and concentric light brown crystals formed. Recrystallisation from warm EtOH to yielded 1.2997 g of oxanorbornene **2.6** (69%) as short white needles. MP: 98-99°C. ^{1}H NMR ($CDCl_3$, 400 MHz): δ = 6.53 (s, 2H), 5.28 (s, 2H), 3.61 (t, 2H, *J* = 6.2 Hz), 2.88 (s, 2H), 2.49 (t, 2H, *J* = 6.2 Hz). ^{13}C NMR ($CDCl_3$, 100 MHz): δ = 176.20, 136.54, 80.89, 56.50, 52.09, 47.48, 45.45, 36,90. HRMS (ESI+ of M+H): *m/z* calculated for $C_{12}H_{17}N_2O_3^+$: 237.1239, found 237.1243.

General Polymerisation Procedure. [Under N_2]. A Schlenk flask containing the appropriate monomer(s) **2.5** and **2.6** (total 0.2 mmol) was treated with 2 mL (0.013 mmol) of a solution of first generation Grubbs catalyst prepared as a $6x10^{-3}$ M solution in anhydrous deoxygenated DCM. The solution was left to stir under N_2 for 2 hours. The living polymerization was terminated with excess ethyl vinyl ether and stirred for a further 30 minutes exposed to air. The solution was poured into cold Et_2O, either vacuum filtered or evaporated to dryness, and washed several times with Et_2O.

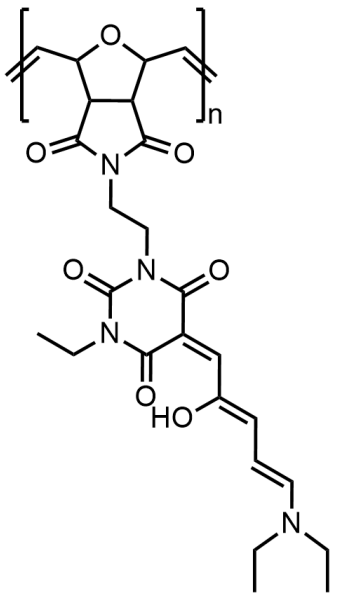

Synthesis of DASA Polymer (2.5p). A solution of DASA monomer **2.5** (99.72 mg, 0.20 mmol) was polymerised with Grubb's catalyst (10.48 mg, 0.013 mmol) yielding 67.81 mg of polymer **2.5p** after precipitation with cold Et_2O (68%). Polymer **2.5p** is completely insoluble in all common laboratory solvents, and was only characterised by diamond ATIR with comparison to monomer **2.5**. ν (in cm^{-1}) = 3459 (O-H), 1699 (C=O, amide), 1586 (C=O, carboximide), 1496 (C-N), 970 (O-C-O).

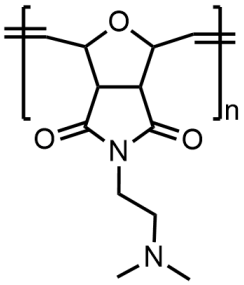

Synthesis of control Polymer (2.6p). A solution of control monomer **2.6** (47.22 mg, 0.20 mmol) was polymerised with Grubb's catalyst (10.48 mg, 0.013 mmol) yielding 11.33 mg of polymer **2.6p** after precipitation with cold Et_2O (24%). ^1H NMR ($CDCl_3$, 400 MHz): δ = 6.08 (s, 2H trans), 5.80 (s, 2H cis), 4.94 (s, 2H cis), 4.45 (s, 2H trans), 3.58 (s, 2H), 3.33 (s, 2H). 2.48 (s, 2H), 2.21, (s, 6H). ^{13}C NMR ($CDCl_3$, 100 MHz): δ = 175.68, 130.92, 81.08, 65.64, 55.89, 45.18, 36.62, 15.08.

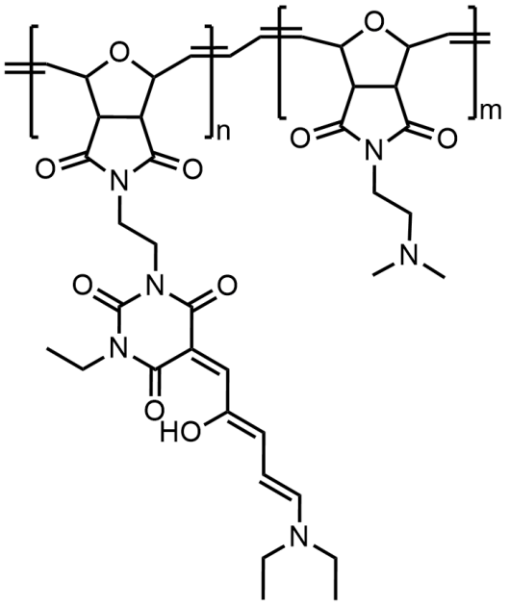

Synthesis of copolymer (2.7a). A solution of DASA monomer **2.5** (49.85 mg, 0.10 mmol) control monomer **2.6** (23.63 mg, 0.10 mmol) was polymerised with Grubb's catalyst (10.48 mg, 0.013 mmol) yielding 57.37 mg of polymer **2.7a** after precipitation with cold Et_2O (78%).

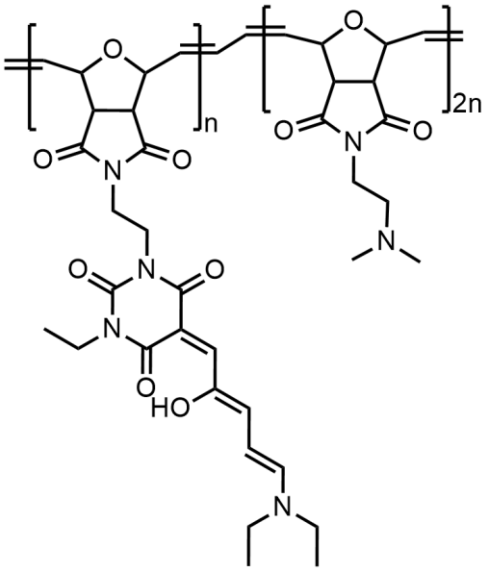

Synthesis of copolymer (2.7b). A solution of DASA monomer **2.5** (33.24 mg, 0.07 mmol) control monomer **2.6** (31.55 mg, 0.13 mmol) was polymerised with Grubb's catalyst (10.48 mg, 0.013 mmol) yielding 59.32 mg of polymer **2.7b** after rotary evaporation and washing with cold Et_2O (91%).

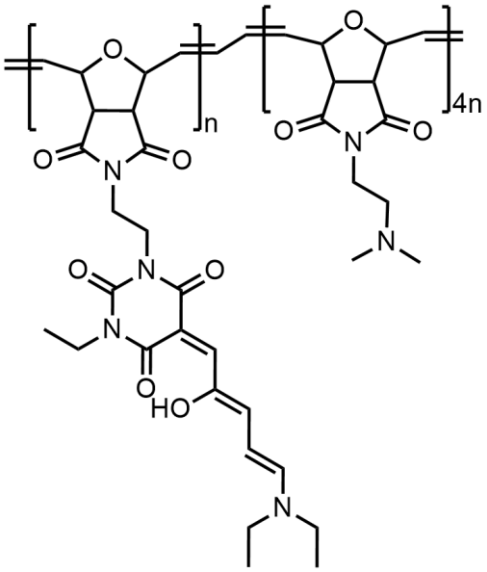

Synthesis of copolymer (2.7c). A solution of DASA monomer **2.5** (19.90 mg, 0.04 mmol) control monomer **2.6** (37.82 mg, 0.16 mmol) was polymerised with Grubb's catalyst (10.48 mg, 0.013 mmol) yielding 47.51 mg of polymer **2.7c** after rotary evaporation and washing with cold Et_2O (82%).

References

(1) Lee, H.; Lee, B. P.; Messersmith, P. B. *Nature* **2007**, *448* (7151), 338–341.

(2) Li, Y.; Krahn, J.; Menon, C. *J. Bionic Eng.* **2016**, *13* (2), 181–199.

(3) Sahay, R.; Low, H. Y.; Baji, A.; Foong, S.; Wood, K. L. *RSC Adv.* **2015**, *5* (63), 50821–50832.

(4) Hawkes, E. W.; Jiang, H.; Cutkosky, M. R. *Int. J. Rob. Res.* **2016**, *35* (8), 943–958.

(5) Wang, B.; Jeon, Y. S.; Bhang, S. H.; Kim, J.-H. *Express Polym. Lett.* **2017**, *11* (8), 601–610.

(6) Kord Forooshani, P.; Lee, B. P. *J. Polym. Sci. Part A Polym. Chem.* **2017**, *55* (1), 9–33.

(7) Brennan, M. J.; Kilbride, B. F.; Wilker, J. J.; Liu, J. C. *Biomaterials* **2017**, *124*, 116–125.

(8) Penkov, O. V.; Pukha, V. E.; Starikova, S. L.; Khadem, M.; Starikov, V. V.; Maleev, M. V.; Kim, D. E. *Biomaterials* **2016**, *102*, 130–136.

(9) Johnson, K. L. *Journal of the American Chemical Society*. 1985, pp 1–17.

(10) Barthel, E. *J. Phys. D. Appl. Phys.* **2008**, *41* (16), 163001.

(11) Boesel, L. F.; Cremer, C.; Arzt, E.; Campo, A. Del. *Adv. Mater.* **2010**, *22* (19), 2125–2137.

(12) Northen, M. T.; Turner, K. L. *Nanotechnology* **2005**, *16* (8), 1159–1166.

(13) Weck, M.; Schwab, P.; Grubbs, R. H. *Macromolecules* **1996**, *29* (5), 1789–1793.

(14) Autumn, K.; Sitti, M.; Liang, Y. A.; Peattie, A. M.; Hansen, W. R.; Sponberg, S.; Kenny, T. W.; Fearing, R.; Israelachvili, J. N.; Full, R. J. *Proc. Natl. Acad. Sci.* **2002**, *99* (19), 12252–12256.

(15) Im, H.; Kim, J.; Han, S.; Kim, T. *Polymers (Basel).* **2016**, *8* (9), 326.

(16) Eui, H.; Lee, J.; Kim, H. N.; Moon, S. H.; Suh, K. Y.; Langer, R.; Eui, H.; Leeb, J. J.; Nam, H.; Moonb-, S. H.; Suhac-, K. Y. **2017**, *106* (14), 5639–5644.

(17) Balamurugan, A.; Lee, H. Il. *Macromolecules* **2016**, *49* (7), 2568–2574.

(18) Autumn, K. *J. Exp. Biol.* **2006**, *209* (18), 3569–3579.

(19) Izadi, H.; Stewart, K. M. E.; Penlidis, A. *J. R. Soc. Interface* **2014**, *11* (July), 2014.0371.

(20) Atkins, P. W. *Physical Chemistry*; 1994.

(21) Camesano, T. a.; Logan, B. E. *Environ. Sci. Technol.* **2000**, *34* (16), 3354–3362.

(22) Mills, A. L.; Herman, J. S.; Hornberger, G. M.; Dejesús, H.; Dejesust, T. H. **1994**, *60* (9), 3300–3306.

(23) Lau, T.-L.; Kim, C.; Ginsberg, M. H.; Ulmer, T. S. *EMBO J.* **2009**, *28* (9), 1351–1361.

(24) Jucker, B. a; Jucker, B. a; Harms, H.; Harms, H.; Zehnder, A. J. B.; Zehnder, A. J. B. *Microbiology* **1996**, *178* (18), 5472–5479.

(25) Gao, H.; Yao, H.; Achenbach, J. D.; May, N.; Gao, H.; Yao, H. **2016**, *101* (21), 7851–7856.

(26) Kang, E. T.; Neoh, K. G.; Li, Z. F.; Tan, K. L.; Liaw, D. J. *Polymer (Guildf).* **1998**, *39* (12), 2429–2436.

(27) Tannouri, P.; Arafeh, K. M.; Krahn, J. M.; Beaupré, S. L.; Menon, C.; Branda, N. R. *Chem. Mater.* **2014**, *26* (15), 4330–4333.

(28) Park, J.; Feng, D.; Yuan, S.; Zhou, H. C. *Angew. Chemie - Int. Ed.* **2015**, *54* (2), 430–435.

(29) Kopelman, R. A.; Snyder, S. M.; Frank, N. L. *J. Am. Chem. Soc.* **2003**, *125* (45), 13684–13685.

(30) Shao, N.; Jian, Y. J.; Wang, H.; Zhang, Y.; Rong, H. Y.; Wing, H. C. *Anal. Chem.* **2008**, *80* (9), 3466–3475.

(31) Öge, T.; Zentel, R. *Macromol. Chem. Phys.* **1996**, *197* (6), 1805–1813.

(32) Kim, Y.; Phillips, J. a; Liu, H.; Kang, H.; Tan, W. *Proc. Natl. Acad. Sci. U. S. A.* **2009**, *106* (16), 6489–6494.

(33) Schlenoff, J. B. *Langmuir* **2014**, *30* (32), 9625–9636.

(34) Liu, Q.; Li, W.; Wang, H.; Newby, B. M. Z.; Cheng, F.; Liu, L. *Langmuir* **2016**, *32* (31), 7866–7874.

(35) Fritzsche. *J. für Prakt. Chemie* **1867**, *101* (1), 333–343.

(36) Dürr, H. In *Photochromism*; 2003; pp 1–14.

(37) Crano, J. C.; Guglielmetti, R. J. *Organic Photochromic and Thermochromic Compounds*; Crano, J. C., Guglielmetti, R. J., Eds.; Springer US: New York, NY, 1999; Vol. 1.

(38) Feringa, B. L. *Molecular Switches*; Feringa, B. L., Ed.; WILEY-VCH Verlag GmbH, 2001; Vol. 3.

(39) Minkin, V. I. *Chem. Rev.* **2004**, *104* (5), 2751–2776.

(40) Helmy, S.; Leibfarth, F. A.; Oh, S.; Poelma, J. E.; Hawker, C. J.; De Alaniz, J. R. *J. Am. Chem. Soc.* **2014**, *136* (23), 8169–8172.

(41) Lewis, K. G.; Mulquiney, C. E. *Tetrahedron* **1977**, *33* (5), 463–475.

(42) Honda, K.; Komizu, H.; Kawasaki, M. *J. Chem. Soc. Chem. Commun.* **1982**, No. 4, 253–254.

(43) Šafář, P.; Považanec, F.; Prónayová, N.; Baran, P.; Kicklebick, G.; Kožíšek, J.; Breza, M. *Collect. Czech. Chem. Commun.* **2000**, *65* (12), 1911–1938.

(44) Helmy, S.; Oh, S.; Leibfarth, F. A.; Hawker, C. J.; Alaniz, J. R. de A. *J. Org. Chem.* **2014**, *79*, 11316–11329.

(45) Helmy, S.; Oh, S.; Leibfarth, F. A.; Hawker, C. J.; Read De Alaniz, J. *J. Org. Chem.* **2014**, *79* (23), 11316–11329.

(46) Hemmer, J. R.; Poelma, S. O.; Treat, N.; Page, Z. A.; Dolinski, N. D.; Diaz, Y. J.; Tomlinson, W.; Clark, K. D.; Hooper, J. P.; Hawker, C.; Read De Alaniz, J. *J. Am. Chem. Soc.* **2016**, *138* (42), 13960–13966.

(47) Mallo, N.; Brown, P. T.; Iranmanesh, H.; MacDonald, Alaniz, J. R. de. et al. *Chem. Commun.* **2016**, *352* (Scheme 1), 1443–1445.

(48) Laurent, A. D.; Medved', M.; Jacquemin, D. *ChemPhysChem* **2016**, *17*, 1846–1851.

(49) Lerch, M. M.; Wezenberg, S. J.; Szymanski, W.; Feringa, B. L. *J. Am. Chem. Soc.* **2016**, *138* (20), 6344–6347.

(50) Patel, D. G.; Paquette, M. M.; Kopelman, R. A.; Kaminsky, W.; Ferguson, M. J.; Frank, N. L. *J. Am. Chem. Soc.* **2010**, *132* (36), 12568–12586.

(51) Mason, B. P.; Whittaker, M.; Hemmer, J.; Arora, S.; Harper, A.; Alnemrat, S.; McEachen, A.; Helmy, S.; Read De Alaniz, J.; Hooper, J. P. *Appl. Phys. Lett.* **2016**, *108* (4).

(52) Poelma, S. O.; Oh, S. S.; Helmy, S.; Knight, A. S.; Burnett, G. L.; Soh, H. T.; Hawker, C. J.; Read de Alaniz, J. *Chem. Commun.* **2016**, *52* (69), 10525–10528.

(53) Lerch, M. M.; Hansen, M. J.; Velema, W. a; Szymanski, W.; Feringa, B. L. *Nat. Commun.* **2016**, *7* (May), 12054.

(54) Wang, B.; Chen, L.; Abdulali-Kanji, Z.; Horton, J. H.; Oleschuk, R. D. *Langmuir* **2003**, *19* (23), 9792–9798.

(55) Lee; Park; Whitesides. *Anal. Chem. Dc-* **2003**, *75* (23), 6544–6554.

(56) Mukhopadhyay, R. *Anal. Chem.* **2007**, *79* (9), 3248–3253.

(57) Almutairi, Z.; Ren, C. L.; Simon, L. *Colloids Surfaces A Physicochem. Eng. Asp.* **2012**, *415*, 406–412.

(58) Samy, R.; Glawdel, T.; Ren, C. L. *Measurement* **2008**, *80* (2), 4117–4123.

(59) Yao, M.; Fang, J. *J. Micromechanics Microengineering* **2012**, *22* (2), 25012.

(60) Binder, W. H.; Pulamagatta, B.; Kir, O.; Kurzhals, S.; Barqawi, H.; Tanner, S. *Macromolecules* **2009**, *42* (24), 9457–9466.

(61) Czelusniak, I.; Khosravi, E.; Kenwright, A. M.; Ansell, C. W. G. *Macromolecules* **2007**, *40* (5), 1444–1452.

(62) France, M. B.; Alty, L. T.; Earl, T. M. **1999**, *76* (5), 659–660.

(63) Hersey, J. S.; Meller, A.; Grinstaff, M. W. *Anal. Chem.* **2015**, *87* (23), 11863–11870.

(64) Harris, D. C. *Quantitative chemical analysis*, 8th ed.; W.H. Freeman and Company: New York, NY, 2010.

(65) Billmeyer, F. W.; Wiley, J. *Textbook of Polymer Science*; Wiley India: New Delhi, 1984.

(66) IUPAC. *Compendium of Chemical Technology*, 2nd ed.; McNaught, A. D., Wilkinson, A., Eds.; Blackwell Scientific Publications: Oxford, UK, 1997.

(67) Girolami, G. *J. Chem. Educ.* **1994**, *71*, 962–964.

(68) Myles, A. J.; Branda, N. R. *Macromolecules* **2003**, *36* (2), 298–303.

(69) Förch, R.; Schönherr, H.; Jenkins, A. *Surface Design: Applications in Bioscience and*; Förch, R., Schönherr, H., Jenkins, T., Eds.; WILEY-VCH Verlag GmbH, 2009.

(70) Yuan, Y.; Lee, T. R. In *Springer Series in Surface Sciences Techniques*; Bracco, G., Holst, B., Eds.; Springer, Berlin, Heidelberg: Berlin, 2013; Vol. 51.

(71) Holmes-Farley, S. R.; Reamey, R. H.; McCarthy, T. J.; Deutch, J.; Whitesides, G. M. *Langmuir* **1985**, *1* (6), 725–740.

(72) Chuah, Y. J.; Koh, Y. T.; Lim, K.; Menon, N. V.; Wu, Y.; Kang, Y. *Sci. Rep.* **2016**, *5* (1), 18162.

Appendix A. – NMR Spectroscopy

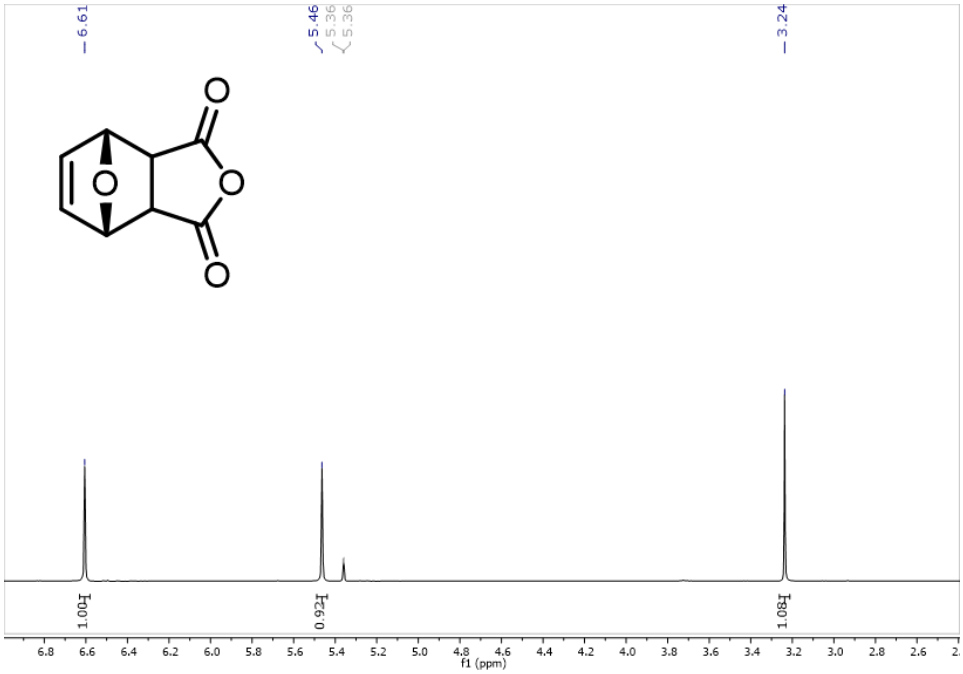

Figure A.1. ***^{1}H NMR of 7-oxabicyclo[2.2.1]hept-5-ene-2,3-dicarboxylic anhydride, 2.1 (400 MHz, chloroform-d)***

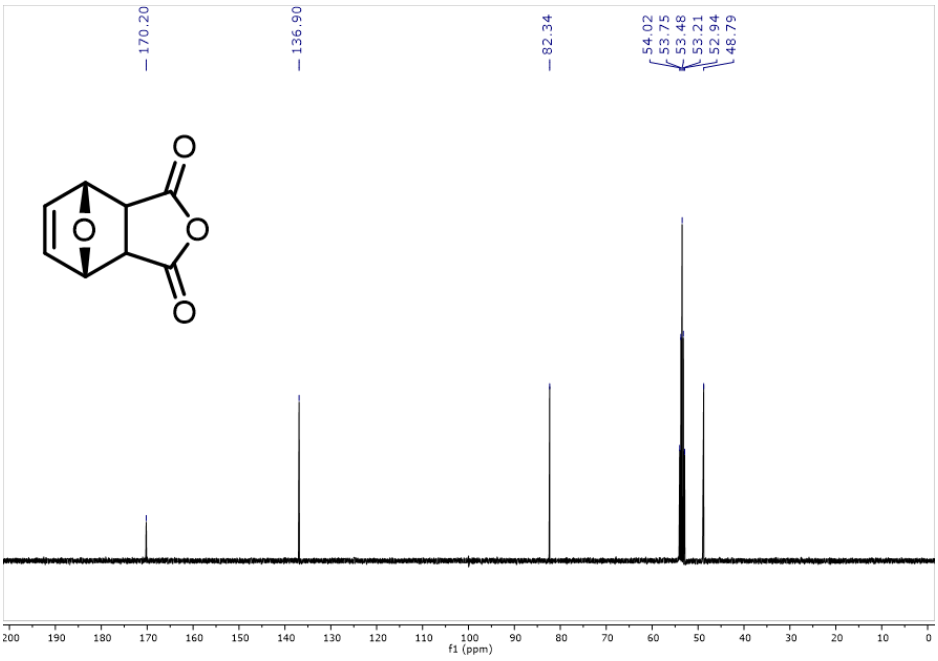

Figure A.2. ***^{13}C NMR of 7-oxabicyclo[2.2.1]hept-5-ene-2,3-dicarboxylic anhydride, 2.1 (100 MHz, DCM-d2)***

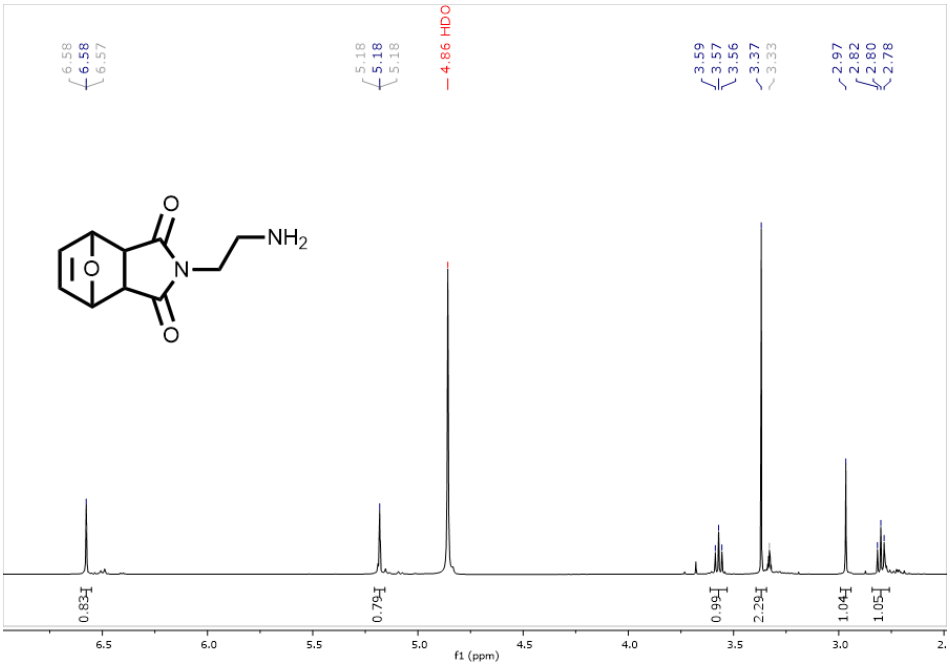

Figure A.3. ***^{1}H NMR of N-(2-aminoethyl)-7-oxabicyclo[2.2.1]hept-5-ene-2,3-dicarboximide, 2.2 (400 MHz, methanol-d4)***

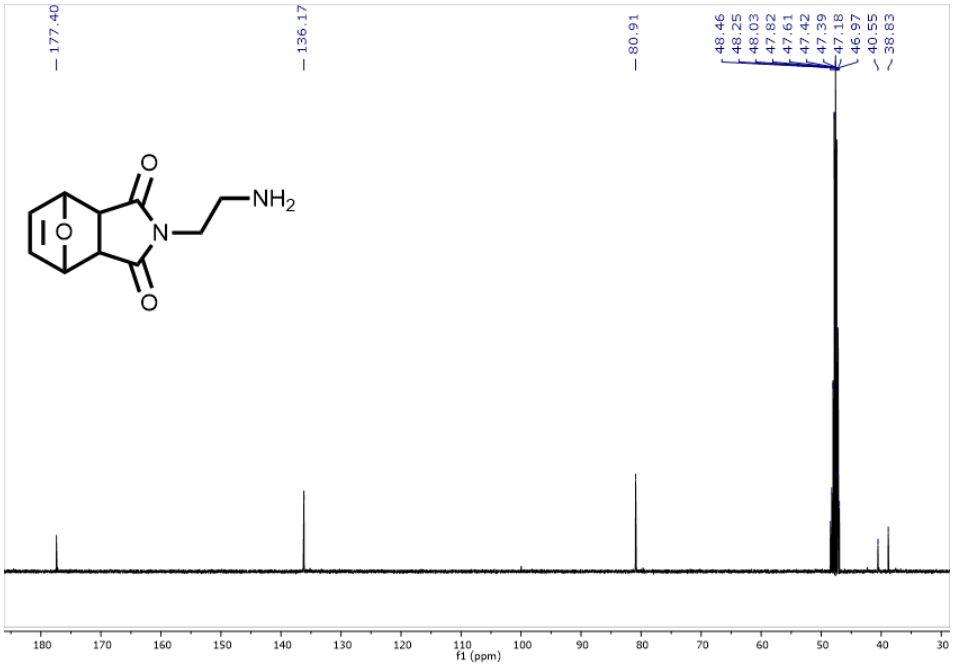

Figure A.4. ***^{13}C NMR of N-(2-aminoethyl)-7-oxabicyclo[2.2.1]hept-5-ene-2,3-dicarboximide, 2.2 (100 MHz, methanol-d4)***

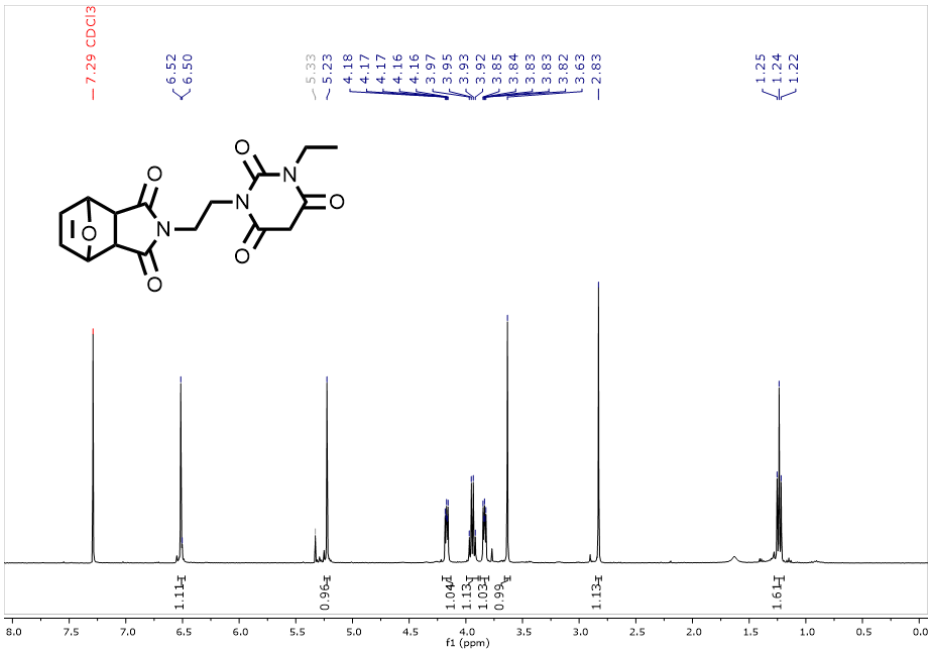

Figure A.5. ***^{1}H NMR of 1-(7-oxabicyclo[2.2.1]hept-5-ene-2,3-dicarboximidoethyl)-3-ethylbarbituric acid, 2.3 (400 MHz, chloroform-d)***

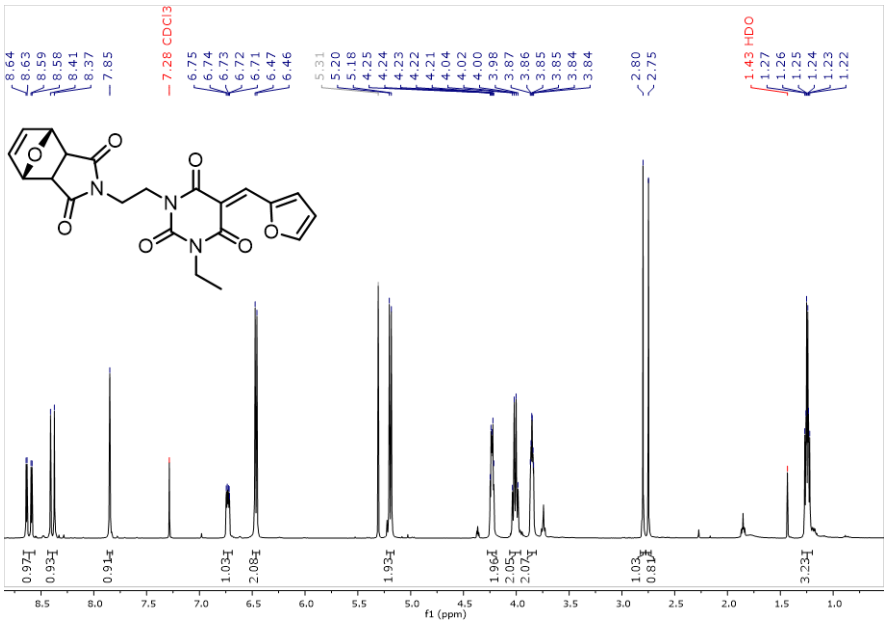

Figure A.6. ***^{1}H NMR of 3-ethyl-5-(furan-2-ylmethylene)-1-(7-oxabicyclo[2.2.1]hept-5-ene-2,3-dicarboximidoethyl)barbituric acid, 2.4 (400 MHz, chloroform-d)***

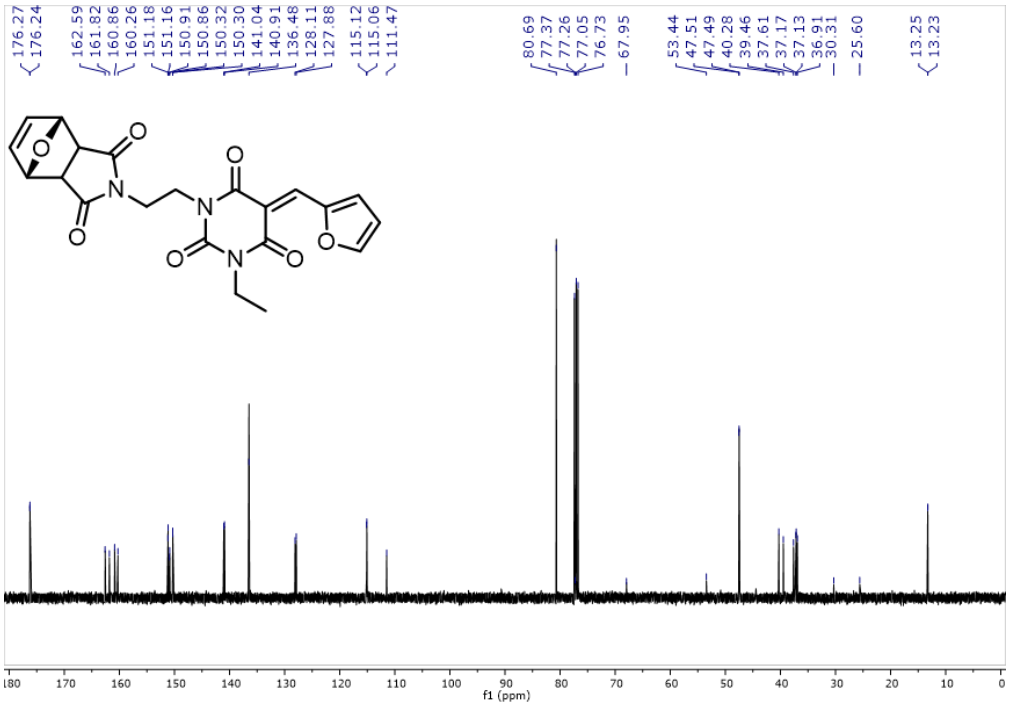

Figure A.7. ***^{13}C NMR of 3-ethyl-5-(furan-2-ylmethylene)-1-(7-oxabicyclo[2.2.1]hept-5-ene-2,3-dicarboximidoethyl)barbituric acid, 2.4 (100 MHz, chloroform-d)***

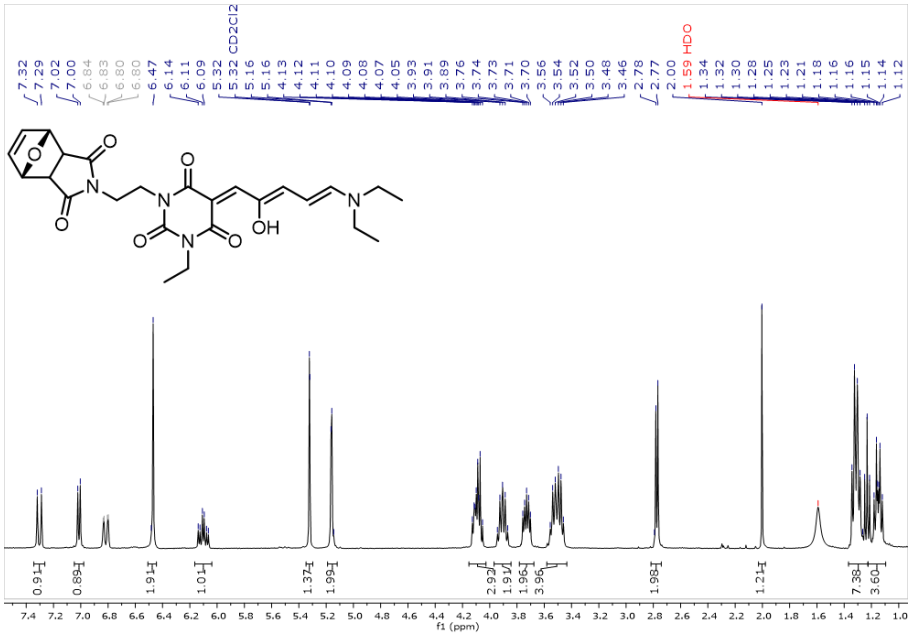

Figure A.8. ***^{1}H NMR of (E)-5-((2Z,4E)-5-(N,N-diethylamino)-2-hydroxypenta-2,4-dien-1-ylidene)3-ethyl-5-(furan-2-ylmethylene)-1-(7-oxabicyclo[2.2.1]hept-5-ene-2,3-dicarboximidoethyl)barbituric acid, 2.5 (400 MHz, DCM-d2)***

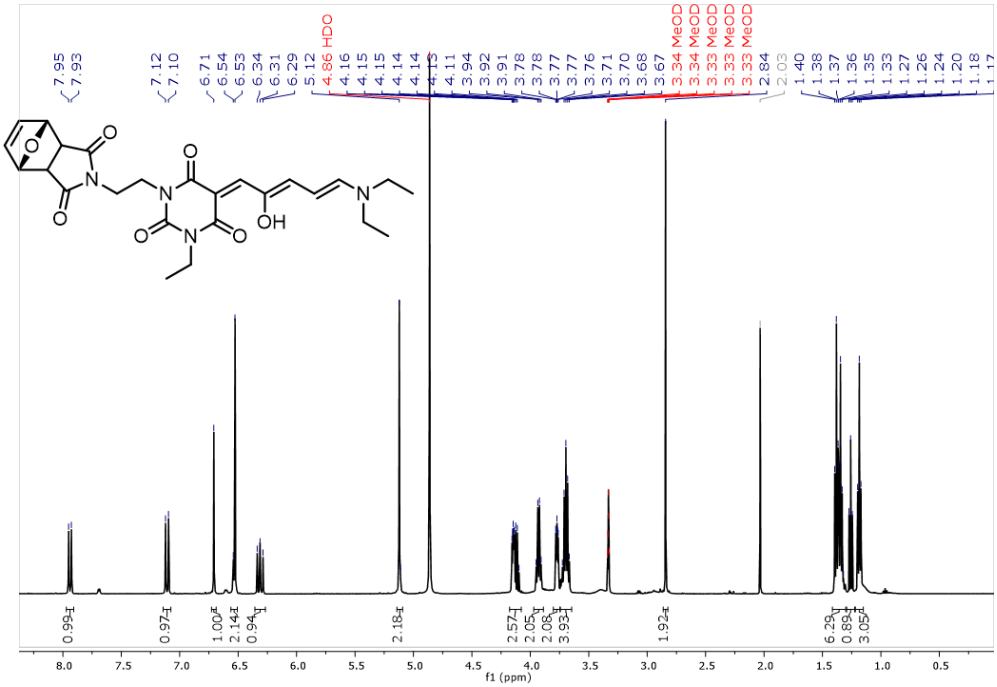

Figure A.9. ***^{1}H NMR of (E)-5-((2Z,4E)-5-(N,N-diethylamino)-2-hydroxypenta-2,4-dien-1-ylidene)3-ethyl-5-(furan-2-ylmethylene)-1-(7-oxabicyclo[2.2.1]hept-5-ene-2,3-dicarboximidoethyl)barbituric acid, 2.5 (400 MHz, 1:1 methanol-d_4:water-d_2)***

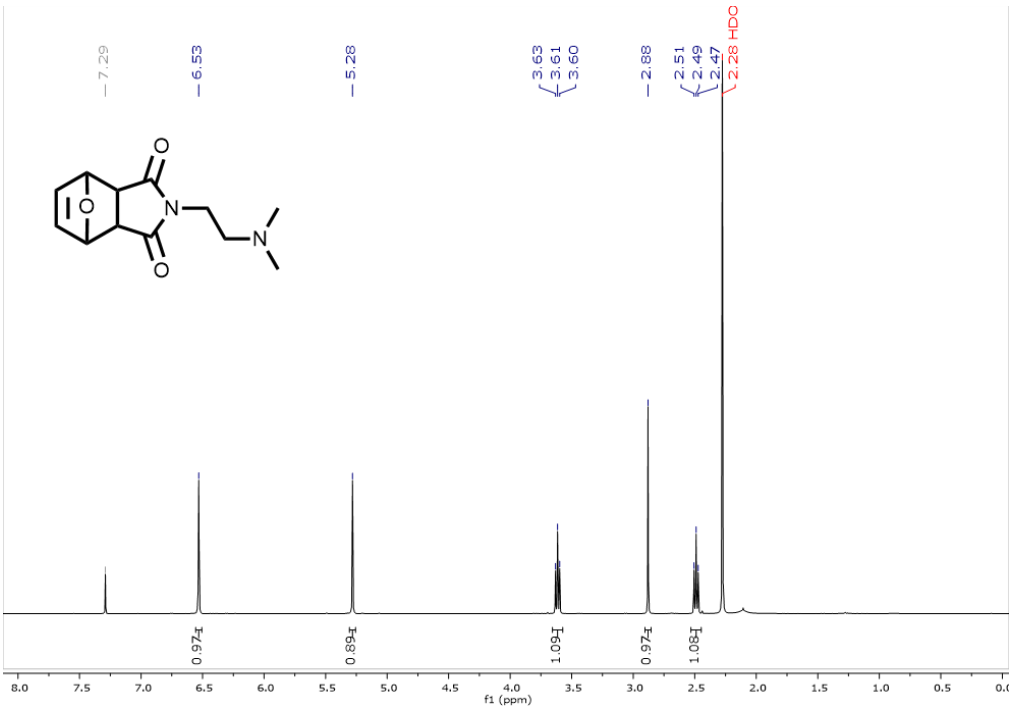

Figure A.10. ***^{1}H NMR of N-(2-(dimethylamino)ethyl)-7-oxabicyclo[2.2.1]hept-5-ene-2,3-dicarboximide, 2.6 (400 MHz, chloroform-d)***

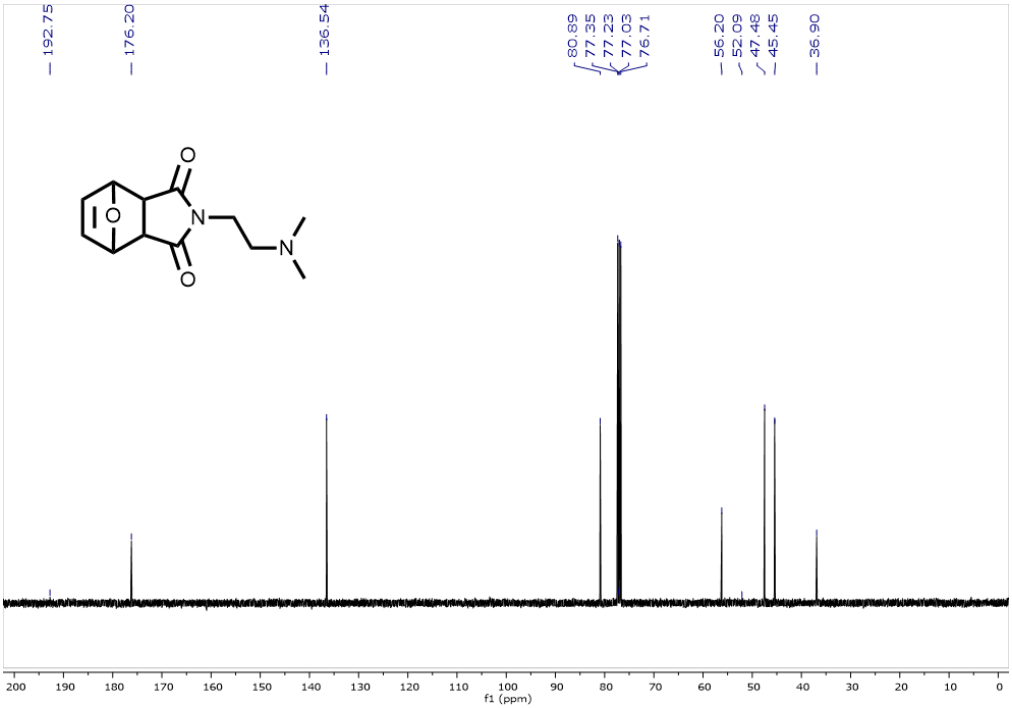

Figure A.11. ***^{13}C NMR of N-(2-(dimethylamino)ethyl)-7-oxabicyclo[2.2.1]hept-5-ene-2,3-dicarboximide, 2.6 (100 MHz, chloroform-d)***

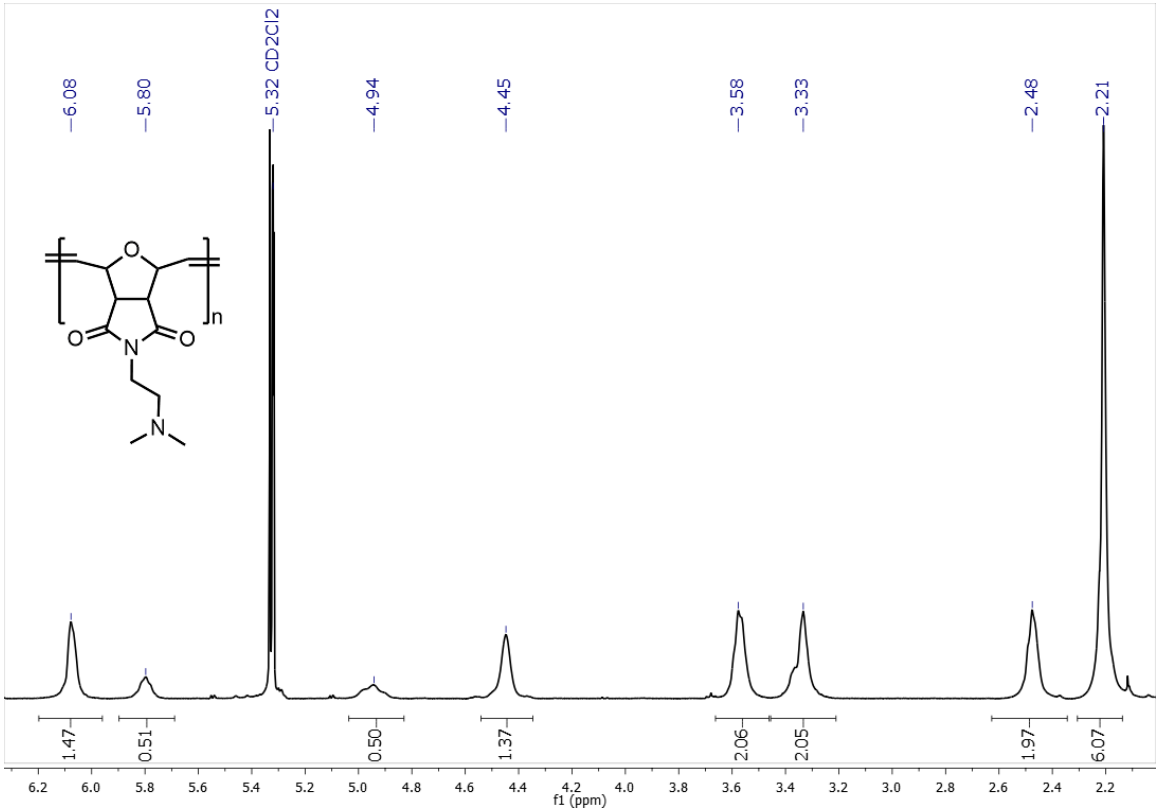

Figure A.12. ***^{1}H NMR of polymer 2.6p (400 MHz, DCM-d2)***

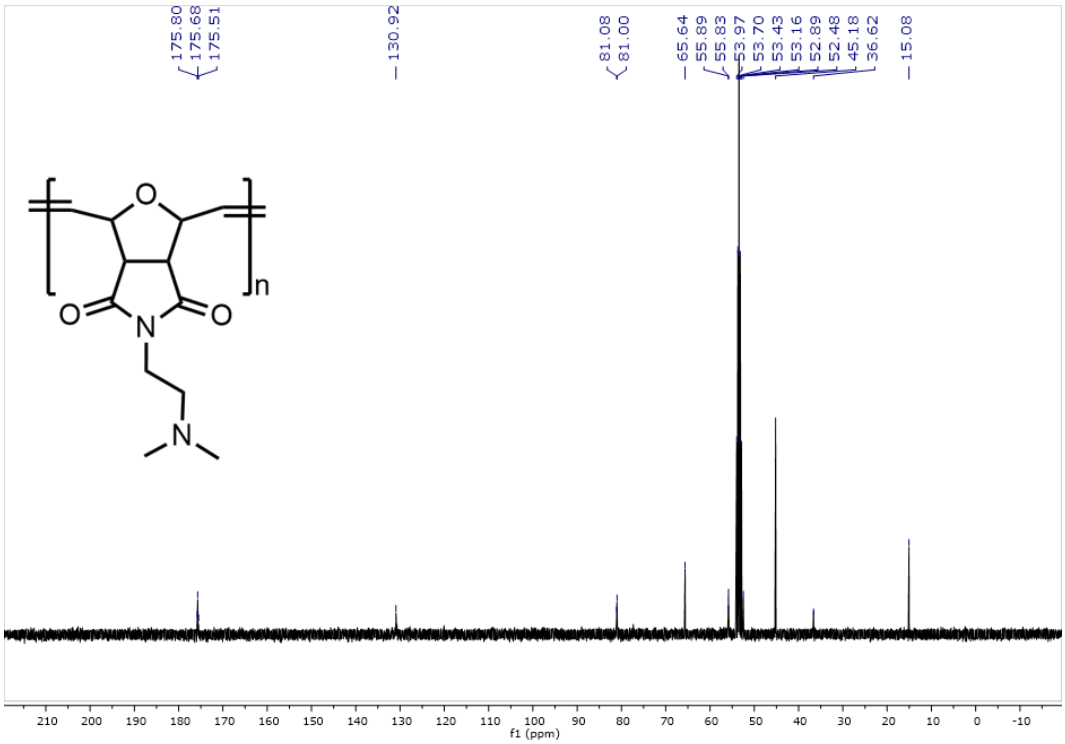

Figure A.13. ***^{13}C NMR of polymer 2.6p (100 MHz, DCM-d2)***

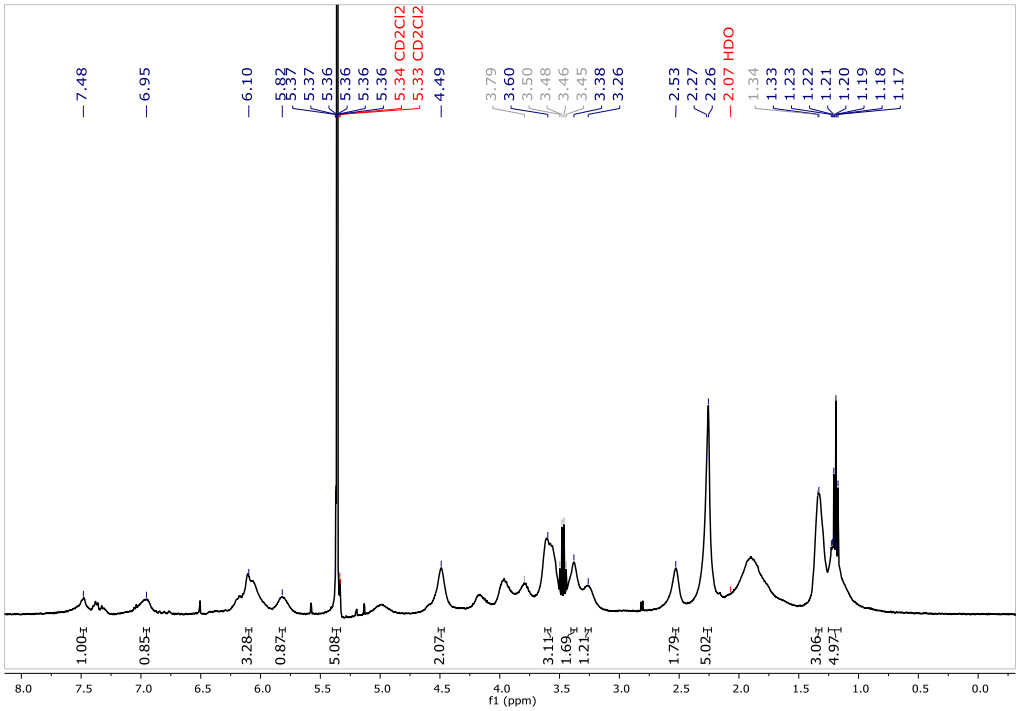

Figure A.14. ***^{1}H NMR of polymer 2.7a (400 MHz, DCM-d2)***

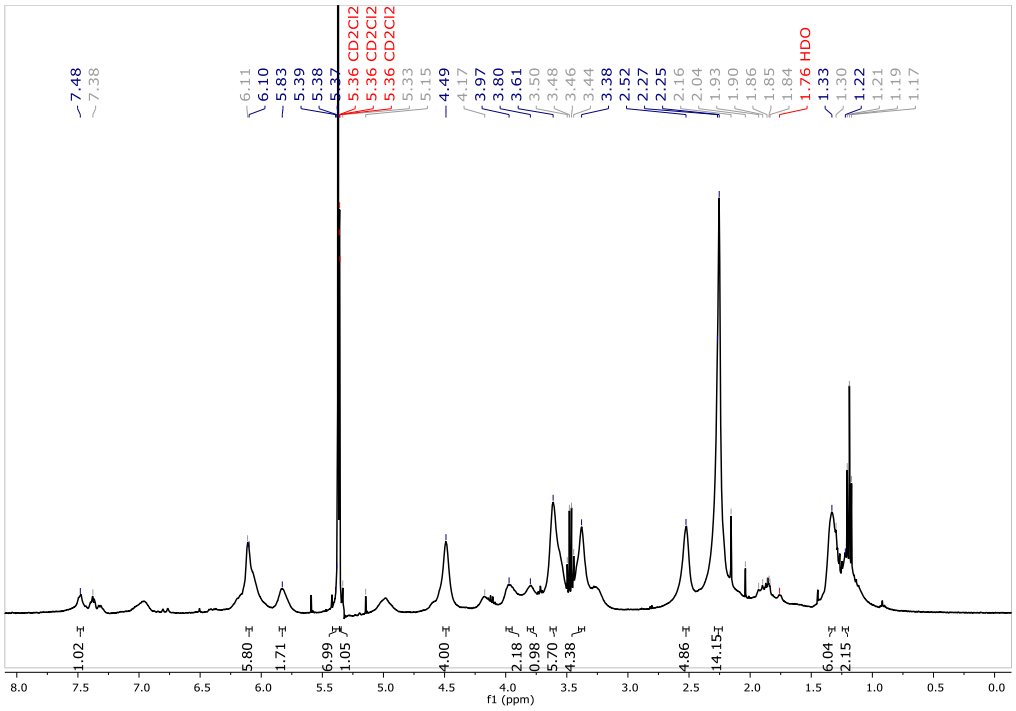

Figure A.15. ^{1}H NMR of polymer 2.7b (400 MHz, DCM-d2)

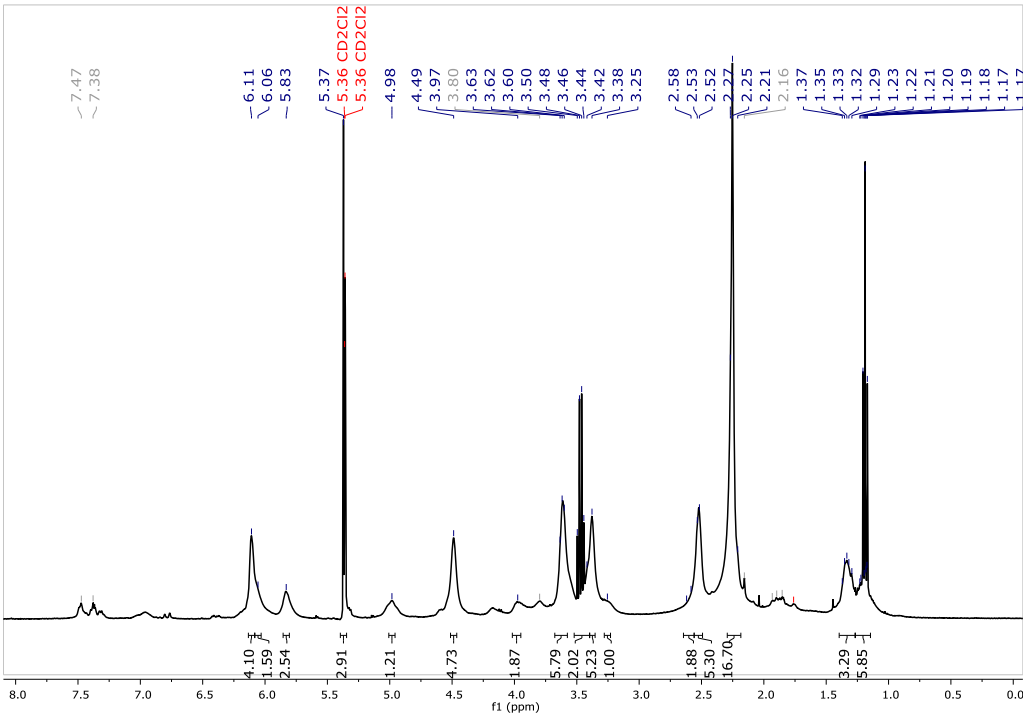

Figure A.16. ^{1}H NMR of polymer 2.7c (400 MHz, chloroform-d)

Appendix B. – GPC Chromatograms

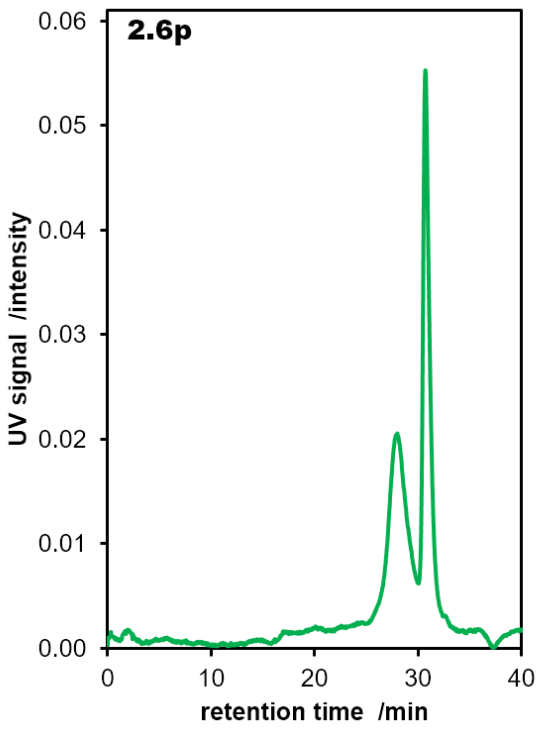

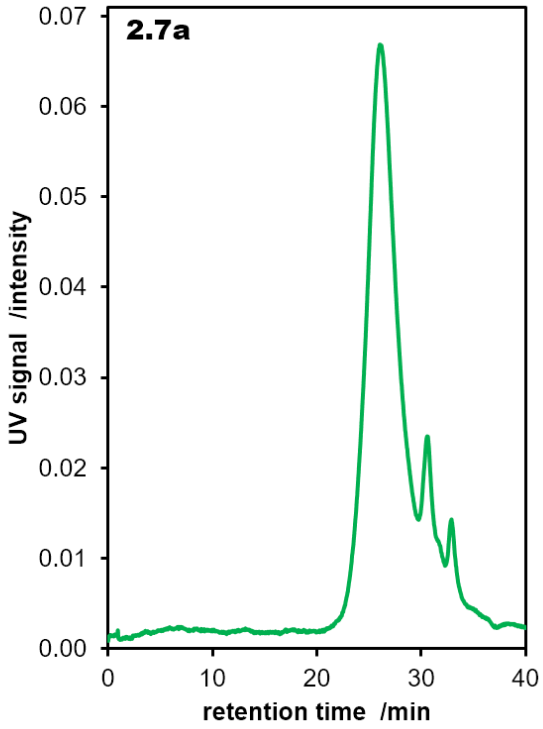

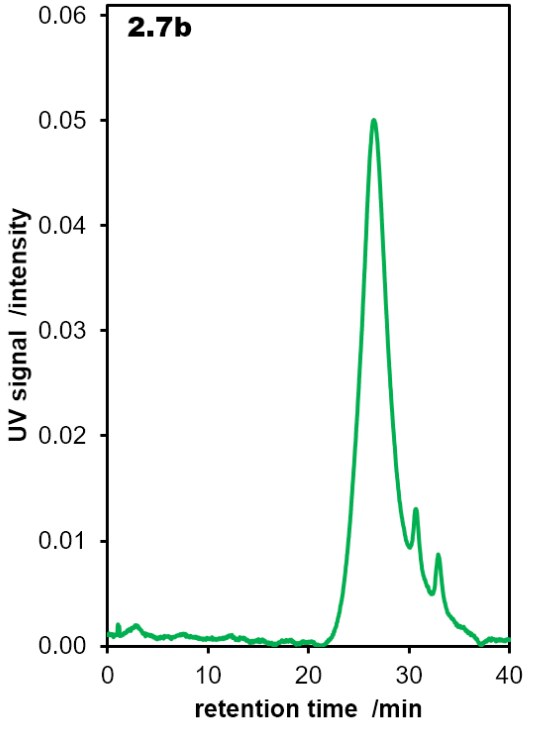

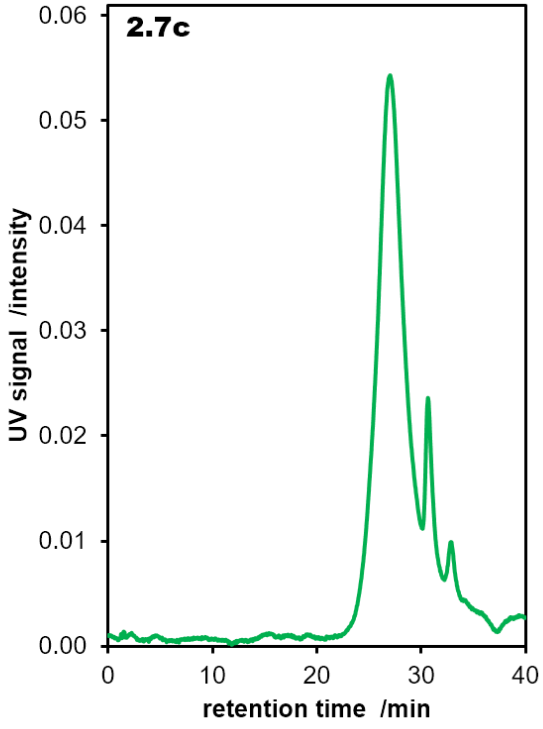

Appendix C. – Calculation of Switch/Control Ratio

Calculation for Polymer 2.6p

Polymer $\bar{M}_w$ from DSC: 21500 g·mol^{-1}; Control molecular weight: 236.272 g·mol^{-1}

y(236.272 g·mol^{-1}) = 21500 g·mol^{-1}

y = 91

Therefore, there is an average of 91 control units, which is consistent with the number of units expected from synthesis (~100).

Calculation for Polymer 2.7a

Polymer $\bar{M}_w$ from DSC: 41000 g·mol^{-1}; Control molecular weight: 236.272 g·mol^{-1}; DASA switch molecular weight: 498.538 g·mol^{-1}

Therefore, x amount of switch and y amount of control sum to the polymer $\bar{M}_w$

x(498.538 g·mol^{-1}) + y(236.272 g·mol^{-1}) = 41000 g·mol^{-1}

Additionally the ratio of control:switch is known from the synthesis as 1:1, and therefore x=y so a substitution can be made, giving:

x(498.538 g·mol^{-1}) + x(236.272 g·mol^{-1}) = 41000 g·mol^{-1}

x = y = 56

Therefore, there are an average of 56 switch units and 56 control units per polymer strand. This sums to 110 units per polymer chain, which is consistent with the number of units expected from synthesis (~100).

Calculation for Polymer 2.7b

Polymer $\bar{M}_w$ from DSC: 38000 g·mol^{-1}; Control molecular weight: 236.272 g·mol^{-1}; DASA switch molecular weight: 498.538 g·mol^{-1}

Therefore, x amount of switch and y amount of control sum to the polymer $\bar{M}_w$

$x(498.538\ g{\cdot}mol^{-1}) + y(236.272\ g{\cdot}mol^{-1}) = 38000\ g{\cdot}mol^{-1}$

Additionally the ratio of control:switch is known from the synthesis as 1:2, and therefore x=2y so a substitution can be made, giving:

$x(498.538\ g{\cdot}mol^{-1}) + 2x(236.272\ g{\cdot}mol^{-1}) = 41000\ g{\cdot}mol^{-1}$

x = 78 and y = 39

Therefore, there are an average of 39 switch units and 78 control units per polymer strand. This sums to 117 units per polymer chain, which is consistent with the number of units expected from synthesis (~100).

Calculation for Polymer 2.7c

Polymer $\bar{M}_w$ from DSC: 31000 $g{\cdot}mol^{-1}$; Control molecular weight: 236.272 $g{\cdot}mol^{-1}$; DASA switch molecular weight: 498.538 $g{\cdot}mol^{-1}$

Therefore, x amount of switch and y amount of control sum to the polymer $\bar{M}_w$

$x(498.538\ g{\cdot}mol^{-1}) + y(236.272\ g{\cdot}mol^{-1}) = 31000\ g{\cdot}mol^{-1}$

Additionally the ratio of control:switch is known from the synthesis as 1:2, and therefore x=4y so a substitution can be made, giving:

$x(498.538\ g{\cdot}mol^{-1}) + 4x(236.272\ g{\cdot}mol^{-1}) = 41000\ g{\cdot}mol^{-1}$

x = 86 and y = 21

Therefore, there are an average of 21 switch units and 86 control units per polymer strand. This sums to 108 units per polymer chain, which is consistent with the number of units expected from synthesis (~100).

Appendix D. – DSC Thermograms

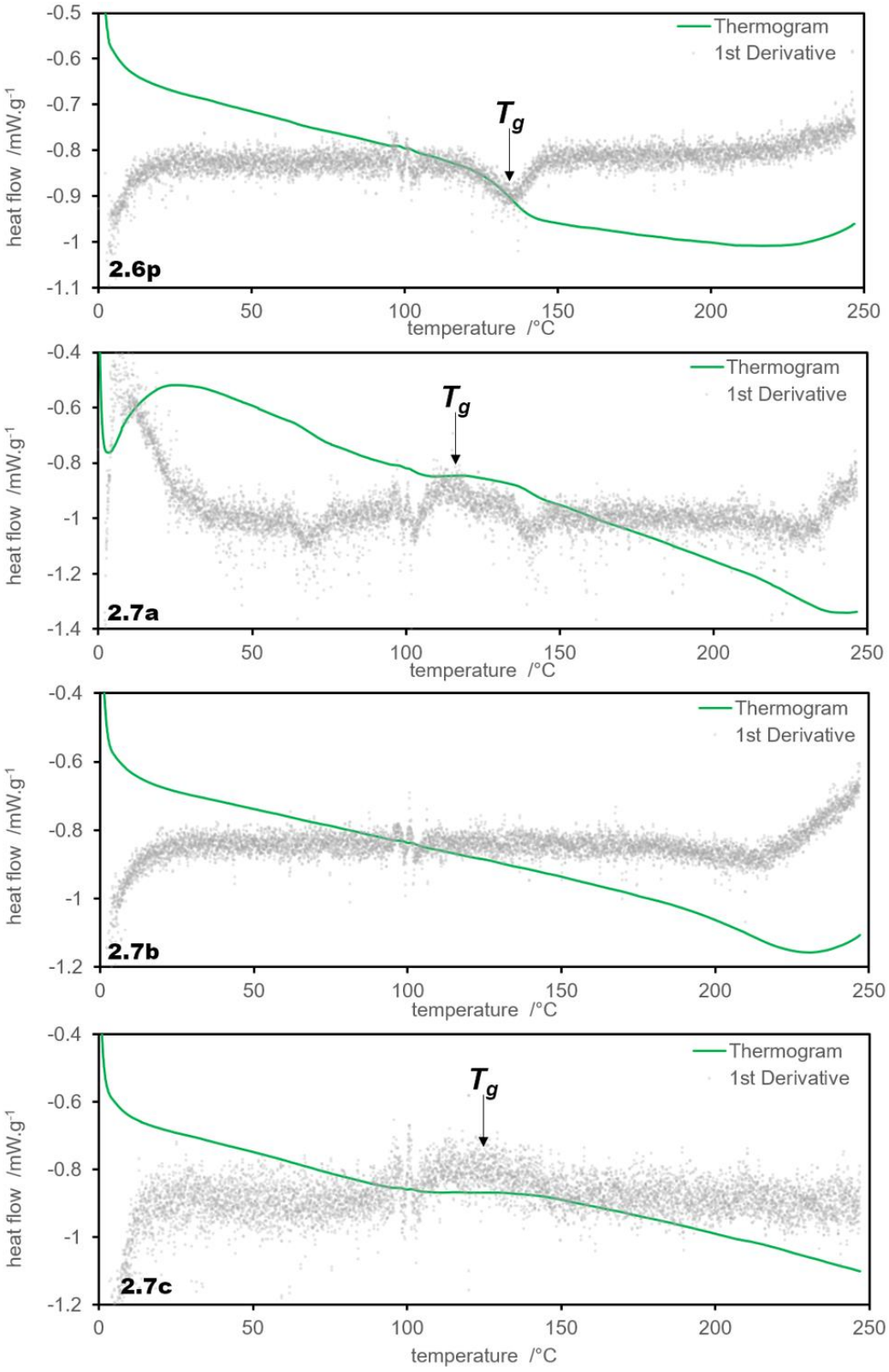

Appendix E. – PSS and Thermal Reversion

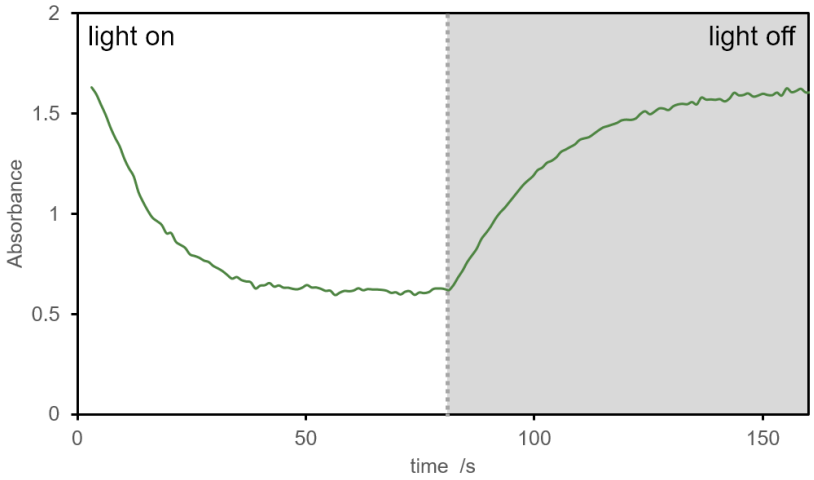

Figure E.1. *DASA 2.5 (2x10^{-5} M in o-xylene) showing irradiation to photostationary state at ~60s and thermal reversion in the dark over ~80s.*

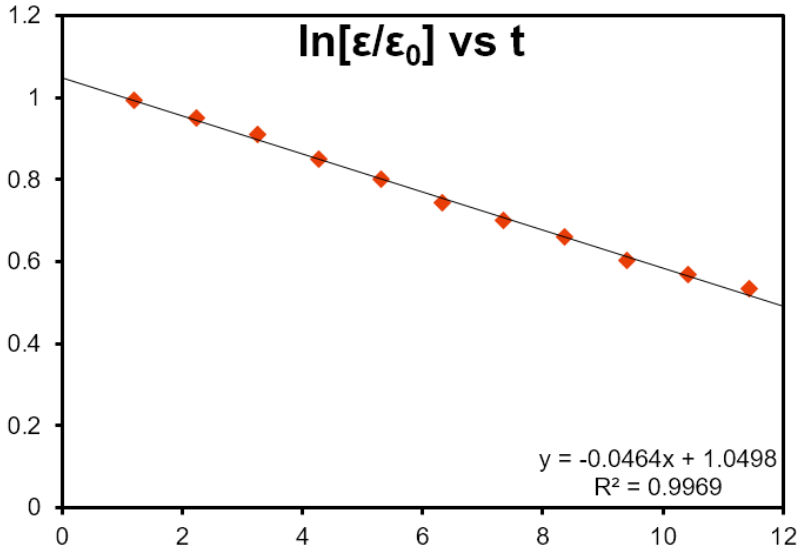

Figure E.2. *DASA 2.5 (2x10^{-5} M in o-xylene) showing relaxing from closed to open form in the dark. The plot of ln(absorbance) with respect to time gives a straight line, and the rate constant can be extracted from the intercept of the graph (0.0464 s^{-1}). $\varepsilon/\varepsilon_0$ is used to produce data for the isomerisation to the open form, rather than data of disappearance of the closed form.*

Equation E.1. Half-life for isomerisation to open form: $t_{1/2} = \frac{0.693}{k} = \frac{0.693}{0.0464} \approx 16s$

Appendix F – Density and Thin Film Calculations

The "back of the envelope" density approximations outlined by Girolami[67] make use of the approximate relative volume of the atoms in a structure by assigning them a value (C,N,O = 2; H =1), and then using a specific factor for the molecular interactions (1.3) and solid state packing interactions (1.4). These calculations give densities within 10%, even for complex molecular systems.

$$\rho = \frac{1.3 \cdot W}{5 \cdot 1.4 \cdot V_s}$$

ρ = density
W = molecular weight
V_s = sum of relative volume
5 is a factor that allows expression in g·cm^{-3}
1.4 takes into account the solid state packing
1.3 takes into account the molecular interactions

For these polymer systems, the important V_s are of the constituent molecules, and then the number average of each in the final polymer (calculated in Appendix C) can be used to ascertain the density of the polymer system.

Calculation of V_s for DASA **2.5**	Calculation of V_s for Control **2.6**
W = 498.538 g·mol^{-1}	W = 236.272 g·mol^{-1}
V_s = (36 × 2) + (30 × 1) = 102	V_s = (17 × 2) + (16 × 1) = 50

Calculation for Polymers; $V_s = n_{(switch)} \cdot V_{s(switch)} + n_{(control)} \cdot V_{s(control)}$

2.6p	V_s = (0 × 102) + (91 × 50) = 4550 $\rho = \frac{1.3 \cdot 21500}{6.4 \cdot 4550} = \mathbf{0.960\ g \cdot cm^{-3}}$
2.7a	V_s = (56 × 102) + (56 × 50) = 8481 $\rho = \frac{1.3 \cdot 41000}{6.4 \cdot 8481} = \mathbf{0.982\ g \cdot cm^{-3}}$
2.7b	V_s = (39 × 102) + (78 × 50) = 7905 $\rho = \frac{1.3 \cdot 38000}{6.4 \cdot 7905} = \mathbf{0.976\ g \cdot cm^{-3}}$
2.7c	V_s = (21 × 102) + (86 × 50) = 6485 $\rho = \frac{1.3 \cdot 31000}{6.4 \cdot 6485} = \mathbf{0.971\ g \cdot cm^{-3}}$

From these density calculations the thickness of the thin films can be calculated:

$$t = \frac{m}{A \cdot \rho}$$

t = thickness (of film)
m = mass of polymer used to make the film
A = surface area covered by film
ρ = density (calculated above)

Calculation for Polymers; m = 3 mg for all films, and A = 10 cm^2

2.6p	$t = \frac{0.003\ g \times 10^4 \mu m \cdot cm^{-1}}{10\ cm^2 \cdot 0.960\ g \cdot cm^{-3}} = \mathbf{3.12\mu m}$
2.7a	$t = \frac{0.003\ mg \times 10^4 \mu m \cdot cm^{-1}}{10\ cm^2 \cdot 0.982\ g \cdot cm^{-3}} = \mathbf{3.05\mu m}$
2.7b	$t = \frac{0.003\ mg \times 10^4 \mu m \cdot cm^{-1}}{10\ cm^2 \cdot 0.976\ g \cdot cm^{-3}} = \mathbf{3.07\mu m}$
2.7c	$t = \frac{0.003\ mg \times 10^4 \mu m \cdot cm^{-1}}{10\ cm^2 \cdot 0.960\ g \cdot cm^{-3}} = \mathbf{3.09\mu m}$

Therefore, these thin films (as prepared) are approximately 3μm thick.

Appendix G – UV-vis Spectroscopy

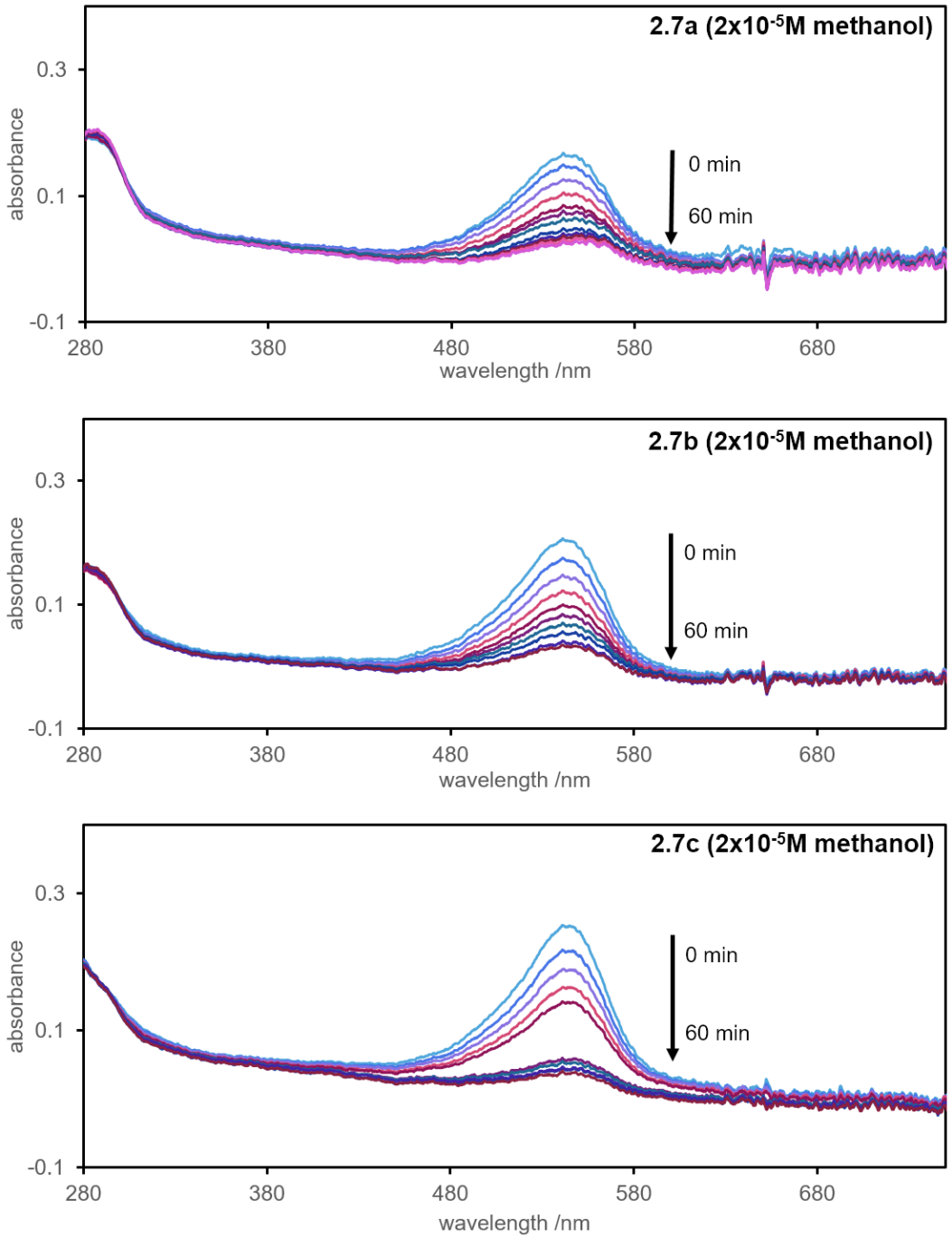

Figure F.1. ***Polymer solutions in methanol. Solutions are 2.5x10^{-5}M in the photoswitching component.***

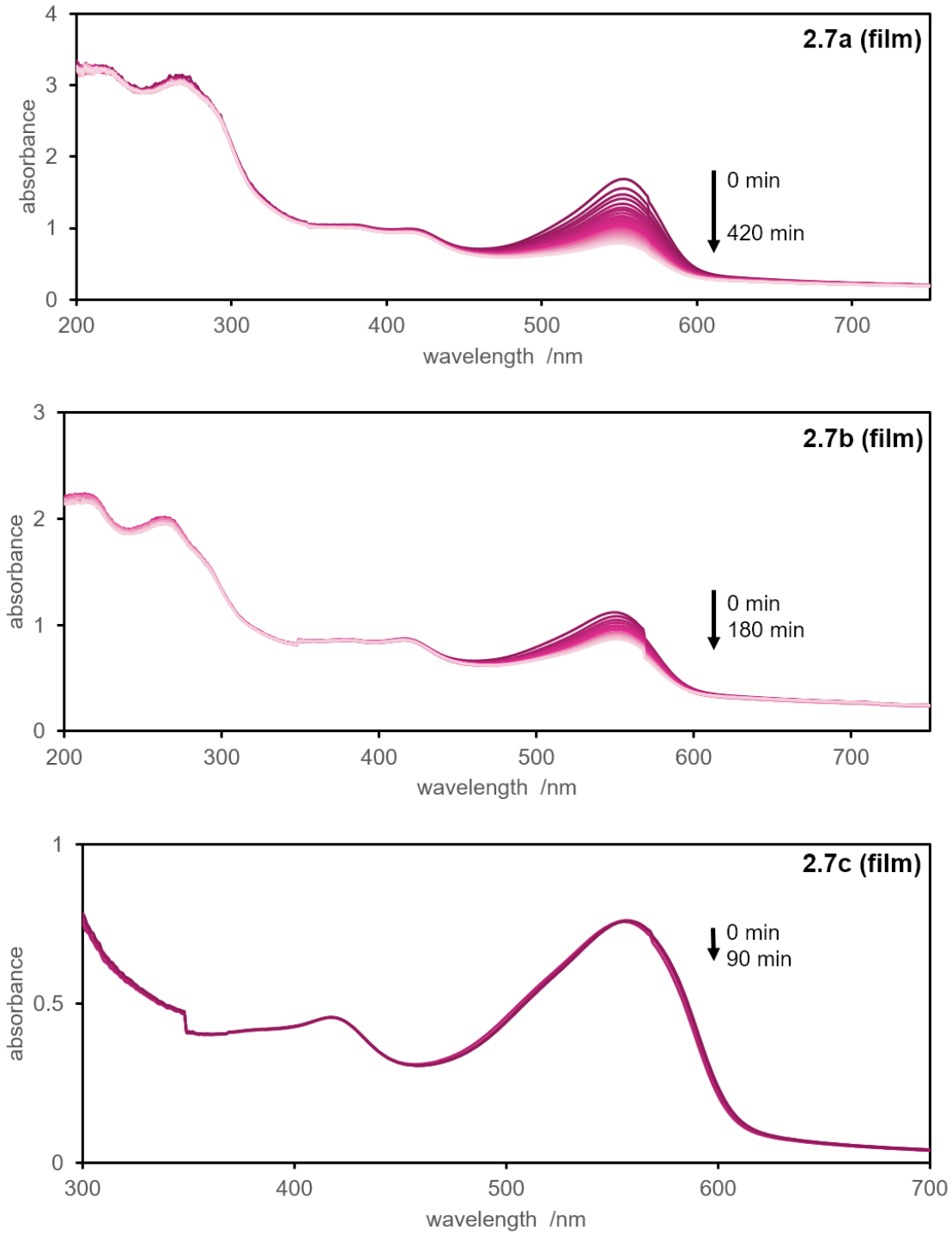

Figure F.2. ***Thin films of polymer on quartz (2.7a,2.7b) and glass (2.7c).***

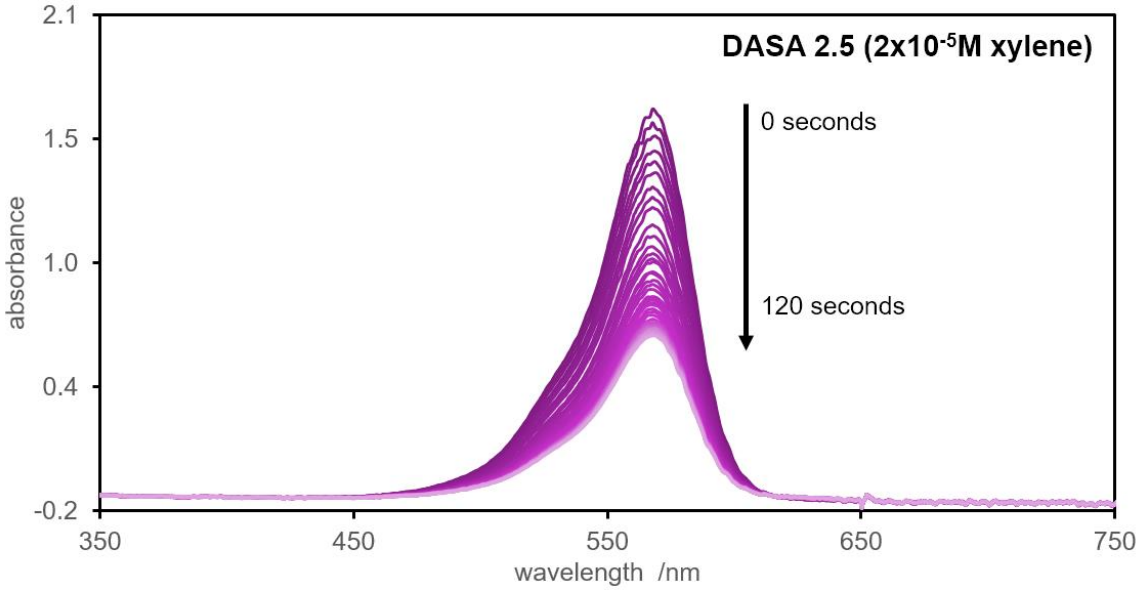

Figure F.3. ***UV-visible absorption spectrum of compound 2.5, 2×10^{-5} M in xylene. Irradiation with >520 nm light yields the PSS at 60 s.***

Appendix H. – Contact Angle Goniometry

Table G.1. Contact angle measurements for water droplets on top of thin films before and after irradiation with >520 nm light source for one hour. The first repeat set of data for **2.7a** is missing as the site was damaged when removing the water droplet.

Polymer 2.6p			
Dark		**Light**	
theta L	theta R	theta L	theta R
14.1	12.7	Not Taken	
21.3	22.7		
18.9	23.8		
27.4	20.6		
32.7	26.2		

Polymer 2.7a			
Dark		**Light**	
theta L	theta R	theta L	theta R
76.7	76.4		
73.0	72.7	57.1	54.0
73.6	73.0	56.1	55.7
72.4	72.1	54.6	53.7
73.7	72.4	56.0	55.5

Polymer 2.7b			
Dark		**Light**	
theta L	theta R	theta L	theta R
67.0	68.3	62.4	62.9
63.2	65.1	66.5	70.8
67.9	65.8	68.5	68.8
62.6	63.1	69.5	68.3
68.4	68.2	70.5	65.2

Polymer 2.7c			
Dark		**Light**	
theta L	theta R	theta L	theta R
49.0	51.3	57.0	54.4
49.5	51.8	52.6	52.8
55.1	55.1	58.0	59.1
52.5	52.4	54.2	50.8
46.9	50.7	58.5	59.9